INTERNAL STRUCTURE AND GEOCHRONOLOGY OF THE GERREI UNIT IN THE FLUMENDOSA AREA, VARISCAN EXTERNAL NAPPE ZONE, SARDINIA, ITALY

by

Ashley V. Dack

A thesis

submitted in partial fulfillment

of the requirements for the degree of

Master of Science in Geology

Boise State University

Summer 2009

BOISE STATE UNIVERSITY GRADUATE COLLEGE

DEFENSE COMMITTEE AND FINAL READING APPROVALS

of the thesis submitted by

Ashley V. Dack

Thesis Title: Internal structure and geochronology of the Gerrei Unit in the Flumendosa area, Variscan External Nappe Zone, Sardinia, Italy

Date of Final Oral Examination: 13 May 2009

The following individuals read and discussed the thesis submitted by student Ashley V. Dack, and they also evaluated her presentation and response to questions during the final oral examination. They found that the student passed the final oral examination, and that the thesis was satisfactory for a master's degree and ready for any final modifications that they explicitly required.

Clyde J. Northrup, Ph.D.	Chair, Supervisory Committee
Mark D. Schmitz, Ph.D.	Member, Supervisory Committee
Karen Viskupic, Ph.D.	Member, Supervisory Committee

The final reading approval of the thesis was granted by Clyde J. Northrup, Ph.D., Chair of the Supervisory Committee. The thesis was approved for the Graduate College by John R. Pelton, Ph.D., Dean of the Graduate College.

DEDICATION

To my Mom, Mommom, Dada, Alyssa, and Lindsay.

I love you more than you will ever know. Thank you for being everything to me.

ACKNOWLEDGEMENTS

Nothing is more difficult for me than trying to express my gratitude in words when everything but giving these people the world seems inadequate. That being said, I will attempt to thank the many people that have gotten me to where I am now.

First I must thank my advisor, Dr. CJ Northrup, for his support and giving me this opportunity. My summers would not have been the same without Dr. Claude Spinosa, who became my Sardinian husband, an adopted grandfather and a cherished friend all in one. Another Sardinian connection that forever changed me is Summer Brown, who almost single handedly got me into graduate school; there could never be a better field partner.

My thanks would be incomplete without acknowledging the influence three very special professors had on my undergraduate career at North Carolina: Dr. Drew Coleman, Dr. Allen Glazner, and Dr. Kevin Stewart. No matter how far away I am, I will forever be grateful for the encouragement you all gave me. Go Heels!

My graduate experience would not have been the same without the faculty and other graduate students at Boise State University. Dr. Walt Snyder, thank you for helping me in every way that you could. Thank you to Dr. Craig White, Dr. Dave Wilkins, Dr. Jen Pierce, Dr. Michelle Stoklosa, Charla Adams, Joni Hadden, Dr. Bill Clement, Debbie Pierce, Dr. Kasper van Wijk, Dr. Mila Adams, Joshua Wilkins, John Dye, Thomas Blum,

Gene Kurz, Jess Sousa, and Emily Hinz. You all helped me with projects, volunteering, talks, lab work, book club, and for being there for me when my family couldn't be. Thank you for making Boise a home away from home.

A special thanks to Liz Johansen, for always being there for me, and to Dr. Jim Crowley, for all the help in the lab, skiing, and biking. Thank you Nick Vetz for all the entertainment and Dylan Mikesell, a simple thank you that covers a lot. Three people that deserve more thanks than I can give them are Kyle Tumpane, AJ Zenkert, and Kati Carberry. Again words seem inadequate but thank you for all the memories. You are my Boise and the best things I'm taking away from here. I love you all and I'll see you some Thursday at the Dutch Goose or a Friday morning at Bogus.

Of course, I saved the impossible thanks for last. Dr. Karen Viskupic and Dr. Mark Schmitz can never know how important they are to me. Thank you for trusting me with Gus and allowing me to watch him grow up. He is very lucky to have you two as parents. Mark, I am honored to be able to call you a friend. My respect for you is higher than I thought possible and I thank you for all of your support, inspiration, and for entertaining me. Karen, I am at a loss for words. You made me a better person and gave me someone to look up too. You believe in me, you shared your family with me, and you took care of me from the day to day to the life changing things. Thank you for absolutely everything and I can't wait for Kiawah. I love you all to the moon and back twice.

Thank you also to my Chapel Hill family, Leigh-Ervin Stewart, and Jackie Henderson, who never stopped being there for me, even when I moved to Idaho. And to Mom, Mommom, Dada, Alyssa, and Lindsay, you all are my world.

ABSTRACT

To investigate the stratigraphy and structural evolution of the Variscan Orogen of the External Nappe Zone, Sardinia, Italy, field work and geochronologic analyses were combined to assess both regional and orogen scale issues. Geologic mapping, structural analysis, and sampling in the Flumendosa area coupled with high-precision U-Pb zircon geochronology were used to determine the duration of Ordovician magmatic activity and the structural evolution of the Variscan Orogen.

To constrain the duration of magmatism for the Flumendosa area, U-Pb ID/TIMS zircon analyses were performed on samples from a lower volcanic flow of the Ordovician Volcanic Unit and an upper, syn to post-magmatic porphyry. The analyses yielded ages of 457 and 452 Ma respectively. The start of magmatic activity at 457 Ma also marks the end of an unconformity found throughout the External Nappe Zone and provides evidence for correlation with the Sardic Unconformity of the Foreland Zone. Associations of the data with similar-aged Ordovician volcanic rocks and metagranitoids from the Mediterranean realm suggest either: (1) a Rheic wide magmatic event assuming the Posada-Asinara Line (PAL) represents the suture between Laurentia and Gondwana, or (2) the Southern Variscides collisional system of Europe occurred between Gondwana-derived terranes that composed the Hun Superterrane and Laurentia, correlating microterranes throughout the Mediterranean with the northern Gondwanan margin

Within the study area, field evidence exists for four phases of deformation related to the Variscan Orogeny. The initial deformational phase (D1) is evidenced by a south-directed thrust fault related to the amalgamation of the composite Variscan nappe stack, indicating a N-S directed contractional event. The second phase of deformation (D2) is defined by the folding of the D1 thrust by the Flumendosa antiform, indicating a NE-SW directed contractional event. The third phase (D3) is expressed by top-to-the-east-southeast movement of the upper thrust sheet evidenced by penetrative deformation, shear, and a domino style series of N-S striking, high-angle faults within the lower sheet. This phase is interpreted to represent a transition from contraction to extension involving orogen-parallel transport. The evidence for the top-to-the-east D3 allows for a reinterpretation of the nature of the contact between the Sarrabus Unit, the last nappe sheet emplaced, and the Gerrei Unit as a strike-slip fault on the side flank of the indenting nappe. The fourth deformational event (D4) produced brittle fractures within the shale that cross-cut the penetrative deformation. Slickensides indicate a transport direction of 014°, 13°, consistent with extensional reactivation of the N-dipping D1 thrust surface during late stages of orogenic evolution.

A post-D3 dike that contains the brittle fractures of D4 yielded a U-Pb ID/TIMS age of 302 Ma that constrains the transition between D3 and D4. A post-D4 granitoid of the Sardic Batholith yielded a U-Pb ID/TIMS age of 287 Ma that constrains the end of deformation for the Variscan Orogeny within the External Nappe Zone. These new age constraints are consistent with existing geochronologic data for the Variscan Orogen of Sardinia.

TABLE OF CONTENTS

LIST OF TABLES

LIST OF FIGURES

INTRODUCTION

Collisional orogens generally involve early contractional deformation followed by syn- to post-collisional extension (Malaveille, Guilhot, Costa, Lardeaux, and Gardien, 1990; Platt, 1993; LePichon, Henry, and Goffé, 1997; Milnes, Wennberg, Skår, and Koestler, 1997; Anderson, 1998; Leech, 2001). The geometric and kinematic interaction between these processes is a fundamental aspect governing the evolution of many collisional orogenic systems, including the Apennines (Carmignani and Kligfield, 1990; Scisciani, Tavarnelli, and Calamita, 2002), Betic Cordillera (Vissers, Platt, and van der Wal, 1995), Caledonides (Gee, Lobkowicz, and Singh, 1994; Northrup, 1996; Anderson, 1998), and Himalayas (Burchfiel et al., 1992). The structural features and patterns of 3-D movement that accommodate the transition between contraction and extension are, however, poorly understood for many orogens.

Several authors have documented contractional and extensional deformational features of Sardinian geology related to the Variscan Orogeny. The External Nappe Zone, located in the southeast section of the island, was determined to have undergone contraction and later extension related to the Variscan orogeny (Carmignani et al., 1994). Conti, Carmignani, and Funedda (2001) further interpreted three phases of deformation: early contraction, followed by orogen parallel transport, then extension.

This study consisted of two major goals to analyze the Gerrei Unit of the External Nappe Zone within the context of the regional tectonic evolution. The organizational structure of this thesis is based on these two major goals, with both local and regional

interpretations related to each. The first goal was to gain an understanding of the Early Paleozoic stratigraphy to determine the duration of magmatic activity that marked the end of an unconformity and to evaluate the potential correlation of this unit with other Ordovician volcanic rocks and the Sardic Unconformity of the Foreland Zone. The second goal was to determine the deformational history of the External Nappe Zone with particular focus on the Gerrei Unit. To address these goals, detailed field and geochronologic analyses were performed. The Flumendosa study area was chosen because the stratigraphy and internal structure of the Gerrei Unit are well exposed at this location. The approach to this thesis was to write each chapter as independent manuscripts. So, some repetition within the sections, particularly introductory material, was necessary.

The first chapter of the thesis is a summary of previous work to provide a framework for the results of this study. The summary includes overviews of the pre-Variscan history (Cambrian-Devonian), the Variscan Orogeny of western Europe (500-250 Ma), the Variscan Orogeny of Sardinia (360-280 Ma), post-Variscan rifting and subsequent rotation of Sardinia-Corsica (20.5-15 Ma), the Alpine Orogeny (40 Ma-present), and present day tectonics.

The second chapter discusses the stratigraphy and U-Pb ID/TIMS ages from the Ordovician volcanic package of the Gerrei Unit. Constraints on the ages of the stratigraphic units have been limited to fossil identification with sparse geochronologic data for the island (Carmignani et al., 1994). Whole grain zircons were analyzed for one of the lowermost sections within the unit and tips and whole grain zircons were analyzed

for a syn- to post-volcanic porphyry interpreted as a late stage intrusion. The results suggest the magmatic activity lasted from approximately 457-452 Ma. The base of the volcanic unit is marked by an unconformity. Therefore, the beginning of magmatism at 457 Ma also represents the end of the time gap recorded by the unconformity. This constraint provides support for the correlation of the unconformity within the Gerrei Unit with the Sardic Unconformity defined in the Foreland Zone.

Chapter 3 is a synthesis of structural and geochronologic analyses related to the deformational history of the Variscan Orogeny. Field evidence suggest a four-stage deformational history: two north-south oriented contractional events (D1 and D2), followed by a transitional phase of orogen-parallel extension (D4) and a final phase of north-south oriented extension (D4). The evidence for D3 is consistent with a new interpretation of the emplacement of the Sarrabus Unit via dextral strike-slip faulting along the contact between the Sarrabus and Gerrei Units rather than a thrust fault. If true, then the emplacement of the Sarrabus Unit occurred after the second contractional event, later than previously thought.

Works Cited

Anderson, T.B., 1998, Extensional tectonics in the Caledonides of southern Norway, an overview: Tectonophysics, v. 285, p. 333–351.

Burchfiel, B.C., Ziliang, C., Hodges, K. V., Yuping, L., Royden, L.H., Chanrong, D., and Jiene, X., 1992, The South Tibetan Detachment System, Himalayan Orogen: Extension contemporaneous with and parallel to shortening in a collisional mountain belt: Spec. Pap. Geol. Soc. America, v. 269.

Carmignani, L., Carosi, R., Di Pisa, A., Gattiglio, M., Musumeci, G., Oggiano, G., and Pertusati, P.C., 1994, The Hercynian chain in Sardinia (Italy): Geodinam. Acta., v. 7, p. 31-47.

Carmignani, L. and Kligfield, R., 1990, Crustal extension in the northern Appenines: the transition from compression to extension in the Alpi Apuane core complex: Tectonics, v. 9, p. 1275-1303.

Conti, P., Carmignani, L., and Funedda, A., 2001, Change of nappe transport direction during the Variscan collisional evolution of central-southern Sardinia (Italy): Tectonophysics, v. 332(1-2), p. 255-273.

Gee, D. G., Lobkowicz, M., and Singh, S., 1994, Late Caledonian extenision in the Scandinavian Caledonides-The Roragen Detachment revisited: Tectonophysics, v. 231, p. 139-155.

Leech, M., 2001, Arrested orogenic development: eclogitization, delamination, and tectonic collapse: Earth and Planetary Science Letters, v. 185(1-2), p. 149-159.

LePichon, X., Henry, P., and Goffé, B., 1997, Uplift of Tibet: from eclogites to granulites-implications for the Andean Plateau and the Variscan belt: Tectonophysics, v. 273**,** p. 57–76.

Malaveille, J., Guihot, E, Costa, S., Lardeaux, J.M. and Gardien, V., 1990, Collapse of the thickened Variscan crust in the French Massif Central: Mont Pilat extensional shear zone and St. Etienne Late Carboniferous basin: Tectonophysics, v. 177, p. 139-149.

Milnes, A.G., Wennberg, O.P., Skår, Ø., and Koestler, A.G., 1997, Contraction, extension and timing in the south Norwegian caledonides: the Songefjord transect: J.-P. Burg, M. Ford (Eds.), Orogeny Through Time: Geological Society Special Publication No. 121, p. 123–148.

Northrup, C. J., 1996, Structural expressions and tectonic implications of general noncoaxial flow in the midcrust of a collisional orogen: the Northern Scandinavian Caledonides: Tectonics, v. 15, p. 490-505.

Platt, J.P., 1993, Exhumation of high-pressure rocks: a review of concepts and processes: Terra Nova, v. 5, p. 119–133.

Scisciani V., Tavarnelli, E., and Calamita, F., 2002, The interaction of extensional and contractional deformations in orogenic belts: the example of the central Apennines, Italy: Journal of Structural Geology, v. 10, p. 1647–1658.

Vissers, R. L. M., Platt, M. J., and van der Wal, D., 1995, Late orogenic extenision of the Betic Cordillera and Alboran Domain: A lithospheric view: Tectonics, v. 14, p. 786-803.

A REVIEW OF PREVIOUS WORK: SARDINIA, ITALY

Introduction

The tectonic history of Sardinia involves a series of complex events. This presents a synthesis of previous work as an overview of the pre-Variscan history (Cambrian-Devonian), the Variscan Orogen (500-250 Ma), the Variscan Orogen focused on Sardinia (360-280 Ma), post-Variscan rifting and drifting of Sardinia-Corsica (20.5-15 Ma), the Alpine Orogen (40 Ma-present), and present-day tectonics. The purpose of this review is to present a framework for the stratigraphic and structural analyses. Key aspects for contextual support are the stratigraphic unit descriptions and previous structural interpretations for Sardinia, especially those focused on the External Nappe Zone of southeast Sardinia.

Pre-Variscan History (Cambrian-Devonian)

The lack of information concerning the pre-Variscan tectonics of Western Europe is due to the sparse geologic record of older events, significant Varicscan metamorphic overprinting, limited paleomagnetic data and effects of strike-slip faulting. There are two models that interpret the pre-Variscan paleogeography of the three distinct Sardinian crustal blocks: (1) the northeastern block of Sardinia is Laurentia-derived and the central and southern blocks are Gondwana-derived (Cappelli et al., 1992; Figure 1.1), and (2) the whole crustal block of Sardinia is of Gondwana origin (Stampfli and Borel, 2002; Figure

1.2). The first model proposes that prior to collision, the northeastern block was on the Laurentia margin and the central and southern blocks were on the Gondwana margin. The second model proposes the northeastern block of Sardinia was part of the Hun Superterrane that consisted of Gondwana-derived mircocontinents that rifted from the northern Gondwana margin approximately 420 Ma and sutured to Laurentia approximately 360 Ma (Stampfli and Borel, 2002; Figure 1.2). Therefore, in the second model, all of Sardinia was associated with Gondwana prior to rifting of the Hun Superterrane and the collision of the Hun Superterrane with Laurentia to the north and later Gondwana to the south.

The immediate pre-collisional history is generally divided into ocean formation, subduction, and obduction (Matte, 1991). Two major oceans are proposed to have been present at approximately 490-480 Ma: the Galicia-Massif Central Ocean in the north and the Rheic Ocean (proto-Tethys) to the south (Matte, 1991; Matte, 2001). The approximate size of the Galicia-Massif Central Ocean is estimated to be relatively small due to the similarities across fauna, sedimentary facies, paleomagnetic inclinations and metamorphic ages and subduction-related mafic protoliths of the Barrandian-Central and Galicia-Massif Central-Gföhl terranes. These terranes were sutured along the Massif Central Suture (Figure 1.3). Evidence for the small extent of the Rheic Ocean is from the lack of formation of a volcanic arc during subduction of the Rheic Ocean (Matte, 1991; Lefort and Max, 1992). High-grade rocks with the geochemical signature of island arcs in the Massif Central, a Variscan suture, and I-type granites in basement thrust sheets of the Alps are evidence that early Paleozoic subduction occurred within the region (Brown,

1983; Gardien, Lardeaux, and Misseri, 1988; Finger and Steyrer, 1990). According to Matte (1991), high-pressure metamorphic rocks in the Massif Central, Coimbra-Cordoba, and Münchberg-Tepla sutures are associated with obduction at approximately 430-420 Ma, concluding the last stage before collision of the supercontinents Laurentia and Gondwana.

The Variscan Orogen of Western Europe (~ 500-250 Ma)

The formation of Pangaea during the Paleozoic was a result of several collisional systems that made up a roughly continuous belt. Resulting from the convergence and collision of Laurentia-Baltica from the north and Gondwana from the south between 500 and 250 Ma, the belt as a whole was a 1,000 km broad and 8,000 km long system that extended from the Appalachian and Ouachita Mountains of North America to the Bohemian Massif in Czechoslovakia and Poland (Matte, 1991; Figure 1.4). The belt was subsequently segmented and dismembered during the Mesozoic rifting and opening of the Atlantic Ocean (Matte, 1986; Ziegler, 1989).

The Variscan Orogen of Western Europe was part of the later stages of Pangaea assembly that occurred during the Ordovician-Permian (Matte, 2001). Considered a classical obduction-collision orogen, the intraoceanic subduction and resulting closure of the Rheic Ocean and Galicia-Massif Central Ocean (proto-Tethys) lasted from roughly 480-290 Ma (Matte, 1991; Matte, 2001). The extent of the Western European Variscan Orogen is approximately 3,000 km long and 700-800 km wide, based upon the linking of stable massifs with basement outcrops and the pre-Mesozoic position of the Iberian and

Corsica-Sardinian blocks (Matte, 1991; Figure 3). To the north, the boundary of the Variscan orogenic belt is defined in southern Ireland by a succession of flat N-facing thrusts that compose the Stavelot-Venn Massif of the Variscan front (Teichmüller and Teichmüller, 1979; Meissner, Barthelsen, and Murawski, 1981; Raoult and Meilliez, 1986; Cazes and Torreilles, 1988; Le Gall, 1990; as referenced in Matte, 1991). The belt is obliquely cut and offset by the Elbe and Tornquist faults to the northeast (Figure 1.3). These large, dextral faults form the boundary of the Russian platform (Arthaud and Matte, 1977). The southern boundary of the Variscan orogenic belt is poorly constrained because the relative movements between Africa and Europe, deformation from the Alpine Orogen and recent oceanization have strongly altered the Variscan belt around the Mediterranean (Matte, 1991).

Metamorphism and crustal melting in Britain, the Massif Central, and Spain indicate that collision between the northernmost terranes and Laurentia began at approximately 380 Ma, with a minimum age constraint of 360-350 Ma from S-type granites and intra-continental basins in the Massif Central of France (Matte, 1991; Figure 1.3). The Variscan orogen is interpreted to have a bilateral symmetrical structure based on seismic data and surface geometry. Symmetrical subduction of opposing plates led to the deformation and metamorphism occurring progressively both to the north and south from approximately 380-300 Ma. Three indentors have been suggested for different regions of the orogen: the Ibero-Armorican arc (Brun and Burg, 1982; Matte, 1986); the Armorican block (Lefort and Max, 1992); and the Vindelician block (Vollbrecht, Weber, and Schmoll, 1989). Each of these caused symmetrical, opposing stike-slip movements

on either side of the leading edge of the indentor. Post-Variscan batholiths, such as the Sardic Batholith, yield a range of ages on a regional basis that provide the minimum age for Variscan deformation (Chapter 2; Figure 1.5).

The Variscan Orogen in Western Europe has been divided into sections based upon stratigraphy and varying structural history (Hutton and Sanderson, 1984; Franke, 1989, 1992; Neugebauer, 1989; Matte, Maluski, Rajlich, and Franke, 1990; Matte, 1991; Dallmeyer, Franke, and Weber, 1992; Figure 1.3). Therefore, the Variscan orogenic belt can be described based upon units (Matte, 1991) or terranes based on the rock units (Windley, 1995; Figure 1.3). For the purposes of this chapter, the more general tectonic framework will be described below.

The Northern Foreland

The Northern Foreland is the northernmost zone located between the Caledonian suture to the north and the Northern Variscan Front to the south (Matte, 1991; Figure 1.3). This zone consists of a Precambrian to Caledonian basement that was only mildly deformed during the Variscan, overlain by Devonian sandstones and an early Carboniferous carbonate shelf. The only structural expression of the Variscan Orogeny in the Northern Foreland is in folds within the carbonate shelf (Windley, 1995).

Cornwall-Rhenish Terrane

The Cornwall-Rhenish Terrane is bounded to the north by the Northern Variscan Front and to the south by the Lizard-Rhenish suture (Matte, 1991; Figure 1.3). The

Northern Variscan Front is marked by a north-verging, shallow-dipping thrust stack that emplaced Cambrian to Lower Carboniferous sediments structurally above mid-late Carboniferous foredeep molasse basins and the foreland (Flueh, Klaeschen, and Meissner, 1990; Le Gall, 1990, 1991). The terrane was formed from a continental margin sedimentary prism that reconstructions indicate experienced approximately 350 km of shortening (Behrmann et al., 1991). North-directed nappes and thrusts are characteristic of the French, German, and English sections of the terrane (Matte, 1991). The Irish segment developed as a northward-propagating surge zone (Murphy, 1990). There is also evidence that the south Portugese zone correlates with a segment of the Cornwall-Rhenish Terrane, and that the Ossa Morena suture is an extension of the Lizard-Rhenish suture. The Lizard-Rhenish suture contains underlying MORB-type basalts interpreted to be an accretionary prism (Anderson, 1975) and as a trench-slope-break complex (Franke and Engel, 1986). Along with seismic reflectors indicating ophiolite slices, the accretionary prism and trench-slope-break suggest the presence of a suture. The proposed location of the suture is in close proximity to rocks derived from the northern Rheic Ocean (Matte, 1991; Windley, 1995). One interpretation of this terrane proposes that southward subduction of the northern Rheic Ocean formed the arc, closed the ocean, and led to north-directed thrusting of the nappes upon collision of this terrane and the other terranes bounding the suture to the south (Floyd and Leveridge, 1987).

Channel-Saxothuringian Terrane

The Channel-Saxothuringian Terrane is the next terrane to the south, bounded by the Lizard-Rhenish suture to the north and the Münchberg-Tepla suture to the south (Matte, 1991). Offset by a dextral strike- slip fault, the two areas of outcrop are located in the Spessart anticlinal nappe stack in Germany and in the Bohemian Massif (Matte et al., 1990). This terrane is composed of high-grade orthogneisses, S-type granites and granulites, and low-grade Lower Paleozoic sediments (Franke, 1989; Matte, 1991). Rocks of the Saxothuringian terrane may have originally formed in a closed Cambro-Ordovician rift basin (Franke, 1993). The Münchberg-Tepla suture potentially extends in Portugal as the Coimbra-Cordoba suture zone, thus associating the Ossa-Morena zone with the Channel-Saxothuringian Terrane (Matte, 1991).

North Brittany Terrane

The North Brittany Terrane is bounded to the north by the Münchberg-Tepla suture and to the south by the Central Armorican Zone. The Central Armorican Zone is a dextral shear zone formed by an indenter (Matte, 1991; Windley, 1995). This terrane is composed of the 2.5-2.0 Ga Precambrian North Brittany block, intruded by a granitic batholith at 650-550 Ma, with an unconformable Cambrian-Ordovician sedimentary cover thrusted northwards in the Bray nappe (Matte, 1991).

Barrandian-Central Brittany Terrane

The Barrandian-Central Brittany Terrane is bounded to the north by the Central Armorican Zone and to the south by the Massif Central suture. High-pressure metamorphism of eclogites and blueschists within the Massif Central suture is dated at 420-360 Ma (Ballèvre, Kienast, and Paquette, 1987). The Barrandian section of this terrane consists of Cambrian-Devonian sediments unconformably overlying Proterozoic sediments and basaltic volcanics (Matte, 1991). The Central Brittany section is characterized by Upper Precambrian meta-pelites, Cambrian-Devonian sediments and 450-600 Ma orthogneisses (Matte, 1991). This section was transported in the south-directed South Brittany nappes (Windley, 1995).

Galicia-Massif Central-Gföhl Terrane

As indicated by the name, the Galicia-Massif Central-Gföhl terrane is divided into three sections. The Galicia subterrane is a 3-4 km thick nappe composed of an ophiolitic complex and allochthon of high-pressure granulites, and eclogites (Peucat et al., 1990). The Massif Central section is a 1-5 km thick nappe composed of high-grade gneisses, mafic-ultramafic rocks, and anatectic gneisses (Downes, Bodinier, Dupuy, Leyreloup, and Dostal, 1989). The Gföhl section is a 2 km thick nappe composed of gneisses, amphibolites, metagabbros, eclogites, serpentinites, and granulites (Wendt, Kröner, Fiala, and Todt, 1994). Metamorphic ages from eclogites within the Galicia section are 420 Ma and associated with the closure of a back-arc basin whereas zircons from granulites

within the Gföhl section yield ages of 346-351 Ma (Peucat et al., 1990; Wendt et al., 1994).

Vendée-Cévennes-Drosendorf Terrane

The Vendée-Cévennes-Drosendorf Terrane displays the arcuate nature of the Variscan orogen in Western Europe. This terrane arcs from central Spain, France, through part of the Bohemian Massif and Sardinia (Matte, 1991). The section in Galicia is composed of Ordovician to Silurian-Devonian pelites and quartzites whereas the section in France consists of mica schists and quartzites. The third section located in the Bohemian Massif contains felsic gneisses and mica schists with lenses of marble, graphitic phyllite and mafic volcanic rocks (Matte et al., 1990).

Aquitaine-Montagne Noire-Moravian Terrane

This terrane outcrops in the southern Massif Central to the eastern Pyrenees and is the southernmost terrane in the Variscan Orogeny. The Montagne Noire nappe is composed of fossiliferous sediments of Lower Cambrian to Upper Visean age (Echtler, 1990).

Variscan Zones of Sardinia (360-280 Ma)

The Variscan exposures of Sardinia have been divided into three major zones based on the degree of metamorphism and tectonic structure: the Axial/Internal Zone, the Nappe Zone and the Foreland Zone (Conti, Carmignani, and Funedda, 2001; Figure 1.6).

The Posada-Asinara Line (PAL), a Variscan suture (Cappelli et al., 1992), lies within the Axial Zone and the Arburesi Fault separates the Nappe and Foreland zones.

The Axial/Internal Zone

The northernmost section of the island, the Axial/Internal zone, is composed of migmatites and migmatitic gneisses that experienced epidote-amphibolite facies metamorphism related to the Variscan Orogeny (Carmignani et al., 1994; Franschelli, Memmi, and Ricci, 1982; Figures 1.5 and 1.6). Units in the area are large roof pendants in the late-orogenic calcalkaline batholith and are assumed have Precambrian protoliths based on the Ordovician-age orthogneisses (458 ± 31 Ma) that intrude the complex (Di Simplicio et al., 1974). Present within the migmatites is evidence for a polymetamorphic history from mafic and ultramafic rocks that display an early granulitic stage overprinted by a retrograde amphibolite phase (Carmignani et al., 1994). The Axial/Internal Zone has been interpreted as a Lower Carboniferous south-directed crustal nappe that was emplaced above the units that lie south of the Posada-Asinara Line (Carmignani et al., 1992). Matte (1991) suggests that the Axial/Internal Zone correlates to the Galicia-Massif Central-Gföhl Terrane (Figure 1.3).

The Posada-Asinara Line (PAL): a Variscan Suture

Composed of amphibolite facies micaschists, paragneisses, and quartzites, the Posada-Asinara Line (Figure 1.5) is a narrow, mylonitic belt that trends N100-140E (Carmignani et al., 1994). This belt contains small bodies of amphibolitic rocks with

relics of granulite and eclogite facies, along with relict mylonitic textures (Ghezzo, Memmi, and Ricci, 1982; Cappelli et al., 1992; Carosi and Elter, 1989). The PAL was derived in part from metamorphosed basalts of tholeiitic affinity based on the major element composition of amphibolites (Carmignani et al., 1994). Analyses of rare earth elements and the relative abundances of high field strength elements further indicate an oceanic basaltic protolith (Carmignani et al., 1994). There are two models concerning the interpretation of the PAL as a collisional thrust zone. In the first, the PAL is interpreted as a suture between Laurussia (the Axial/Internal Zone) and Gondwana (the Nappe Zone) (Carmignani et al., 1992; Figure 1.1). The second model interprets the PAL as the suture between the Hun Superterrane consisting of Gondwana-derived-microcontinents and Gondwana (Stampfli and Borel, 2002; Figure 1.2). The significant difference for these models is the origin of the Axial/Internal Zone as Laurentian (model 1) or Gondwanan (model 2). Following collision, the PAL acted as a dextral wrench shear zone during late stages of the Variscan Orogeny which, under some reconstructions, is thought to be related to the tightening of the Ibero-Armorican arc by west-directed thrusting of the Cantabrian indentor (Elter, Musumeci, and Pertusati, 1990; Conti et al., 2001).

The Nappe Zone

The Nappe Zone lies in central Sardinia between the northern Axial/Internal Zone and the southern Foreland Zone (Figure 1.6). The nappe stack contains greenschist to non-metamorphosed units ranging from Cambrian to Early Carboniferous in age (Carmignani et al., 1994; Figure 1.5). The fold vergence and shear sense in mylonites

indicate the nappes were emplaced through top-to-the-SSW transport, with one exception of top-to-the-west (Carmignani and Pertusati, 1979; Carmignani, Cocozza, Ghezzo, Pertusati, and Ricci, 1982; Carosi, Musumeci, and Pertusati, 1991; Conti et al., 2001). Emplacement of the nappes occurred during the Early Carboniferous Variscan Orogeny (Conti et al., 2001; Carmignani et al., 1982; Carosi et al., 1991). The Nappe Zone is further divided into the "Internal Nappes," composed of the Nurra, Anglona, Goceano, Baronie, and Barbagia Units, and the "External Nappes," consisting of the Meana Sardo, Riu Gruppa, Gerrei, Sarrabus (including what used to be separated out as the Arburese Unit), and Grighani Units (Carmignani et al., 1994; Conti et al., 2001; Figure 1.5). According to Matte (1991), the Nappe Zone correlates to the Vendée-Cévennes-Drosendorf Terrane (Figure 1.4).

The Internal Nappes

The northern section of the Nappe Zone is considered the Internal Nappes, ranging from the PAL to where the Barbagia Unit comes in contact with the Meana Sardo Unit of the External Nappes. The sequence of rock units that compose these nappe units are similar the sequence for the External nappes: quartzites, phyllites, metasandstones, black shales and marbles (Pili and Saba, 1975). The difference between the Internal and External Nappe Zones is the lack of Ordovician metavolcanic rocks and Devonian limestones in the Internal Nappe sequence (Carmignani et al., 1994). The metamorphism in the Internal Nappes ranges from intermediate pressure amphibolite facies in the north, close to the PAL (Baronie, Anglona, and northern Nurra Units) to greenschist facies in the south: Barbagia, Goceano, and southern Nurra Units (Carmignani et al., 1994). Major

structural features within this area are the Barbagia synform and the Gennargentu antiform, both roughly E-W trending folds (Carmignani et al., 1992).

The External Nappes

The External Nappes extend from the Meana Sardo Unit on the north limb of the Flumendosa Antiform to the Arburesi Fault. The lithostratigraphic succession is similar in all the nappe units (bottom to top): Cambrian-Lower Ordovician metasandstones, phyllites and quartzites, Middle Ordovician metaconglomerates and metavolcanic rocks, Upper Ordovician meta-arkoses and metasiltstones, Silurian-Lower Devonian black shales, phyllites, and marbles, Mid-Upper Devonian marbles, and Lower Carboniferous synorogenic flysch that is rarely present (Conti et al., 2001). Emplacement of the Meana Sardo, Gerrei, and Riu Gruppa are interpreted to have top-to-the-south thrusting directions based on shear sense in mylonite zones, stretching lineations, and southward facing folds (Carmignani et al., 1982; Dessau, Duchi, Moretti, and Oggiano, 1982; Carosi and Pertusati, 1990; Carmignani et al., 1994; Conti et al., 2001;). However, kinematic investigations of the Villasalto thrust that bounds the Sarrabus Unit indicate top-to-the-west emplacement (Carmignani and Pertusati, 1979). A major structural feature within this area is the Flumendosa Antiform, a roughly WNW-ESE trending, upright fold (Carmignani et al., 1992). The Arburesi Thrust forms the leading edge of the External Nappes, and juxtaposes the allochthonous nappe stack with the para-autochthonous Foreland Zone (Carmignani et al., 1994).

The Foreland Zone

The Arburesi Fault juxtaposes the autochthonous rocks of the Foreland Zone with the allochthonous units of the Nappes in southwestern Sardinia. This section is composed of the Iglesiente-Sulcis unit that outcrops beneath the Sarrabus Unit (Conti et al., 2001). Major structural features within the unit are the E-W trending Iglesias syncline and the Gonnessa anticline, both interpreted to be pre-Mid Orodovician and associated with Caledonian deformation (most recently, Carmignani et al., 1982). Post-Ordovician rocks also exhibit E-W trending folds associated with Variscan deformation with no post-Variscan overprinting evident. Therefore, Variscan deformation in this area is considered to have tightened the already present Caledonian folds (Conti et al., 2001).

Change in Nappe Transport Direction

As mentioned above, there were two phases of shortening related to nappe emplacement that occurred during the Early Carboniferous (Figure 1.7). The earlier stage was expressed through N-S shortening and top-to-the-south nappe imbrication (Conti et al., 2001). This phase of shortening is related to the emplacement of all the nappes except the Sarrabus Unit. Evidence supporting this conclusion includes isoclinal kilometer scale S-facing folds in the Gerrei Unit, shear sense indicators in the Barbagia Unit and along the Meana thrust, NNE-SSW stretching lineations throughout central Sardinia, and E-W trending folds in the Iglesias Unit in the Foreland Zone (Minzoni, 1975; Carmignani et al., 1982, 1994; Dessau et al., 1982; Carosi and Pertusati, 1990; Gattiglio and Oggiano, 1990; Conti et al., 2001). The second phase of shortening is

characterized by E-W shortening associated with the top-to-the-west transport of the Sarrabus Unit (Carmignani and Pertusati, 1979; Barca and Maxia, 1982; Conti and Patta, 1998; Conti et al., 2001). These authors found west-directed shear sense indicators on the Villasalto thrust (fault bounding the Sarrabus Unit to the north), E-W stretching lineations within the Sarrabus Unit and the floor thrust of the Arburese Unit, W-facing folds in the Sarrabus Unit, and N-S striking folds in the Iglesias Unit of the Foreland. The Foreland Zone is, therefore, the only area that displays evidence of both phases of deformation.

It is difficult to explain the reasoning for the change in transport direction without a definitive reconstruction of the pre-Permian position of the Sardinia-Corsica block. Accepting the reconstruction of Vigliotti and Langenheim (1995), Conti et al. (2001) proposed a model to explain the change in transport direction and related tectonic events concerning the Iberian peninsula and southern France.

Assuming that reconstruction of the pre-rifting Sardinia-Corsica block restores the microplate near the Gulf of Lyon, Conti et al. (2001) correlated the two orthogonal nappe transport directions with Ibero-Armorican arc and the Cantabrian indentor, respectively. This reconstructed location allowed Conti et al. (2001) to correlate the early phase of N-S shortening, (top-to-the-south transport direction), to the collisional evolution of the Ibero-Armorican arc, characterized by an east-west trending subduction zone with northward underthrusting (Brun and Burg, 1982). The later phase of E-W shortening is associated with the westward movement of the Cantabrian indentor resulting in a tightening of the Ibero-Armorican arc (Conti et al., 2001). The Cantabrian indentor model is supported by

evidence of sinistral shear on Iberia, dextral shear on the Armorican peninsula and thrusting on the leading edge of the indentor (Matte and Ribeiro, 1975; Brun and Burg, 1982; Ribeiro, Dias, and Brandão, 1995; Dias and Ribeiro, 1995). Though this model provides tectonic interpretations that are reasonable, further discussion of the ambiguity of the pre-Permian position of the Sardinia-Corsica block is presented in later sections.

Alpine Orogeny (40 Ma-present)

The collision of the Adriatic plate with Europe began during the Miocene, approximately synchronous with rifting of Sardinia-Corsica from mainland Europe. Sardinia was positioned far enough to the southwest of the collision zone with the Adriatic plate that only distal effects of the Alpine event are found on the island (Figure 1.8). The Alpine event produced only local deformation in Sardinia, primarily in the form of NE-trending sinistral strike-slip faults (Chapter 2).

Rifting of Sardinia/Corsica Block (20.5-15 Ma)

The Sardinia-Corsica block remained attached to mainland Europe until rifting began in the Miocene and subsequent counter-clockwise rotation resulted in the present day location and orientation of the island (Figure 1.9). The rifting and rotation has been associated with the opening of the Liguro-Provençal back-arc oceanic basin. This association of the rifting and rotation with basin formation demonstrates its significance in the evolution of the Western Mediterranean (Gattacceca et al., 2007).

The post-rift, pre-drift positioning of the Sardinia-Corisca block is still constroversial, even with several geophysical studies of the nature of the crust below the Liguro-Provençal basin. These studies yielded conflicting results, attributed to the weak magnetic anomaly patterns of the basin (Galdeano and Rossignol, 1977; Gattacecca et al., 2007). However three models have become generally accepted as possible scenarios for the pre-rift position of the Sardinia-Corsica block (Figure 1.8). The first model was based upon a computer fit of 1,000 m isobaths (Westphal, Bardon, Bossert, and Hamzeh, 1973) then was later supported by a similar reconstruction produced from morphological analyses of the Liguro-Provençal basin margin (Réhault, 1981; Gueguen, 1995). The second model was constructed using seismic data to interpret the extent of the oceanic domain of the basin (Burrus, 1984). Model three was based upon paleomagnetic data from Miocene volcanics on Sardinia and magnetic anomalies within the basin (Edel, 1980). The three models are compared in Figure 1.8 (Gattacceca et al., 2007).

Along with the controversy over the pre-rift position of the Sardinia-Corsica microplate, the later drift and contemporaneous counterclockwise rotation with respect to stable Europe also remain indeterminate. Paleomagnetic (Todesco and Vigliotti, 1993; Speranza, 1997 for reviews) and geochronological (Beccaluva, Civetta, Macciota, and Ricci, 1985 for a review; Lecca et al., 1997) studies have demonstrated the uncertainty of constraints on both the timing of rotation and the angle of rotation (Gattacceca et al., 2007; De Jong, Manzoni, and Zijderveld, 1969). Paleomagnetic and K-Ar geochronologic data from Sardinian volcanics done by Montigny, Edle, and Thuizat (1981) were originally interpreted to indicate a 30° counterclockwise rotation between 21

and 19.5 Ma (ages recalculated by Deino, Gattacceca, Rizzo, and Montanari, 2001). However, a re-evaluation of the data taking into consideration the uncertainties in the paleomagnetic pole path concluded that the timing of completion of the rotation could not be estimated (Todesco and Vigliotti, 1993; Speranza, 1997). One of the major issues noted was the potential for bias due to oversampling of some of the volcanic units because of the lack of a precise stratigraphic framework during sampling (Gattacceca et al., 2007). Later work examined the paleomagnetism of well-dated sedimentary sequences (Speranza et al., 2002) and pyroclastic flows (Edel, Dubois, Marchant, Hernandez, and Cosca, 2001), and resulted in the proposal of ~23° rotation after 19 Ma and ~10° rotation after 18 Ma, respectively.

Recent work regarding the timing and magnitude of rotation utilized paleomagnetic and $^{40}Ar/^{39}Ar$ geochronologic data from Miocene calc-alkaline volcanic sequences from northeastern and central Sardinia and interpreted a marked increase in the amount and duration of rotation from previous works (Gattacceca et al., 2007). Gattacceca et al. (2007) proposed a 45° counterclockwise rotation with respect to stable Europe after 20.5 Ma with 30° of rotation between 20.5 and 18 Ma and the culmination of rotation by 15 Ma. The interval between 20.5 and 18 Ma corresponds to the period of maximum volcanic activity in Sardinia and a high rate of drift and oceanic spreading (up to 9 cm yr^{-1} for the southern part), related to slab roll-back of the Adriatic/Ionian slab (Gattacceca et al., 2007). These new conclusions are therefore compatible with Model A of Figure 1.8, the reconstruction based upon the morphological fits of the margins.

The cohesiveness of the Sardinia-Corsica microplate during rotation is also debated. Given the present day north-south nature of the microplate, there are estimates of a gradient in total rotation magnitude ranging from 30° in northwestern Corsica to 113° in central Sardinia (Speranza, 1997; Edel, 2000). Paleomagnetic data from dikes located between Sardinia and Corsica yield a 2° ± 8 counterclockwise rotation of Sardinia relative to Corsica at a 95% confidence interval, thereby indicating no significant rotation between the two islands (Vigliotti, Alvarez, and McWilliams, 1990). Also, geologic evidence indicates that no strike-slip movement has occurred between the islands since the Variscan Orogeny (Arthaud and Matte, 1977); therefore, Gattacceca et al. (2007) concluded that the north-south rotational gradient is present and that the block rotations that did occur, happened before the Liguro-Provençal oceanic basin opened. Thus, the Sardinia-Corsica block can be interpreted as a cohesive microplate.

Present Day Tectonics

Sardinia is currently surrounded by passive margins. Once rotation stopped roughly 15 Ma and rifting jumped from the Liguro basin to the eastern margin of Sardinia, the island has had no recent tectonic activity. The opening of the Tyrenean basin on the east between Sardinia and mainland Italy resulted in the end of rotation and the present day position and tectonic setting of Sardinia.

Figures

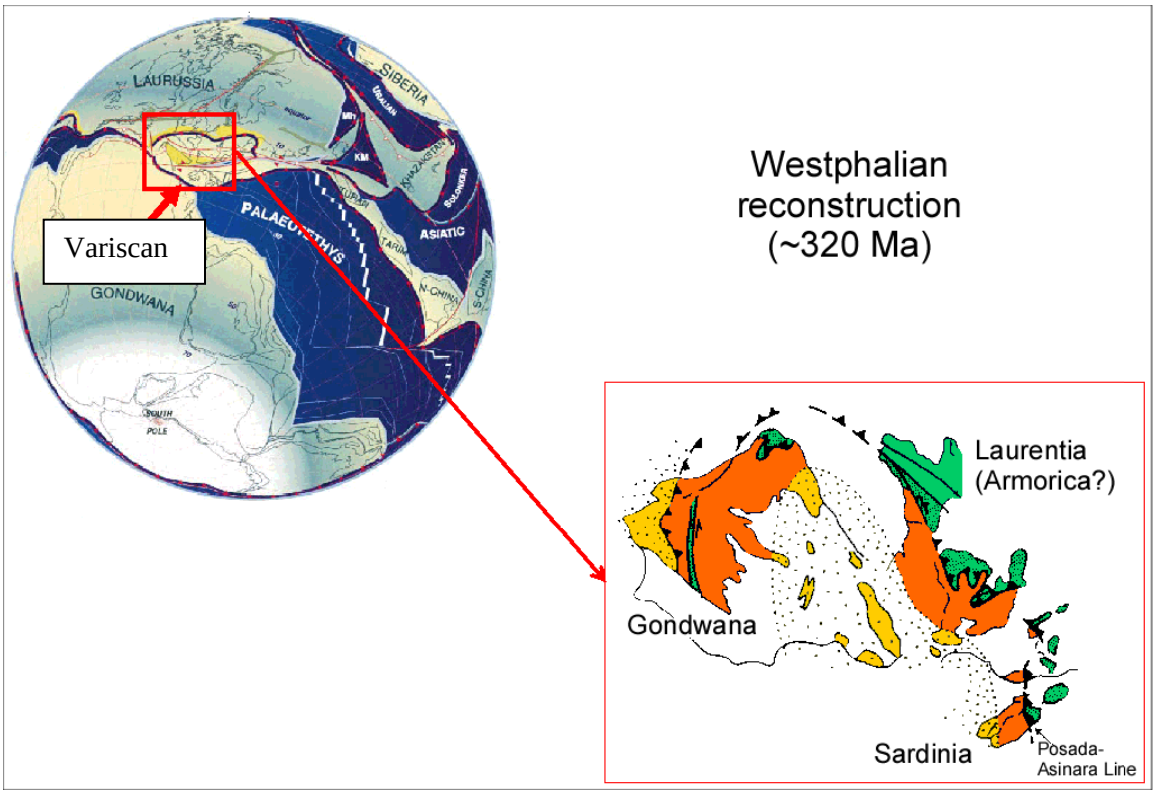

Figure 1.1: Paleogeographic reconstruction of Sardinia within the Variscan orogen based on Matte (1986) and Stampfli and Borel (2002).

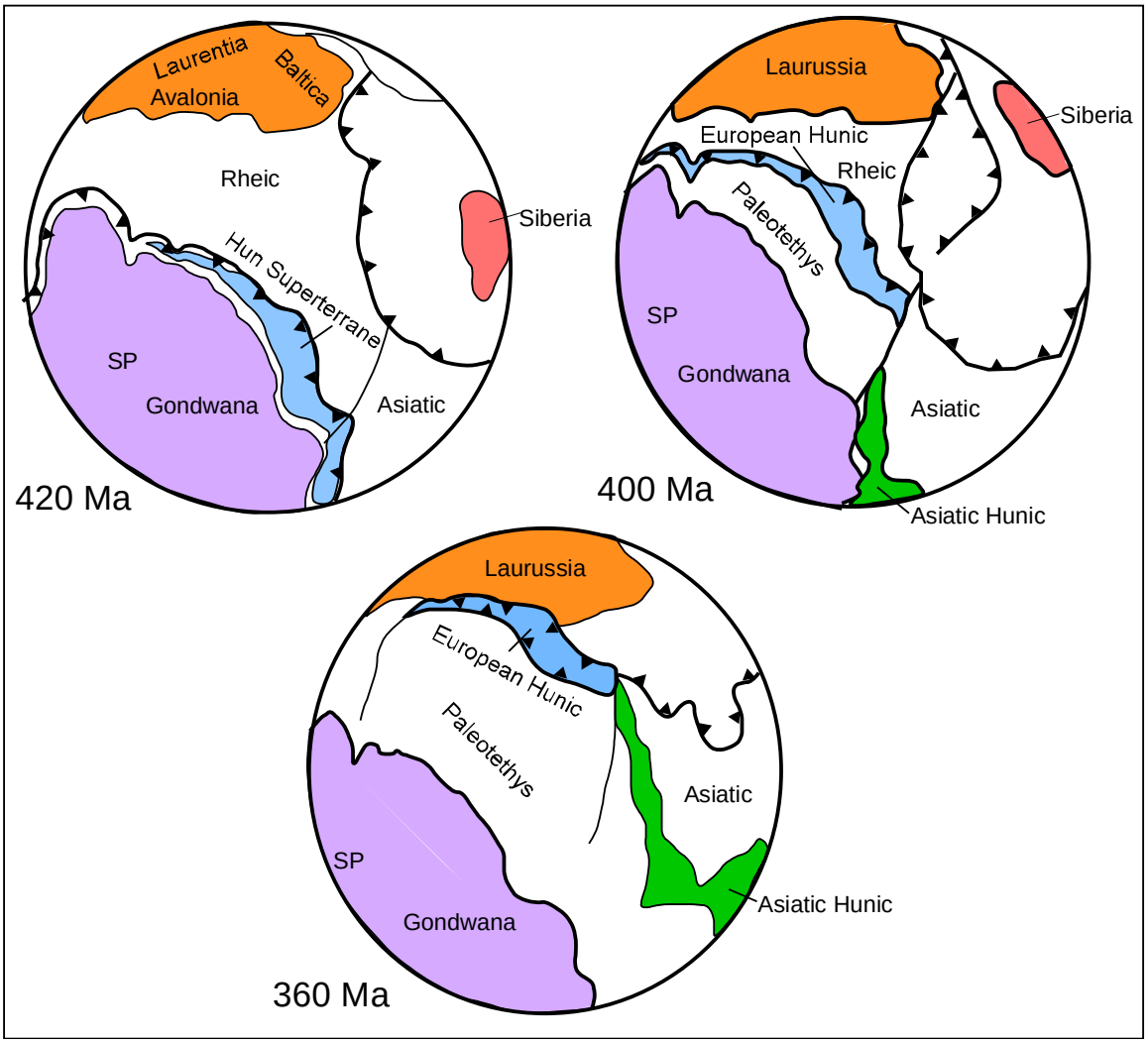

Figure 1.2: Simplified paleographic series of the evolution of the Hun Superterrane (modified from Stampfli and Borel, 2002).

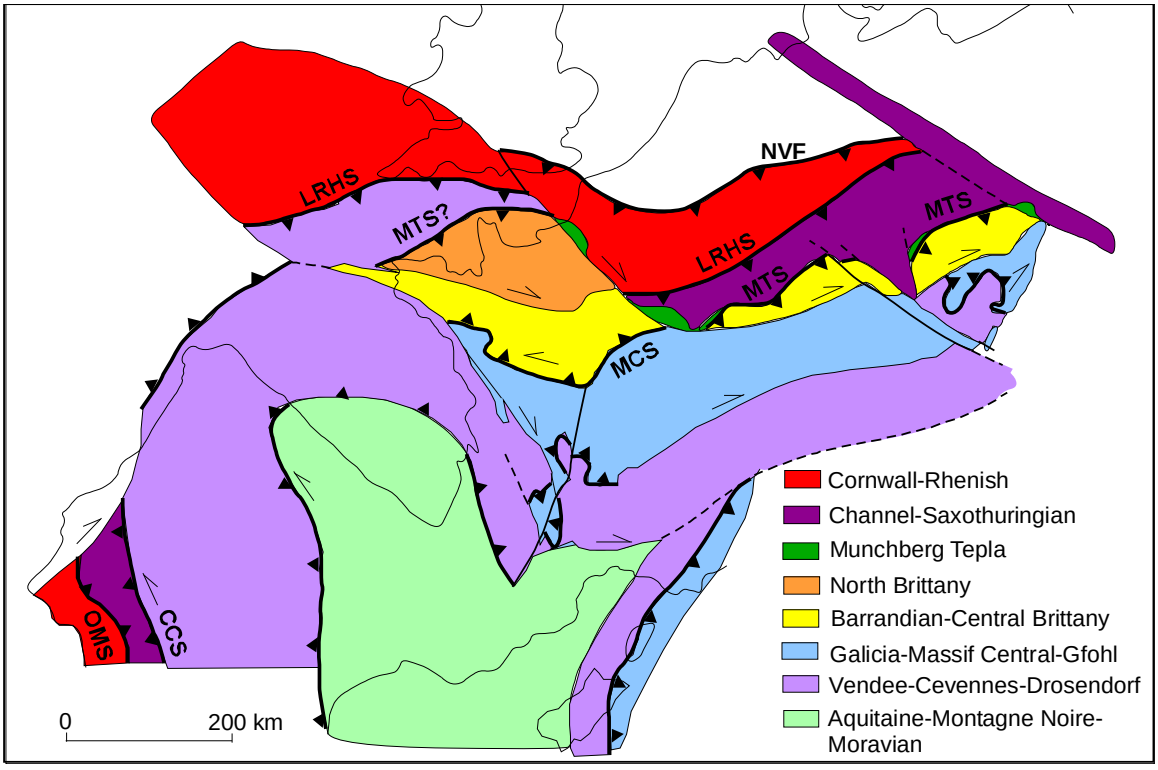

Figure 1.3: Permian reconstruction of Iberian and Sardinia-Corisca blocks relative to mainland Europe. NVF, Northern Variscan Front; LRHS, Lizard-Rhenish suture; MTS, Münchberg-Tepla suture; MCS, Massif Central suture; CCS, Coimbra-Cordoba suture; OMS, Ossa Morena suture (modified from Matte, 1991).

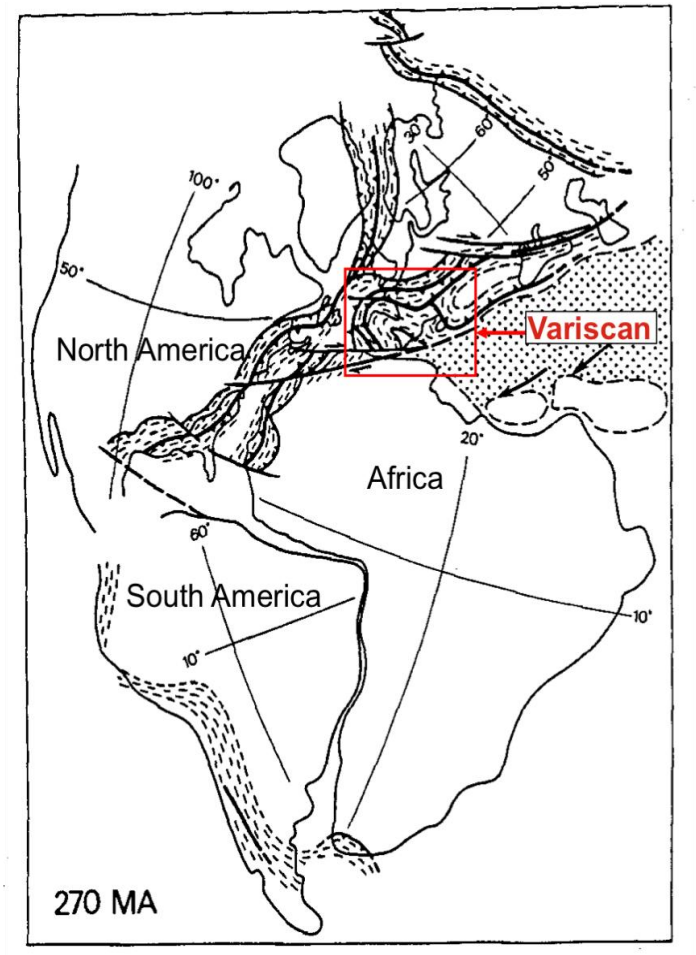

Figure 1.4: Intra-Paleozoic peri-Atlantic orogens with dashed lines representing orogenic zones to demonstrate the extent of this system as a whole (modified from Matte, 1991).

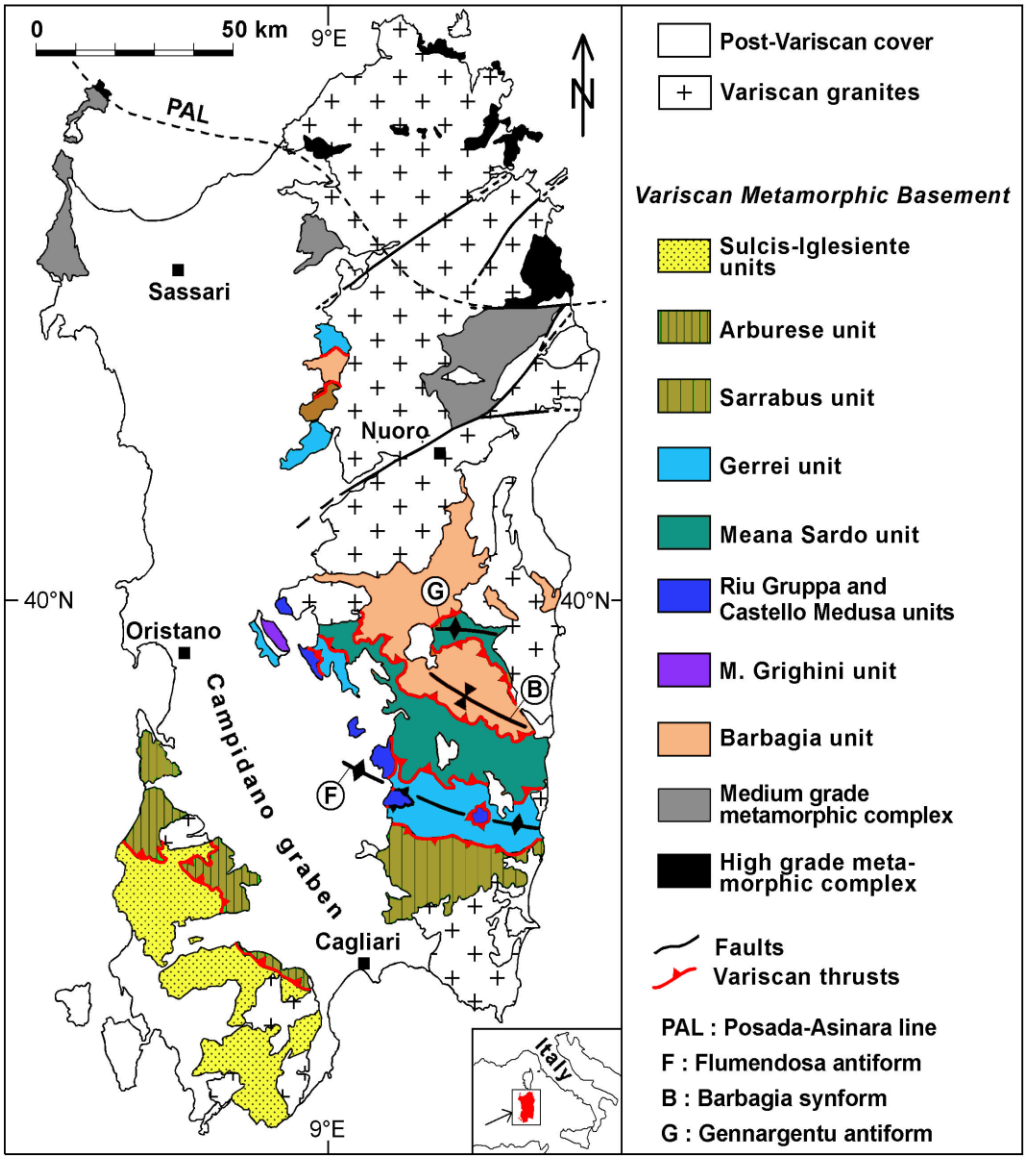

Figure 1.5: Distribution of Variscan exposure on Sardinia, Italy (Carmignani, Cocozza, Ghezzo, Pertusati, and Ricci, 1987).

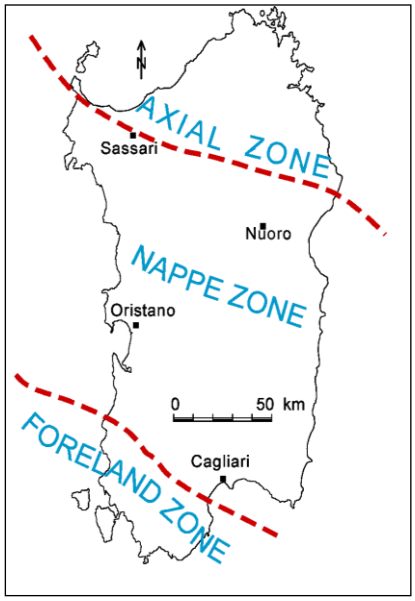

Figure 1.6: Tectono metamorphic zonation of Variscan metamorphism of Sardinia (Carmignani et al., 1987).

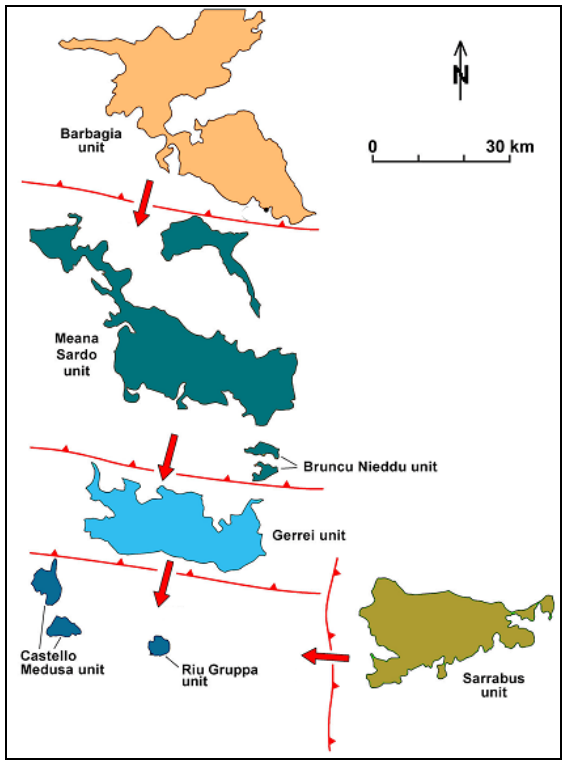

Figure 1.7: Pre-Carboniferous palinspastic reconstruction of the External Nappes of Sardinia. Colors indicate different nappes with labeling to the sides. Arrows indicate mean transport direction (Conti and Patta, 1998).

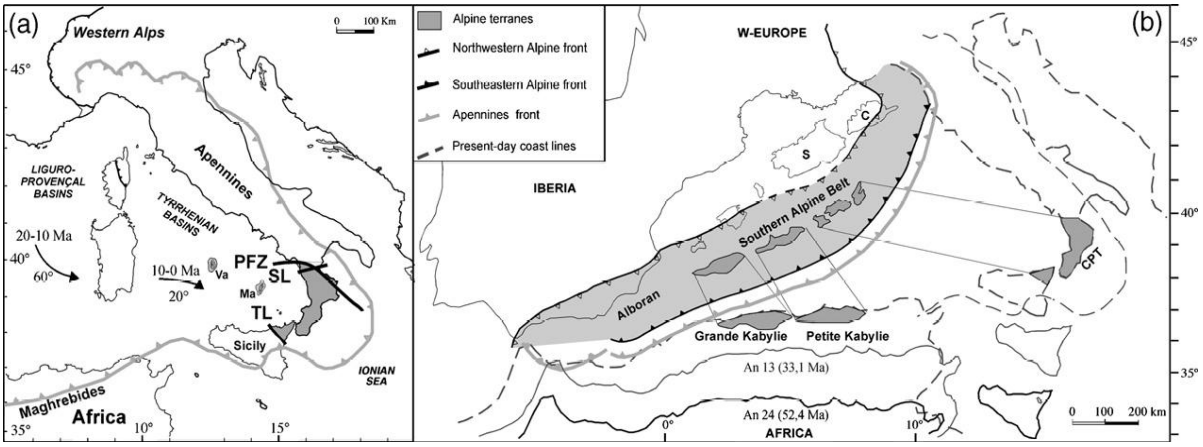

Figure 1.8: (a) Tectonic sketch of the Appenines modified after Guegen et al., 2001. (b) Pre-rift sketch of the Western Mediterranean with present day positions of the Calabria-Peloritani and Kabylie terranes modified from Alvarez, Cocozza, and Wezel (1974) and Gueguen, Doglioni, and Fernandez (1998); (Langone, Gueguen, Prosser, Caggianelli, and Rottura, 2006).

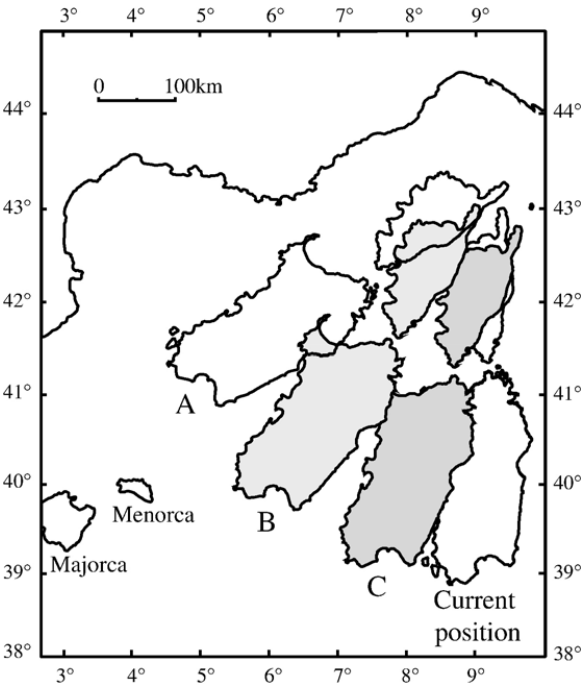

Figure 1.9: Reconstructed positions of the pre-rift/pre-drift location of Sardinia (~20.5 Ma) based on three models: (A) morphological fit of the continental margins of the Liguro-Provençal Basin (Gueguen, 1995); (B) seismic reflections (Burrus, 1984); (C) paleomagnetic data of Sardinia-Corsica (Edel, 1980). Compiled by Gattacceca et al. (2007).

Works Cited

Alvarez, W., Cocozza, T., and Wezel, F.C., 1974, Fragmentation of the Alpine orogenic belt by microplate dispersal: Nature, v. 248, p. 309-313.

Anderson, T.A., 1975, Carboniferous subduction complex in the Harz mountains, Germany: Geol. Soc. Am. Bull., v. 86, p. 77-82.

Arthaud, F. and Matte, P., 1977, Détermination de la position initiale de la Corse et de la Sardaigne à la fin de l'orogenèse hercynienne grâce aux marquers géologiques anté-mésozoïques: Bull. Soc. Gèol. Fr., v. XIX(4), p. 833-840.

Ballèvre, M., Kienast, J.R., and Paquette, J.L., 1987, Le métamorphism éclogitique dans la nappe hercynienne de Champtoceaux (Massif Armorican): C. R. Acad. Sci. Paris, Sér. II, v. 305, p. 127-131.

Barca, S. and Maxia, M., 1982, Assetto stratigrafico e tettonico del Paleozoico del Sarrabus occidentale: Carmignani, L., Cocozza, T., Ghezzo, C., Pertusati, P.C., Ricci, C.A. (Eds.), Guida alla Geologia del Paleozoico sardo. Società Geologica Italiana, Guide Geologiche Regionali, Cagliari, p. 87–93.

Beccaluva, L., Civetta, L., Macciota, G., and Ricci, C.A., 1985, Geochronology in Sardinia: results and problems: Rend. Soc. Ital. Mineral. Petrol., v. 40, p. 57-72.

Behrmann, J., Drozdzewski, G., Heinrichs, T., Huch, M., Meyer, W., and Onsken, O., 1991, Crustal-scale balanced cross-sections through the Variscan fold belt, Germany: the central EGT-segment: Tectonophysics, v. 196, p. 1-21.

Brown, M., 1983, The petrogenesis of some migmatites from the Presue'ile de rhuys, southern Brittany, France: M. P. Atherton and C. D. Gribble (Eds), Migmatites, Melting, and Metamorphism, p. 174-200.

Brun, J. and Burg, J.P., 1982, Combined thrusting and wrenching in the Ibero-Armorican arc: a corner effect during continental collision: Earth Planet. Sci. Lett., v. 61, p. 319-332.

Burrus, J., 1984, Contribution to a geodynamic synthesis of the Provençal basin (north-western Mediterranean): Mar. Geol., v. 55, p. 247-269.

Cappelli, B., Carmignani, L., Castorina, F., Di Pisa, A., Oggiano, G., and Petrini, R., 1992, A Hercynian suture zone in Sardinia: geological and geochemical evidence: Geodinam. Acta., v. 5, p. 101-118.

Carmignani, L., Barca, S., Cappelli, B., Di Pisa, A., Gattiglio, M., Oggiano, G., and Pertusati, P.C., 1992, A tentative model for the Hercynian Basement of Sardinia. In: "Contributions to the Geology of Italy": L. Carmignani and F.P. Sassi (eds)., IGCP N^{o} 276, Newsletter, v. 5, p. 61-82.

Carmignani, L., Carosi, R., Di Pisa, A., Gattliglio, M., Musumeci, G., Oggiano, G., and Pertusati, P.C., 1994, The hercynian chain in Sardinia (Italy): Geodinamica Acta (Paris), v. 7(1), p. 31-47.

Carmignani, L., Cocozza, T., Ghezzo, C., Pertusati, P.C., and Ricci, C.A., 1987, Structural Model of the Hercynian Basement of Sardinia. 1:500,000: Stabilimento L. Salomone, CNR, Progetto Finalizzanto Geodinamica, Roma.

Carmignani, L., Cocozza, T., Ghezzo, C., Pertusati, P.C., and Ricci, C.A., 1982, Lineamenti del basamento sardo: Guida alla Geologia del Paleozoico sardo. Guide Geologiche Regionali. Soc. Geol. It., p. 11-23.

Carmignani, L. and Pertusati, P.C., 1979, Analisi strutturale di un segmento della catena ercinica: il Gerrei (Sardegna SE). Boll. Soc. Geol. It. (1977), v. 96, p. 339-364.

Carosi, R. and Elter, F.M., 1989, Le microstrutture deformative di alto grado delle anfiboliti di Torpè (Sardegna NE): Atti Soc. Tosc. Sc. Nat. Mem., v. 96(A), p. 241-255.

Carosi, R., Musumeci, G., and Pertusati, P.C., 1991, Senso di transporto delle unità tettoniche eriniche della Sardegna dedotto dagli indicatori cinematici nei livelli cataclastico-milonitici: Rend. Soc. Geol. It. (1990), v. 13, p. 103-106.

Carosi, R. and Pertusati, P.C., 1990, Evoluzione strutturale dellle unità tettoniche erciniche nella Sardegna centro-meridionale: Boll. Soc. Geol. It., v. 109, p. 325-335.

Cazes, M. and Torreilles, G., 1988, Etude de la Croûte Terrestre par Sismique Profonde: Profil Nord de la France. Inst. Fr. Pet., INSU, SNEAP, Technip, Paris, 2 Vols.

Conti, P., Carmignani, L., and Funedda, A., 2001, Change of nappe transport direction during the Variscan collisional evolution of central-southern Sardinia (Italy): Tectonophysics, v. 332(1-2), p. 255-273.

Conti, P. and Patta, E., 1998, Large-scale Hercynian West-directed tectonics in southeastern Sardinia (Italy): Geodinamica Acta (Paris), v. 11(5), p. 217-231.

Dallmeyer, R.D., Fanke, W., and Weber, K. (Ed), 1992, Tectonostratigraphic Evolution of the Central and Eastern European Paleozoic Orogens: Berlin: Springer-Verlag.

De Jong, K.A., Manzoni, M., and Zijderveld, A., 1969, Paleomagnetism of the Alghero trachyandesites: Nature, v. 244, p. 67-69.

Deino, A., Gattacceca, J., Rizzo, R., and Montanari, A., 2001, $^{40}Ar/^{39}Ar$ dating and paleomagnetism of the Miocene volcanic succession of Monte Furru (western Sardinia): implications for rotation history of the Corsica-Sardinia microplate: Geophys. Res. Lett., v. 28, p. 3373-3376.

Dessau, G., Duchi, G., Moretti, A., and Oggiano, G., 1982, Geologia della zona del Valico di Correboi (Sardegna centro-orientale), Rilevamento, tettonica e giacimenti minerari: Boll. Soc. Geol. It., v. 101, p. 497-522.

Di Simplicio, P. Ferrara, G., Ghezzo, C., Guasparri, G., Pellizzer, R., Ricci, C.A., Rita, F., and Sabatini, G., 1974, Il metamorfismo e il magmatismo paleozoico della Sardegna: Rend. Soc. It. Min. Petr., v. 30 p. 979-1068.

Dias, R. and Ribeiro, A., 1995, The Ibero-Armorican Arc: a collision effect against an irregular continent?: Tectonophysics, v. 246, p. 113-128.

Downes, H., Bodinier, J.L., Dupuy, C., Leyreloup, A., and Dostal, J., 1989, Isotope and trace-element heterogeneities in high-grade basic metamorphic rocks of Marvejols: tectonic implications for the Hercynian suture of the French Massif Central: Lithos, v. 24, p. 37-54.

Echtler, H., 1990, Geometry and kinematics of recumbent folding and low-angle detachment in the Pardailhan nappe (Montagne Noire, southern French Massif Central): Tectonophysics, v. 177, p. 109-123.

Edel, H.B., 2000, Hypothèse d'une ample rotation horaire tardi-varisque du bloc Maures-Estérel-Corse-Sardaigne: Géol. Fr., v. 1, p. 3-19.

Edel, J.B., 1980, Etude paléomagnétique en Sardaigne. Conséquences pour la géodynamique de la Méditerannée occidentale [Ph.D. Thesis]: Institut de Physique du Globe, Université Louis Pasteur, Strasbourg (France).

Edel, J.B., Dubois, D., Marchant, R., Hernandez, J., and Cosca, M., 2001, La rotation miocène inférieur du bloc corso-sarde. Nouvelles contraintes palémagnétiques sur la fin du movement: Bull. Soc. Géol. Fr., v. 172, p. 275-283.

Elter, F.M., Musumeci, G., and Pertusati, P.C., 1990, Late Hercynian shear zones in Sardinia: Tectonophysics, v. 176, p. 387-404.

Finger, F. and Steyrer, H.P., 1990, I-type granitoids as indicators of a late Paleozoic convergent ocean-continent margin along the southern flank of the central European Variscan orogen: Geology, v. 18, p. 1207-1210.

Floyd, P.A. and Leveridge, B.E., 1987, Tectonic environment of the Devonian Gramscatho basin, south Cornwall: framework mode and geochemical evidence from turbiditic sandstones: J. Geol. Soc. Lond., v. 144, p. 531-542.

Flueh, E.R., Klaeschen, D., and Meissner, R., 1990, Wide-angle Vibroseis data from the western Rhenish Massif: Tectonophysics, v. 173, p. 83-93.

Franke, W., 1993, The Saxonian granulites: a metamorphic core complex?: Geol. Rundsch., v. 82, p. 505-515.

Franke, W., 1992, Phanerozoic structures an events in central Europe. In: Blundell, D., Freemann, R. and Mueller, S., Editors, 1992. A Continent Revealed-The European Geotraverse: Cambridge University Press, Cambridge, p. 164–179.

Franke, W., 1989, Tectonostratigraphic units in the Variscan belt of central Europe: Geol. Soc. Am. Spec. Pap., v. 230, p. 67–90.

Franke, W. and Engel, W., 1986, Synorogenic sedimentation in the Variscan belt of Europe: Bull. Soc. Géol. France, v. 1, p. 25-33.

Franschelli, M., Memmi, I., and Ricci, C.A., 1982, Zoneografia metamorfica dekka Sardegna settentrionale: Guida alla Geologia del Paleozoico sardo. Guide Geologiche. Soc. Geol. It., p. 137-149.

Galdeano, A. and Rossignol, J.C., 1977, Assemblage à altitude constante des cartes d'anomalies magnétiques couvrant l'ensemble du basin occidental de la Méditerranée: Bul. Soc. Géol. France, v. 19, p. 461-468.

Gardien, V., Lardeaux, J.M., and Misseri, M., 1988, Les péridotites des Monts du Lyonnais (MCF): témoins privilégiés d'une subduction de lithosphère palèozoïque: J. Geol. Soc. Lond., v. 307, p. 1961-1972.

Gattacceca, J., Deino, A., Rizzo, R., Jones, D.S., Henry, B., Beaudoin, B., and Vadeboin, F., 2007, Miocene rotation of Sardinia: New paleomagnetic and geochrological constraints and geodynamic implications: Earth and Planetary Science Letters, v. 258, p. 359-377.

Gattiglio, M. and Oggiano, G., 1990, L'unità tettonica di Bruncu Nieddu e i suoi rapporti con le unità della Sardegna sud-orientale: Boll. Soc. Geol. Ital., v. 109, p. 547-555.

Ghezzo, C., Memmi, I., and Ricci, C.A., 1982, Le granuliti e le eclogiti della Sardegna nord-orientale. In: Guida alla Geologia del Paleozoico sardo: Guide Geologiche Regionali. Soc. Geol. It., p. 151-156.

Gueguen, E., 1995, Le bassin Liguro-Provençal: un véritable océan [Ph.D. Thesis]: Université de Bretagne Occidentale, Brest (France).

Gueguen, E., Doglioni, C., and Fernandez, M., 1998, On the post-25 Ma geodynamic evolution of the western Mediterranean: Tectonophysics, v. 298, p. 259-269.

Hutton, D.H.W. and Sanderson, D.J. (Eds), 1984, Variscan Tectonics of the North Atlantic Region. Bath: Gol. Soc. Lond. Spec. Publ.

Langone, A., Gueguen, E., Prosser, G., Caggianelli, A., and Rottura, A., 2006, The Curinga – Girifalco fault zone (northern Serre, Calabria) and its significance within the Alpine tectonic evolution of the western Mediterranean: Journal of Geodynamics, v. 42, p. 140-158.

Le Gall, B., 1991, Crustal evolutionary model for the Variscides of Ireland and Wales from SWAT seismic data: J. Geol. Soc. Lond., v. 148, p. 759-774.

Le Gall, B., 1990, Evidence of an imbricate crustal thrust belt: the south British Variscides. Contribution of SWAT deep seismic reflection profiles recorded through the English Channel and the Celtic sea: Tectonics, v. 9(2), p. 283-302.

Lecca, L. Lonis, R., Luxoro, S., Melis, E., Secchi, F., and Brotzu, P. (1997) Oligo-Miocene volcanic sequences and rifting stages in Sardinia: a review: Per. Mineral. v. 66, p. 7-61.

Lefort, J.P. and Max, M.D., 1992, Structure of the Variscan belt beneath the British and Armorican overstep sequences: Geology, v. 20, p. 979-982.

Matte, P., 2001, The Variscan collage and orogeny (480-290 Ma) and the tectonic definition of the Armorica microplate: a review: Terra Nova, v. 13(2), p. 122-128.

Matte, P., 1991, Accretionary history and crustal evolution of the Variscan belt in Western Europe: Tectonophysics, v. 196, p. 309-337.

Matte, P., 1986, Tectonics and plate tectonic model for the Variscan belt of Europe: Tectonophysics, v. 126, p. 329-374.

Matte, P., Maluski, H., Rajlich, P., and Franke, W., 1990, Terrane boundaries in the Bohemian Massif: Result of large-scale Variscan shearing: Techtonophysics, v. 177, p. 151-170.

Matte, P. and Ribeiro, A., 1975, Forme et orientation de l'ellissoide de déformation dans la virgation de Galice. Relation avec le plissement et hypothèses sur la genèse de l'arc Ibéro-armoricain: C.R. Acad. Sci. Paris, v. 280, p. 2825-2828.

Meissner, R., Barthelsen, H. and Murawski, H., 1981, Thin skinned tectonics in the northern Rhenish Massif, Germany: Nature, v. 290, p. 399-401.

Minzoni, N., 1975, La serie delle formazioni paleozoiche a Sud del Gennargentu: Boll. Soc. Geol. Ital., v. 94, p. 347-365.

Montigny, R., Edle, J.B., and Thuizat, R., 1981, Oligo-Miocene rotation of Sardinia: K/Ar ages and paleomagnetic data of Tertiary volcanics: Earth Planet. Sci. Lett., v. 54, p. 262-271.

Murphy, F.C., 1990, The Irish Variscides: a fold belt developed within a major surge zone: J. Geol. Soc. Lond., v. 147, p. 451-460.

Neugebauer, J., 1989, The Iapetus model: a plate tectonic concept for the Variscan belt of Europe: Tectonophysics, v. 169, p. 229-256.

Peucat, J.J., Bernard-Griffiths, J., Gil Ibarguchi, J.I., Dallmeyer, R.D., Menot, R.P., Cornichet, J., and Iglesias Ponce De Leon, M., 1990, Geochemical and geochronological cross-section of the deep Variscan crust: the Cabo Ortegal high-pressure nappe (NW Spain): Tectonophysics, v. 177, p. 263-292.

Pili, P. and Saba, O., 1975, Presenza di Devoniano a conodonti nelle rocce carbonatiche di Correboi (Sardegna centro-orientale), Boll. Soc. Sarda Sci. Nat. Cagliari, v. 15, p. 3-8.

Raoult, J.F. and Meilliez, F., 1986, Commentaires sur une coupe structurale de l'Ardennes selon le meridian de Dinant: Ann. Soc. Geol. Nord., p. 97-109.

Réhault, J.P., 1981, Evolution tectonique et sédimentaire du bassin ligure (Méditerranée occidentale) [Ph.D. Thesis]: Univ. Paris VI (France).

Ribeiro, A., Dias, R., and Brandão Silva, J., 1995, Genesis of the Ibero-Armorican arc: Geodinam. Acta, v. 8, p. 173-184.

Stampfli, G. and Borel, G., 2002, Paleozoic evolution of pre-Variscan terranes: From Gondwana to the Variscan collision: Geological Society of America Special Paper, v. 364, p. 263-280.

Speranza, F., 1997, Paleomagnetism and the Corsica-Sardinia rotation: a short review: Boll. Soc. Geol. Ital., v. 118, p. 537-543.

Speranza, F., Villa, I.M., Sagnotti, L., Florindo, F., Cosentino, D., Cipollari, P., and Mattei, M., 2002, Age of the Corsica-Sardinia rotation and Liguro-Provençal spreading: new paleomagnetic and Ar/Ar evidence: Tectonophysics, v. 347, p. 231-251.

Stampfli, G. and Borel, G., 2002, A plate tectonic model for the Paleozoic and Mesozoic constrained by dynamic plate boundaries and restored synthetic oceanic isochrones: Earth and Planetary Science Letters, v. 196, p. 17-33.

Teichmüller, M. and Teichmüller, R., 1979, Ein Inkohlungsprofil entlang der linksrheinischen Geotaverse von Schleiden nach Aachen und die Inkohlung in der Nord-Süd Zone der Eifel: Fortschr. Geol. Rheinl. Westfalen, v. 27, p. 323-355.

Todesco, M. and Vigliotti, L., 1993, When did Sardinia rotate? Statistical evaluation of paleomagnetic data: Ann. Geofis., v. 36, p. 119-134.

Vigliotti, L., Alvarez, W., and McWilliams, M., 1990, No relative rotation detected between Corsica and Sardinia: Earth Planet. Sci. Lett., v. 98, p. 313-318.

Vigliotti, L. and Langenheim, V.E., 1995, When did Sardinia stop rotating? New paleomagnetic results: Terra Nova, v. 7, p. 424-435.

Vollbrecht, A., Weber, K., and Schmoll, J., 1989 Structural model for the Saxothuringian-Moldanubian suture in the Variscan basement of the Oberpfalz (northeastern Bavaria, F.R.G) interpreted from geophysical data: Tectonophysics, v. 157, p. 123-133.

Wendt, J.I., Kröner, A., Fiala, J., and Todt, W., 1994, U-Pb zircon and Sm-Nd dating of Moldanubian HP/LT granulites from South Bohemia, Czech Republic: J. Geol. Soc. Lond., v. 151, p. 83-90.

Westphal, M., Bardon, C., Bossert, A., and Hamzeh, R., 1973, A computer fit for Corsica and Sardinia against Southern France: Earth Planet. Sci. Lett., v. 18, p. 137–140.

Windley, B., 1995, The Evolving Continents, 3rd Edition: John Wiley & Sons Ltd, England.

Ziegler, P., 1989, Evolution of Laurussia: Kluwer, Dordrecht.

NEW U-PB ANALYSES FOR ORDOVICIAN VOLCANIC ROCKS IN THE GERREI UNIT, SARDINIA, ITALY: IMPLICATIONS FOR THE SARDIC UNCONFORMITY AND A TETHYAN WIDE ORDOVICIAN VOLCANIC EVENT

Abstract

The volcanic package of the Gerrei Nappe Unit in southeastern Sardinia, Italy, has been broadly interpreted as Middle Ordovician in age and sits directly above an unconformity within the nappes that may correlate with the Sardic Unconformity of the Foreland. New ID-TIMS U-Pb zircon geochronology of volcanic rocks in the vicinity of the Flumendosa Antiform places constraints on the timing and duration of Ordovician magmatism, as well as the hiatus represented by the basal unconformity. Zircon ages from one of the lowermost volcanic layers and a late crosscutting porphyry constrain the timing of magmatism to between 457-452 Ma. Implications include: (1) a relatively late initiation of magmatism, (2) a short duration of magmatic activity, and (3) a longer hiatus for the basal unconformity (10 Ma) than previously interpreted. Rather than Middle Ordovician, new data place the initiation of magmatism in the Late Ordovician. This constraint provides stronger evidence for correlation between the unconformity at the base of the nappes with the Sardic Unconformity defined in the Foreland Zone. Correlating the volcanic package of the Gerrei Unit with other contemporaneous volcanic units in northeast Sardinia, suggests either: (1) a Tethyan wide Ordovician volcanic event, based upon the contrasting Ordovician paleogeographic locations of the volcanic

units-the northeast portion of Sardinia associated with Laurentia and the External Nappe Zone of Gondwanan origin (Matte, 2001); or (2) support for the Southern Variscan collisional system of Europe occurring between Gondwana-derived terranes and Laurentia, associating the whole of the island of Sardinia with Gondwana (Stampfli, von Raumer, and Borel, 2002).

Introduction

The stratigraphy of the nappes that comprise the External Nappe Zone of southeastern Sardinia was investigated in order to constrain the pre-Variscan deposition of these volcanosedimentary units. Little previous geochronological work has been done to provide concrete ages of deposition of these stratigraphic units, including the broadly interpreted Ordovician volcanic rocks within the Gerrei Unit, one of the five nappes that compose the External Nappe Zone. The volcanic sequence is well exposed within the Gerrei Unit and is correlated with volcanic rocks in the other nappes in the region. The age of the volcanic unit is only broadly constrained by the stratigraphic units below and above that are dated as Cambrian and Silurian, respectively, based on fossil assemblages. This paper presents new U-Pb zircon data from the lower and upper sections of the Ordovician volcanic unit that constrain the duration of magmatic activity for the Gerrei Unit. Correlation and comparison with volcanic rocks of similar age in the External Nappe Zone and other regional Ordovician volcanic rocks provides insight into the scale of magmatic activity during the Ordovician.

In addition, these new data help to constrain the timing of the unconformity at the contact between the underlying Cambrian San Vito Sandstone and the overlying Ordovician volcanic rocks. This unconformity can be correlated throughout the External Nappe Zone, and potentially relates to the Sardic Unconformity that is defined within the Foreland Zone. More precise timing of the volcanic sequence within the Gerrei Unit can be used to evaluate this possible correlation.

Regional Setting

Pre-Variscan

Deposition of rock units now contained within the Sardinian Nappes has been interpreted within the framework of four major tectonic settings: a Cambrian passive margin, an Ordovician "Andean Type Margin," the collapse of the volcanic arc, and a Silurian-Devonian passive margin (Carmignani et al., 1994). A Precambrian to Lower Ordovician passive margin is thought to have bounded the southern border of the oceanic domain that existed between northern and central-southern Sardinia (Cappelli et al., 1992). The tectonosedimentary record of central and southern Sardinia is consistent with this interpretation. These metasedimentary sequences are unconformably overlain by metavolcanic rocks in central-southern Sardinia and by the Sardic Unconformity and overlying continental clastic rocks in the Foreland Zone (Carmignani et al., 1994). The Sardic Unconformity has been associated with uplift and subsidence possibly driven by continental volcanic arc activity (Garbarino, Maccioni, Padalino, Tocco, and Violo,

1981) or an orogenic event (Memmi et al., 1983). More recent work, however, supports the continental volcanic arc hypothesis (Carmignani et al., 1994).

The Ordovician system of central-southeastern Sardinia may have formed in an "Andean-type" arc setting as evidenced by different components displayed from NE to SW Sardinia. The stratigraphy of the Internal Nappes contains few metavolcanic rocks of Ordovician age, and thus may represent the arc-trench gap (Carmignani et al., 1992). The basic and intermediate volcanic succession of the Meana Sardo Unit is associated with the inner arc, and the outer arc is represented by acidic volcanics of the Gerrei Unit. The lack of Ordovician volcanic components in the Sulcis-Iglesiente Unit signifies the back-arc area of this system (Carmignani et al., 1994).

The subsequent "collapse" of the volcanic arc may have been related to subduction-termination through ridge-trench collision (Carmignani et al., 1994). One feature interpreted as evidence of this collision is the uniformly deposited Early-Middle Silurian Black Shales Unit that is characteristic of the northern margin of Gondwana. The shales are associated with the end of rifting, and genesis of a transtensive setting in which the arc collapsed (Vai, 1982).

The Silurian and Devonian depositional units of Northern Gondwana are characteristic of a passive margin environment hosting Silurian black shales and Early-Middle Devonian shales and limestones (Carmignani et al., 1994). Pull-apart basins were created in the Late Devonian-Early Carboniferous (Vai and Cocozza, 1986; Vai, 1991) that, combined with intra-plate basaltic magmatism, have been associated with the early

stages of collision between Gondwana and Armorica (Di Pisa, Gattaglio, and Oggiano, 1992).

The Variscan Orogeny

The Variscan belt of Western Europe was one of several collisional systems that were involved in the formation of Pangaea during the Paleozoic. As part of the 1,000 km broad and 8,000 km long system that extended from the Caucasus to the Appalachian and Ouachita Mountains, the Variscan Orogeny occurred in the Carboniferous during the later stages of Pangaea assemblage (Matte, 2001). Some paleogeographic reconstructions place Sardinia at the suture zone between Laurentia-Baltica and Gondwana, suggesting that the mylonite zone known as the Posada-Asianara Line may represent part of a complex, anastomosing suture zone between these two supercontinents (Matte, 1986; Stampfli and Borel, 2002; Figure 2.1). However, other models propose that the Variscan system of Europe occurred between the Hun Superterrane, consisting of terranes derived from Gondwana, and Laurentia, not between the supercontinents of Gondwana and Laurentia (Stampfli, von Raumer, and Borel, 2002; Figure 2.2). This second model interprets the PAL as a suture that occurred along the northern margin of Gondwana that either represents a suture within the Hun Superterrane or the suture between the Hun Superterrane and Gondwana. The significant difference between these models is the interpretation of the crustal rocks from the northeast corner of Sardinia as derived from Laurentia (Matte, 1986; Matte, 1991) or as derived from Gondwana as part of the Hun

Superterrane (Stampfli, von Raumer, and Borel, 2002; von Raumer, Stampfli, and Bussy, 2003).

The Variscan exposures of Sardinia have been divided into three major zones based on the degree of metamorphism and tectonic structure: the Axial/Internal Zone, the Nappe Zone and the Foreland Zone (Figure 2.3; Carmignani, Cocozza, Ghezzo, Pertusati, and Ricci, 1987). The Axial/Internal Zone is located in the northernmost section of the island, contains the Posada-Asinara Line, and comprises rocks metamorphosed to epidote-amphibolite facies. The Nappe Zone lies south of the Axial Zone and contains greenschist to non-metamorphosed units. The Arburesi thrust separates the Nappe and Foreland Zones, juxtaposing the autochthonous units of the Foreland Zone with the allochthonous units of the Nappe Zone.

The Nappe Zone of central Sardinia is composed of several nappes that were imbricated during the Variscan Orogeny (Carmignani et al., 1987). The Nappe Zone is further sub-divided into the northern Internal Nappes and the southern External Nappes. The External Nappe Zone consists of the Grighani Unit, the Rio Gruppa Unit, the Meano Sardo Unit, the Gerrei Unit, and the Sarrabus Unit, from north to south (Carmignani et al., 1994). The first four nappes were structurally emplaced by south-directed thrust faults and the fifth, structurally highest nappe had a west-directed transport direction. The cause of change in transport directions is not known (Conti and Patta, 1998). The study area is located within the Gerrei unit, the third nappe sheet in overall sequence of thrust emplacement (Figure 2.3, see Chapter 3 for detailed structural analysis).

Stratigraphy and Rock Unit Descriptions

Five rocks units comprise the Gerrei nappe, but only four of them are found within the study area: the Cambrian San Vito Sandstone, Ordovician Volcanic Unit, Gennemesa Formation, and the Silurian Shale (Figure 2.4). Devonian Limestone is present regionally in the Gerrei Unit, but not within the study area and will not be described (see Carmignani et al., 2001 for description).

Cambrian San Vito Sandstone

The San Vito Sandstone is composed of very fine to medium grained, tan to dark grey Cambrian sands. The age of this unit is based on regional fossils of acritarchs, jellyfish prints, ichnofossils, and trilobites, including one locality near the study area (Carmignani et al., 2001). It is moderately to well sorted and cross-bedding is present locally. The unit was metamorphosed under lower greenschist facies conditions. The San Vito can be distinguished in outcrop by its blocky appearance and darker color. Seen in all of the thrust sheets regionally, the San Vito Sandstone is the lowest stratigraphic unit. The depositional base of the unit is not visible.

Ordovician Volcanic Rocks

The Ordovician Volcanic unit is an undifferentiated package of volcanic and shallow intrusive rocks. The basal contact is sharp and unconformable with the Cambrian San Vito Sandstone. The lowermost layers are characterized by interbedded volcanic rocks and lenses of metaconglomerates with clasts composed of the underlying

San Vito Sandstone. The volcanic rocks contain variable amounts of quartz, potassium feldspar, and hornblende phenocrysts ranging in size from 0.5-3 mm, within a dull light tan to light grey fine-grained matrix. The uppermost layers of this unit are intruded by crosscutting porphyries. The age of the unit is constrained by two new U-Pb zircon ages for a basal volcanic and upper crosscutting porphyry, as discussed below.

The Gennemesa Formation

The Ordovician Gennamesa Formation is a light tan to grey arkosic sandstone. This unit is composed largely of reworked phenocrysts derived from the underlying volcanic sequence. Clear to milky quartz grains compose approximately 85% of the rock along with 1-3 mm, equant feldspars. Grain size varies throughout the unit from medium to very coarse sand. The unit is characterized by its cliff forming outcrops present in the central portion of the mapped area. The basal contact is not seen within the map area, but regionally is sharp and unconformable on the volcanic section (Carmignani et al., 1994).

Silurian Shales

Stratigraphically highest in the study area are the Silurian Black Shales (Figure 2.4). The age is based upon the graptolite assemblages found regionally within the unit (Carmignani et al., 2001). This unit is lustrous light to dark gray. The grain size is very fine and the rock displays well-developed penetrative foliation. The base of the unit is characterized by a less than 5m thick zone of darker gray, blocky outcrops with a higher

resistance to weathering. The basal contact is sharp and conformable with the Gennamesa Formation.

U-Pb Geochronology Methods

Zircon was subjected to a modified version of the chemical abrasion method of Mattinson (2005), reflecting a preference to prepare and analyze carefully selected single crystals or crystal fragments. Zircon separates were placed in a muffle furnace at 900°C for 60 hours in quartz beakers. Single crystals were then transferred to 3 ml Teflon PFA beakers, rinsed twice with 3.5 M HNO_3, and loaded into 300 µl Teflon PFA microcapsules. Fifteen microcapsules were placed in a large-capacity Parr vessel, and the crystals partially dissolved in 120 µl of 29 M HF with a trace of 3.5 M HNO_3 for 10-12 hours at 180°C. The contents of each microcapsule were returned to 3 ml Teflon PFA beakers, the HF removed and the residual grains rinsed in ultrapure H_2O, immersed in 3.5M HNO_3, ultrasonically cleaned for an hour, and fluxed on a hotplate at 80°C for an hour. The HNO_3 was removed and the grains were again rinsed in ultrapure H_2O or 3.5M HNO_3, before being reloaded into the same 300 µl Teflon PFA microcapsules (rinsed and fluxed in 6 M HCl during crystal sonication and washing) and spiked with the Boise State University mixed ^{233}U-^{235}U-^{205}Pb tracer solution (BSU-1B). These chemically abraded grains were dissolved in Parr vessels in 120 µl of 29 M HF with a trace of 3.5M HNO_3 at 220°C for 48 hours, dried to fluorides, and then re-dissolved in 6M HCl at 180°C overnight. U and Pb were separated from the zircon matrix using an HCl-based anion-

exchange chromatographic procedure (Krogh, 1973), eluted together and dried with 2 µl of 0.05 N H_3PO_4.

Pb and U were loaded on a single outgassed Re filament in 2 µl of a silica-gel/phosphoric acid mixture (Gerstenberger and Haase, 1997), and U and Pb isotopic measurements made on a GV Isoprobe-T multicollector thermal ionization mass spectrometer equipped with an ion-counting Daly detector. Pb isotopes were measured by peak-jumping all isotopes on the Daly detector for 100 to 150 cycles, and corrected for 0.22 ± 0.04%/a.m.u. mass fractionation. Transitory isobaric interferences due to high-molecular weight organics, particularly on ^{204}Pb and ^{207}Pb, disappeared within approximately 30 cycles, while ionization efficiency averaged 10^4 cps/pg of each Pb isotope. Linearity (to ≥1.4 x 10^6 cps) and the associated deadtime correction of the Daly detector were monitored by repeated analyses of NBS982, and have been constant since installation. Uranium was analyzed as UO_2+ ions in static Faraday mode on 10^{11} ohm resistors for 150 to 200 cycles, and corrected for isobaric interference of $^{233}U^{18}O^{16}O$ on $^{235}U^{16}O^{16}O$ with an $^{18}O/^{16}O$ of 0.00205. Ionization efficiency averaged 20 mV/ng of each U isotope. U mass fractionation was corrected using the known $^{233}U/^{235}U$ ratio of the BSU-1B tracer solution.

U-Pb dates and uncertainties were calculated using the algorithms of Schmitz and Schoene (2007), a $^{235}U/^{205}Pb$ ratio for BSU-1B of 77.93 ± 0.05, and the U decay constants recommended by Steiger and Jager (1977). $^{206}Pb/^{238}U$ ratios and dates were corrected for initial ^{230}Th disequilibrium using a Th/U[magma] of 3 ± 1 using the algorithms of Crowley, Schoene, and Bowring (2007), resulting in a systematic increase

in the $^{206}Pb/^{238}U$ dates of ~90 kyrs. Common Pb in analyses up to 1 pg was attributed to laboratory blank and subtracted based on the measured laboratory Pb isotopic composition and associated uncertainty. This simple correction is typical of most analyses; occasional analyses with common Pb in excess of 1 pg were assumed to contain initial Pb within mineral inclusions, which was subtracted based on the model two-stage Pb isotope evolution of Stacey and Kramers (1975). U blanks are difficult to precisely measure, but are <0.1 pg. Over the course of the experiment, isotopic analyses of the TEMORA zircon standard yielded a weighted mean $^{206}Pb/^{238}U$ age of 417.43 ± 0.06 (n=11, MSWD = 0.8).

Data

Volcanic Sample (SAR-08-04)

Sampling location

The lowermost volcanic sample was taken from location A in Figure 5, in the south-central portion of the field area. The base of the volcanic unit, as described above, is characterized by discontinuous lenses of metaconglomerates. Selection of this sample was based on its proximity to a lens of metaconglomerate consistent with the lowermost stratigraphic position within the unit.

U-Pb data

Eight whole zircon grains were analyzed from this sample using the U-Pb ID-TIMs method (Table 2.1). Two of the grains fall to younger and older $^{206}Pb/^{238}U$ ages of

452.63 and 457.29 Ma respectively. The remaining six grains yielded a weighted mean $^{206}Pb/^{238}U$ age for the volcanic sample of 456.91 ± 0.11 Ma (Figure 2.6). Given the stratigraphic position of the sample, this is interpreted as the beginning of volcanism.

Porphyry (SAR-08-01)

Sampling location

The porphyry sample was taken from a location outside of the field area with GPS coordinates of 39º28'46.386"N and 9º31'41.544"E projected with NAD 83. The sample was collected approximately 50 meters north of the access road along the north side of the Flumendosa River. The cross-cutting nature and textural characteristics of the porphyry support the interpretation that this porphyry is a late/syn-volcanic hypabyssal intrusion and, therefore, associated with the late stages of volcanic activity.

U-Pb data

Eleven grains were analyzed using the U-Pb ID-TIMS method; nine whole grains and two tips from a single grain (Table 2.1). Preliminary analyses of whole zircon grains from the volcanic sample demonstrated some variability in the U-Pb ID-TIMS zircon ages, with grains ranging from ca. 451-510 Ma. Therefore, further analyses were done to minimize the scatter by breaking the tips off two grains to discern the age of these tips versus other whole grain analyses. These results indicate that zircons from this sample contain a slightly older core with younger rims. Analyses of two whole grain zircons and one tip yielded a weighted mean $^{206}Pb/^{238}U$ date of 452.64 ± 0.36 Ma (Figure 2.7), which

is interpreted as the crystallization age of the porphyry. Given the stratigraphic position of the sample, this age can be interpreted as the approximate end of magmatic activity in this section.

Table 2.1. U-Th-Pb Isotopic Data for SAR-08-01 and SAR-08-04.

							Isotope Ratios								Isotopic Ages					
Sample	$\frac{Th}{U}$	$^{206}Pb^*$ x10^{-13} mol	mol % $^{206}Pb^*$	$\frac{Pb^*}{Pb_c}$	Pb_c (pg)	$\frac{^{206}Pb}{^{204}Pb}$	$\frac{^{208}Pb}{^{206}Pb}$	$\frac{^{207}Pb}{^{206}Pb}$	% err	$\frac{^{207}Pb}{^{235}U}$	% err	$\frac{^{206}Pb}{^{238}U}$	% err	corr. coef.	$\frac{^{207}Pb}{^{206}Pb}$	±	$\frac{^{207}Pb}{^{235}U}$	±	$\frac{^{206}Pb}{^{238}U}$	±
(a)	(b)	(c)	(c)	(c)	(c)	(d)	(e)	(e)	(f)	(e)	(f)	(e)	(f)		(g)	(f)	(g)	(f)	(g)	(f)
SAR-08-01																				
z1	0.296	10.4486	99.88%	242	1.03	15577	0.093	0.058118	0.052	0.660995	0.098	0.082487	0.058	0.903	534.21	1.14	515.22	0.39	510.95	0.28
z2	0.108	7.2818	99.88%	225	0.73	15345	0.034	0.056349	0.053	0.577126	0.096	0.074282	0.054	0.906	466.13	1.16	462.61	0.36	461.90	0.24
z4	0.100	9.9392	99.82%	155	1.43	10619	0.032	0.056301	0.059	0.580733	0.101	0.074545	0.053	0.880	472.13	1.32	464.93	0.38	463.48	0.24
z6*	0.110	7.5298	99.93%	374	0.45	25469	0.034	0.056021	0.046	0.561904	0.093	0.072746	0.055	0.935	453.21	1.03	452.77	0.34	452.68	0.24
z7	0.109	5.9311	99.87%	217	0.61	14785	0.034	0.056071	0.055	0.560828	0.098	0.072541	0.054	0.898	455.20	1.22	452.06	0.36	451.45	0.23
z8*	0.139	5.0076	99.88%	231	0.49	15600	0.043	0.055988	0.056	0.561645	0.098	0.072755	0.053	0.896	451.90	1.25	452.60	0.36	452.73	0.23
z9a*	0.090	0.8571	99.58%	64	0.30	4407	0.028	0.055935	0.117	0.560731	0.157	0.072706	0.065	0.737	449.79	2.61	452.00	0.57	452.44	0.29
z9b	0.114	1.7030	99.77%	117	0.33	7958	0.036	0.056013	0.131	0.563915	0.159	0.073017	0.065	0.605	452.87	2.90	454.07	0.58	454.31	0.29
z10	0.134	2.7406	99.69%	90	0.69	6081	0.042	0.056526	0.104	0.584148	0.142	0.074951	0.066	0.735	473.08	2.29	467.12	0.53	465.91	0.30
z11	0.308	1.2082	99.38%	46	0.62	2999	0.097	0.056051	0.167	0.566346	0.203	0.073282	0.064	0.665	454.40	3.71	455.65	0.74	455.90	0.28
z12	0.125	1.4305	99.28%	38	0.86	2571	0.039	0.055882	0.234	0.561800	0.267	0.072913	0.074	0.551	447.69	5.21	452.70	0.97	453.68	0.32
SAR-08-04																				
z1*	0.367	2.9739	99.69%	93	0.77	5915	0.115	0.056131	0.094	0.568761	0.130	0.073489	0.058	0.754	457.56	2.10	457.21	0.48	457.14	0.26
z2	0.148	4.8204	99.77%	122	0.90	8209	0.046	0.056001	0.080	0.561638	0.117	0.072737	0.058	0.791	452.41	1.77	452.59	0.43	452.63	0.26
z3	0.360	1.8201	99.56%	66	0.66	4234	0.113	0.056127	0.116	0.568907	0.150	0.073514	0.056	0.723	457.38	2.58	457.31	0.55	457.29	0.25
z4*	0.296	2.0289	99.32%	42	1.15	2727	0.093	0.056033	0.145	0.567481	0.185	0.073453	0.058	0.776	453.66	3.22	456.38	0.68	456.92	0.25
z5*	0.397	1.7919	99.18%	36	1.21	2276	0.125	0.056084	0.196	0.567964	0.239	0.073448	0.088	0.625	455.69	4.35	456.70	0.88	456.90	0.39
z6*	0.387	2.4224	99.77%	126	0.47	7953	0.121	0.056115	0.100	0.568113	0.132	0.073427	0.059	0.703	456.93	2.22	456.79	0.49	456.77	0.26
z7*	0.276	1.5447	99.45%	52	0.70	3398	0.086	0.056023	0.182	0.567212	0.209	0.073430	0.067	0.539	453.30	4.04	456.21	0.77	456.79	0.29
z8*	0.401	2.7773	99.72%	104	0.65	6545	0.126	0.056108	0.095	0.568234	0.130	0.073451	0.058	0.741	456.65	2.11	456.87	0.48	456.92	0.26

* labels with asterick were used in the weighted mean calculation

(a) z1, z2 etc. are labels for fractions composed of single zircon grains or fragments; all fractions annealed and chemically abraded after Mattinson (2005).

(b) Model Th/U ratio calculated from radiogenic 208Pb/206Pb ratio and 207Pb/235U age.

(c) Pb* and Pbc represent radiogenic and common Pb, respectively; mol % $^{206}Pb^*$ with respect to radiogenic, blank and initial common Pb.

(d) Measured ratio corrected for spike and fractionation only. Mass fractionation correction of 0.22 ± 0.02 (1-sigma) %/amu (atomic mass unit) was applied to all single-collector Daly analyses, based on analysis of NBS-981 and NBS-982.

(e) Corrected for fractionation, spike, and common Pb; all common Pb was assumed to be procedural blank: 206Pb/204Pb = 18.60 ± 0.80%; 207Pb/204Pb = 15.69 ± 0.32%;

Discussion

New U-Pb zircon ages for the Ordovician Volcanics of the Gerrei Unit provide constraints on the timing and duration of magmatic activity for the unit. The lowermost volcanic sample representing the beginning of magmatism yielded an age of 456.91 ± 0.11 Ma, and a late-stage cross-cutting porphyry representing the end of magmatism yielded an age of 452.64 ± 0.36 Ma. Collectively, these ages indicate that the length of magmatic activity was relatively short-lived (5 Ma) during the Late Ordovician; previous work proposed that the age of the volcanic unit was Middle Ordovician (Carmignani et al., 1994).

At least four tectonic settings could account for the genesis of this unit: 1) rift zone, 2) hot spot, 3) ridge subduction, and 4) volcanic arc. Continental rifting is discounted on the basis of the lack of bimodal volcanism, lack of normal faults and associated immature basin filling sediments of Ordovician age. The hot spot setting is discredited based on the lack of localized short-lived volcanic evidence in other areas and no clear tracking pattern. The ridge subduction setting provides a source for a short-lived magmatic activity along the Gondwana margin (Stampfli, von Raumer, and Borel, 2002). This setting would likely generate peraluminous granites from melting of the accretionary prism. The unit is calc-alkaline, however, inconsistent with this model (Carmignani et al., 2008). The volcanic arc setting also provides a scenario for short-lived magmatic activity and the lack of a conformable basin sequence implies that uplift immediately preceded volcanism. These are also characteristics of the subduction and volcanic arc settings. The geochemical make-up of the volcanic unit as calc-alkaline also supports the

volcanic arc hypothesis (Carmignani et al., 2008). This reconstruction is better constrained by the distribution of other Ordovician volcanic rocks throughout Sardinia and the greater context of Pangaea, along with the correlation of the basal unconformity of the volcanic unit throughout Europe.

The distribution of Ordovician volcanic rocks on Sardinia is not well known due to the lack of a comprehensive geochronologic framework. However, recent studies provide U-Pb zircon analyses of volcanic rocks from units located in both the Foreland and Internal Zones. Volcanic rocks contained in the Bithia Formation of the Foreland Zone, near Capo Spartivento, yielded ages ranging from 458.6 to 457.3 Ma (Pavenetto and Funedda, pers. comm.). Field relations are not fully clear, but the Bithia Unit may represent a klippe of a thrust sheet from the Nappe Zone now isolated within the Foreland Zone. Which specific nappe, however, is unclear. If so, the Bithia volcanic ages provide further constraint on the range of magmatic activity for the Nappe Zone. Helbing and Tiepolo (2005) presented geochronologic data for magmatic units in NE Sardinia of late Ordovician ages of 458 ± 7 Ma for the Tanaunella orthogneiss, 456 ± 14 Ma for the Lodè orthogneiss.

There are two working models within which we must interpret the significance in the similarities of Ordovician age volcanic rocks in the three zones of Sardinia: 1) the PAL represents the major suture between Laurentia (the Internal Zone) and Gondwana (the Nappe Zone), (Matte, 1991) and 2) the PAL represents a minor suture within Gondwana derived terranes that compose the Hun Superterrane (von Raumer, Stampfli, and Bussy, 2003).

The first model associates the Internal Zone with Laurentia and the Nappe Zone with Gondwana, thereby suggesting the PAL is the suture zone between these two supercontinents. The Rheic Ocean separated these regions before they were sutured together as a result of the Variscan Orogeny during the Late Devonian-Mississisippian (Matte 2001; Carmignani et al., 1994). Therefore the correlation of the volcanic units in these two zones based on the closeness in ages for the volcanic packages suggests a wide-spread Ordovician volcanic event. The estimated total area for the magmatic activity is not available as the pre-Variscan paleogeography for the nappes are unknown.

Alternatively, the similarities between these volcanic rocks could provide evidence for the PAL representing a Gondwana marginal suture and not the suture between Laurentia and Gondwana (Stampfli, von Raumer, and Borel, 2002). This proposal suggests that the Variscan system in Europe reflects a collision between Gondwana-derived terranes that sutured together as the Hun Superterrane, and Laurentia. In this scenario, the suture between the Northern Gondwana Hun Superterrane and Laurentia is farther north than the PAL in present-day coordinates, but was not clarified. This interpretation of the PAL suggests that the Internal Zone is of Gondwana origin and was located along the margin of Gondwana during the Ordovician. The existence of the Hun Superterrane is supported by the distribution of Ordovician volcanic rocks throughout other parts of the paleo Gondwana margin and now found in other parts of the Variscan Orogen.

Recent studies have investigated Ordovician granitoids and volcanic rocks throughout the Mediterranean region, and provide support for multiple stages of rifting

and suturing that could be correlated with the formation of the Hun Superterrane (Figures 2.8 and 2.9). The Kapanca metagranitoids located in Turkey yielded an age of 467 ± 4.5 Ma (Okay, Satir, and Shang, 2008). The tectonic setting is interpreted to be rift-related due to the lack of volcanic rocks, even though the geochemistry is consistent with a volcanic arc. The setting is associated with the rifting of Avalonia from the Gondwana margin, which occurred between 480-462 Ma (Prigmore, Butler, and Woodcock, 1997) and comprises one of the fragments of the Hun Superterrane (Stampfli, von Raumer, and Borel, 2002). Other Ordovician magmatic zircons from a meta-litharenite from the Ionoussess Island in Greece yielded ages ranging from 450-485 Ma and also are correlated with Gondwanan-derived sources (Meinhold and Frei, 2008). Occurences of Ordovician magmatism in the Western Mediterranean are summarized in Table 2.2.

Table 2.2: Recognized Ordovician Magmatism in Western Mediterranean Region.

Location	Age	Rock type	Reference
Northwest Iberia	(1) 620-470 Ma (2) 460-450 Ma	(1) Granitoids and volcanic rocks (2) Calc-alkaline gneiss of granodioritic origin; protolith emplacement age	Martinez Catalan et al., 2008
Eastern Pyrenees	(1) 475-446 Ma (2) 475-460 Ma	(1) aluminous to calc-alkaline orthogeneisses (2) aluminous granitic orthogneisses	Castineiras, Navidad, Liesa, Carreras, and Casas, 2008; Cocherie et al., 2005
Southwest Bulgaria	460 Ma	Metagranitoids	Titorenkova, Macheva, Zidarov, von Quadt, and Petcheva, 2003
France	456-450 Ma	Augen orthogneiss; granitic protolith emplacement	Roger, Respaut, Brunel, Matte, and Paquette, 2004
Sicily	456-452 Ma	Felsic porphyroids	Trombetta, Cirricione, Corfu, Mazzoleni, and Pezzino, 2004

Several locations support both rifting and subduction settings within a short time frame (Table 2.2; Figures 2.8 and 2.9). This provides support for multiple stages of opening and closing of narrow ocean basins during the formation of the Hun Superterrane and the subsequent suturing of the Hun Superterrane and Laurentia to the north and Gondwana to the south (Figures 2.8 and 2.9).

Further constraint on the proximity of these various regions at the onset of volcanism was investigated through the correlation of the unconformity within the Gerrei Unit with other regional stratigraphic frameworks. The Sardic Unconformity is defined in the Foreland Zone as a Cambrian to early Ordovician time gap (Carmignani et al.,

1994). Similar to the situation for the Ordovician volcanics in the nappes, there is little geochronologic data to constrain the unconformity in the Foreland. Valverde-Valquero and Dunning (2000) presented U-Pb analyses on early Ordovician gneisses across the Berzosa- Riaza shear zone in Central Spain that range in age from 488-468 Ma. This study proposed that the magmatism is correlative with the overlying units of the Sardic Unconformity and is associated with the felsic magmatic belt that extended through the Central Iberian Zone. Therefore, this correlation provides a potential maximum age constraint on the end of the unconformity, assuming the correlation is valid.

A possible correlation of the age of the unconformity within the Gerrei Unit with similar ages presented for bracketing the Sardic Unconformity strengthens a potential correlation. The unconformity represents a time gap from the Cambrian to the Early Ordovician (Valverde-Valquero and Dunning, 2000). Correlation with the gneisses in Central Spain constrain this gap from the Cambrian to between 488-468 Ma, Early Ordovician (Valverde-Valquero and Dunning, 2000). Though this is 10-30 Ma earlier than the start of magmatism for the Nappe Zone (456.91 ± 0.11 Ma), it is still possible that the unconformity in the Nappe Zone is associated with the Sardic Unconformity if the surface is time transgressive.

Conclusion

New geochronologic data from volcanic rocks in the Gerrei Unit support three major conclusions. First, magmatic activity began at approximately 456.91 ± 0.11 Ma and lasted until approximately 452.64 ± 0.36 Ma. Therefore, magmatism began more

recently than previously thought (Carmignani et al., 1994. Second, the unconformity in the Nappe Zone represents a longer gap in time with potential correlations with the Sardic Unconformity. The third conclusion relates the Gerrei volcanic rocks to other Ordovician aged volcanics in the Axial/Internal Zone. Due to the uncertainties with paleogeographic reconstructions of the Ordovician placing the crustal blocks of Sardinia at (1) opposite sides of the Rheic Ocean within the Tethyan realm requires a Tethyan wide Ordovician volcanic event or (2) as part of the Hun Superterrane that provides more evidence for the close proximity of both crustal blocks of Sardinia during the Ordovician on the margin of Gondwana.

Figures

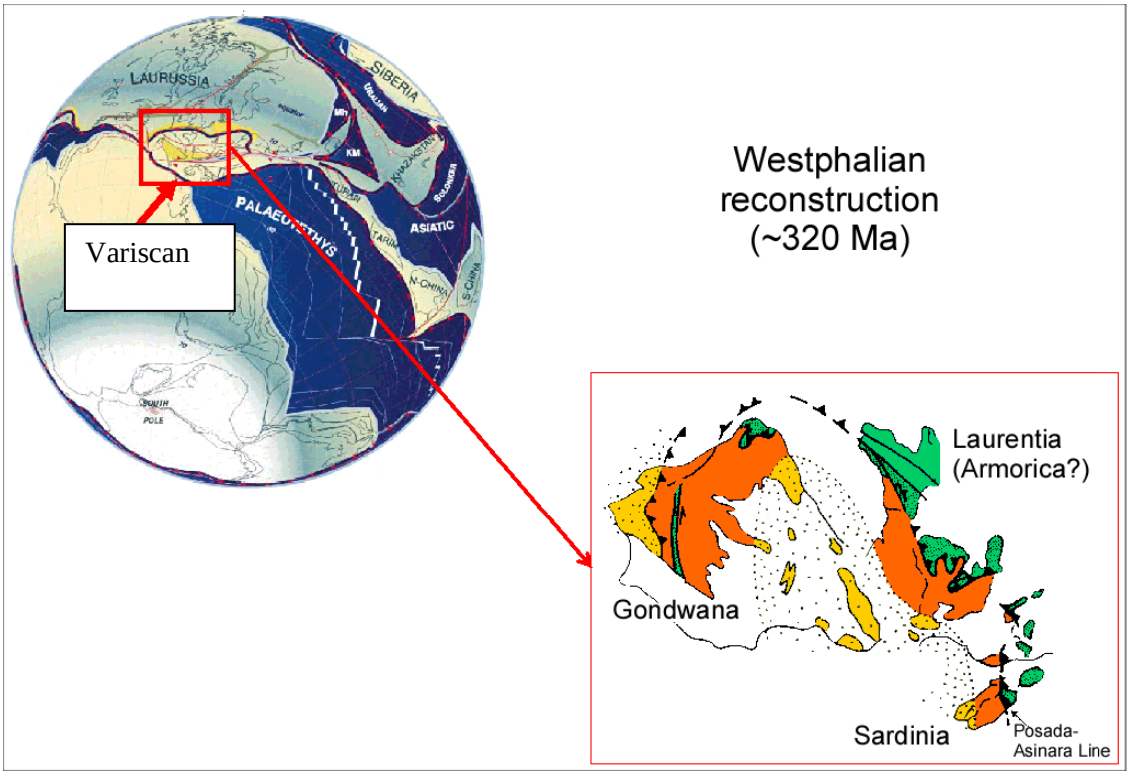

Figure 2.1: Paleogeographic reconstruction of Sardinia within the Variscan orogen based on Matte (1986) and Stampfli and Borel (2002).

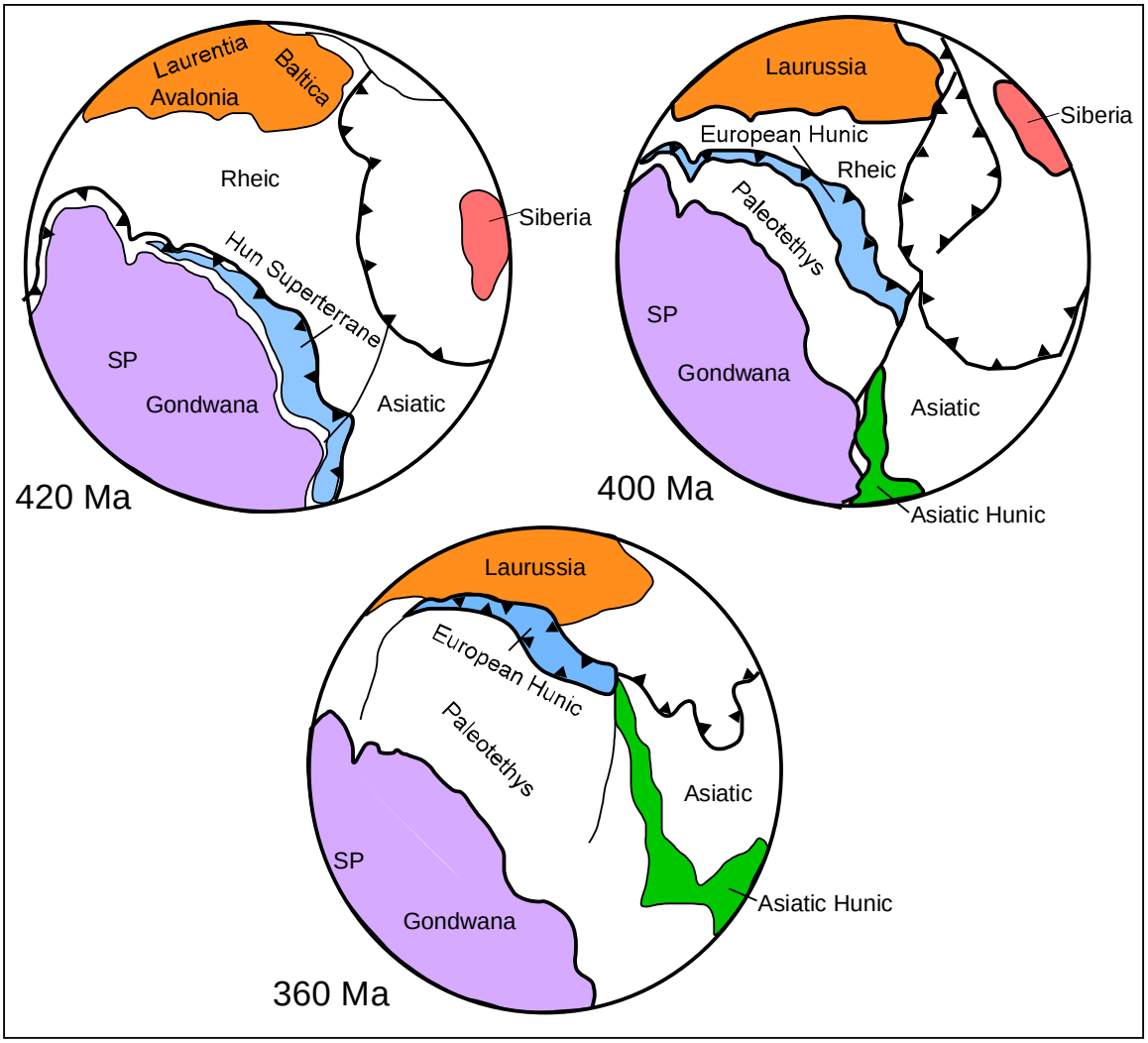

Figure 2.2: Simplified paleographic series of the evolution of the Hun Superterrane (modified from Stampfli, von Raumer, and Borel, 2002)

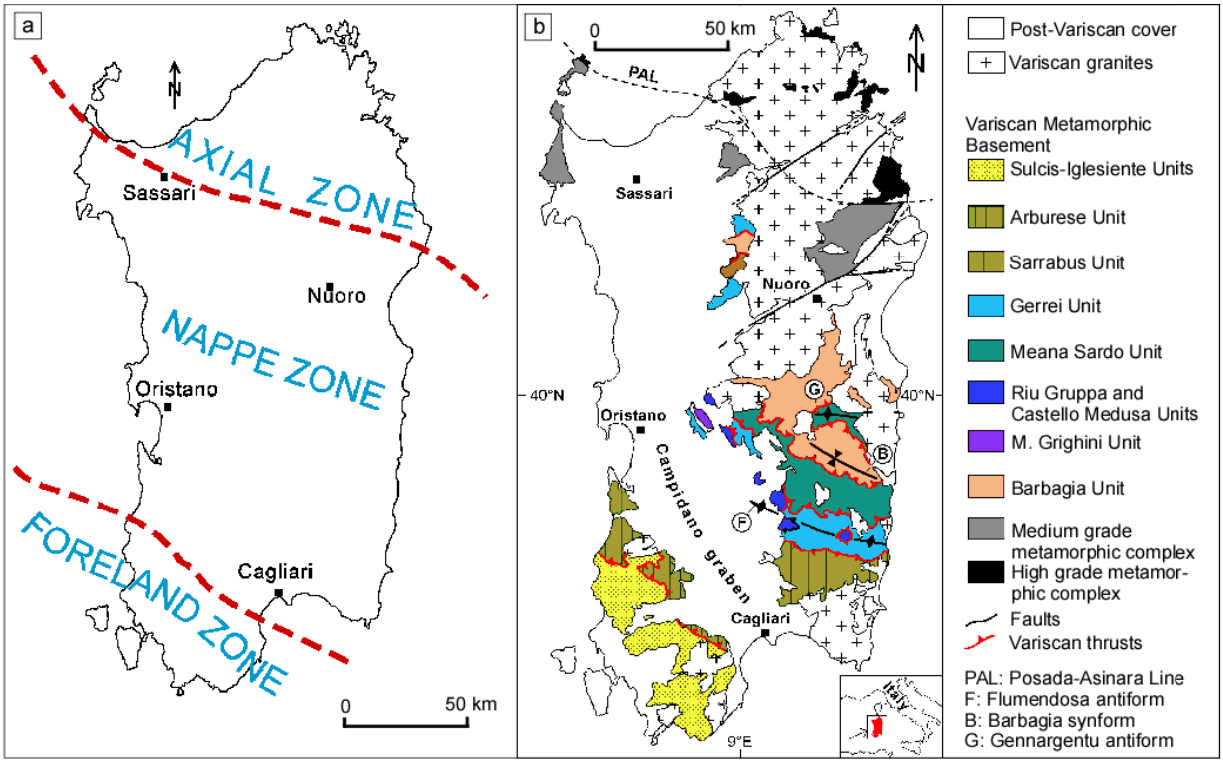

Figure 2.3: Tectono metamorphic zonation of Variscan metamporphism (a) and distribution of exposure (b) on Sardinia composed by Carmignani et al. (1987).

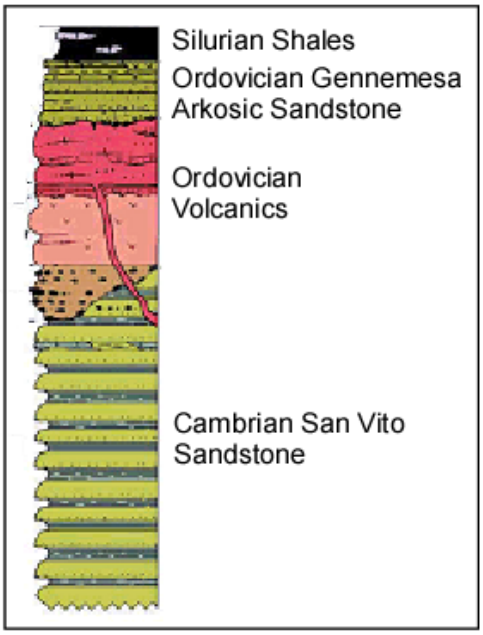

Figure 2.4: Simplified stratigraphic column illustrating the sequence of the rock units in the mapped area. Modified from Carmignani et al. (1994).

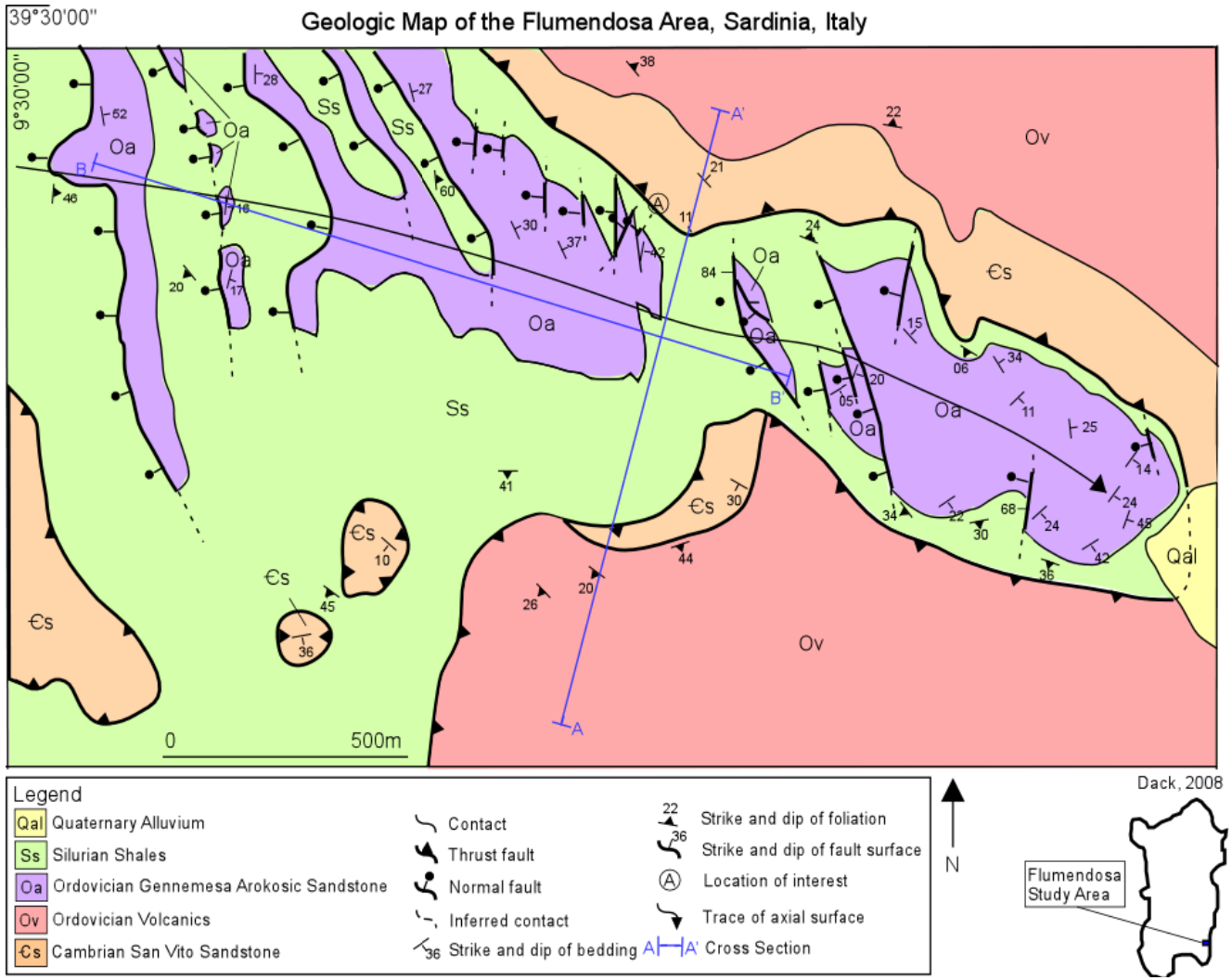

Figure 2.5: Simplified geologic map of the Flumendosa area of southeastern Sardinia with sample location A.

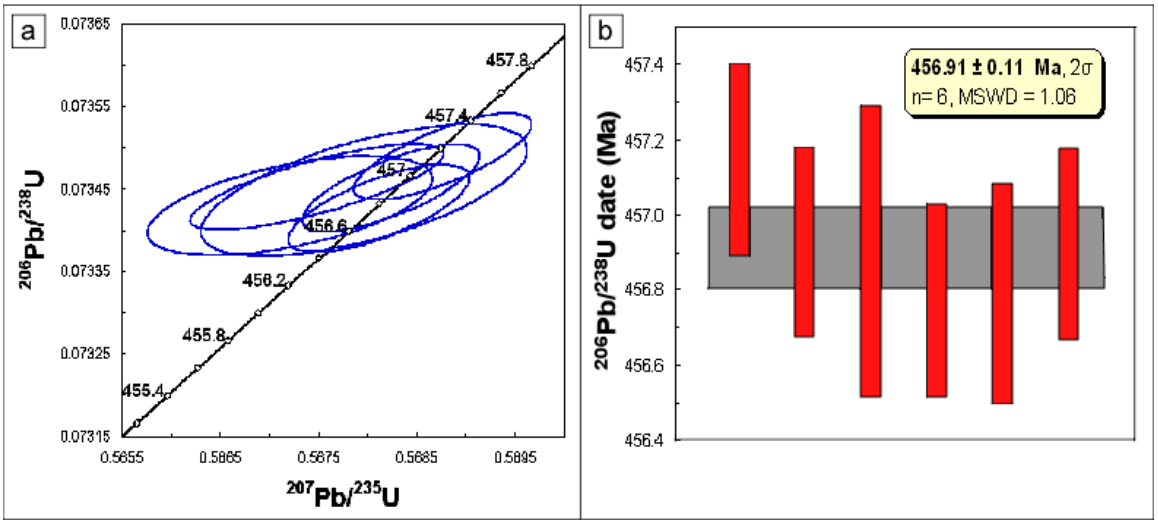

Figure 2.6: A Concordia plot (a) and error bar plot (b) from zircons in the lowest stratigraphic volcanic units (SAR-08-04). The ellipses and bars represent 2σ.

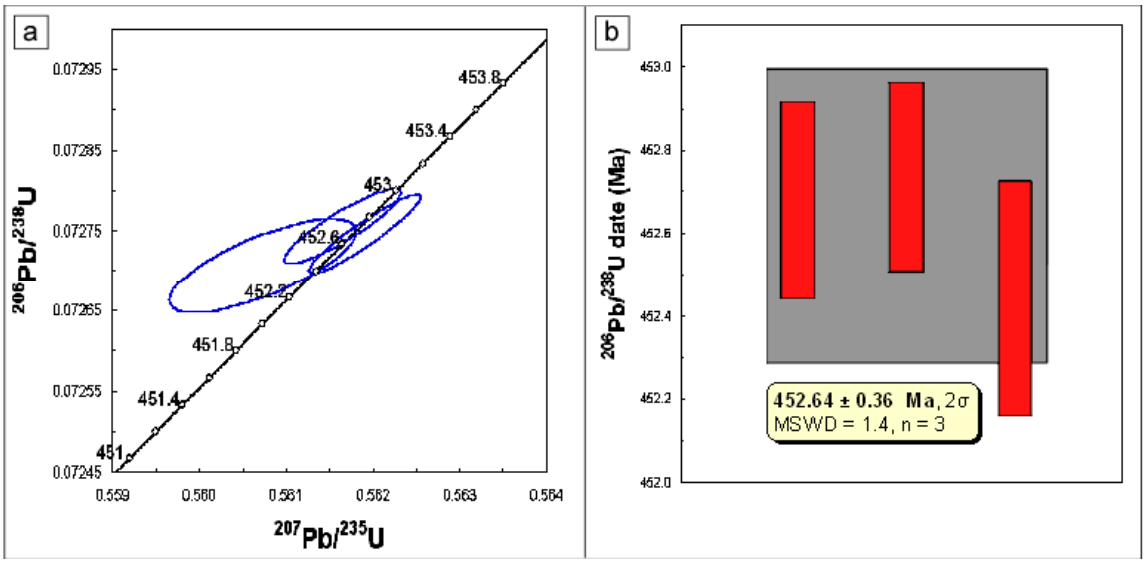

Figure 2.7: Concordia plot (a) and error bar plot (b) from zircons in the porphyry (SAR-08-01). The ellipses and red bars represent 2σ.

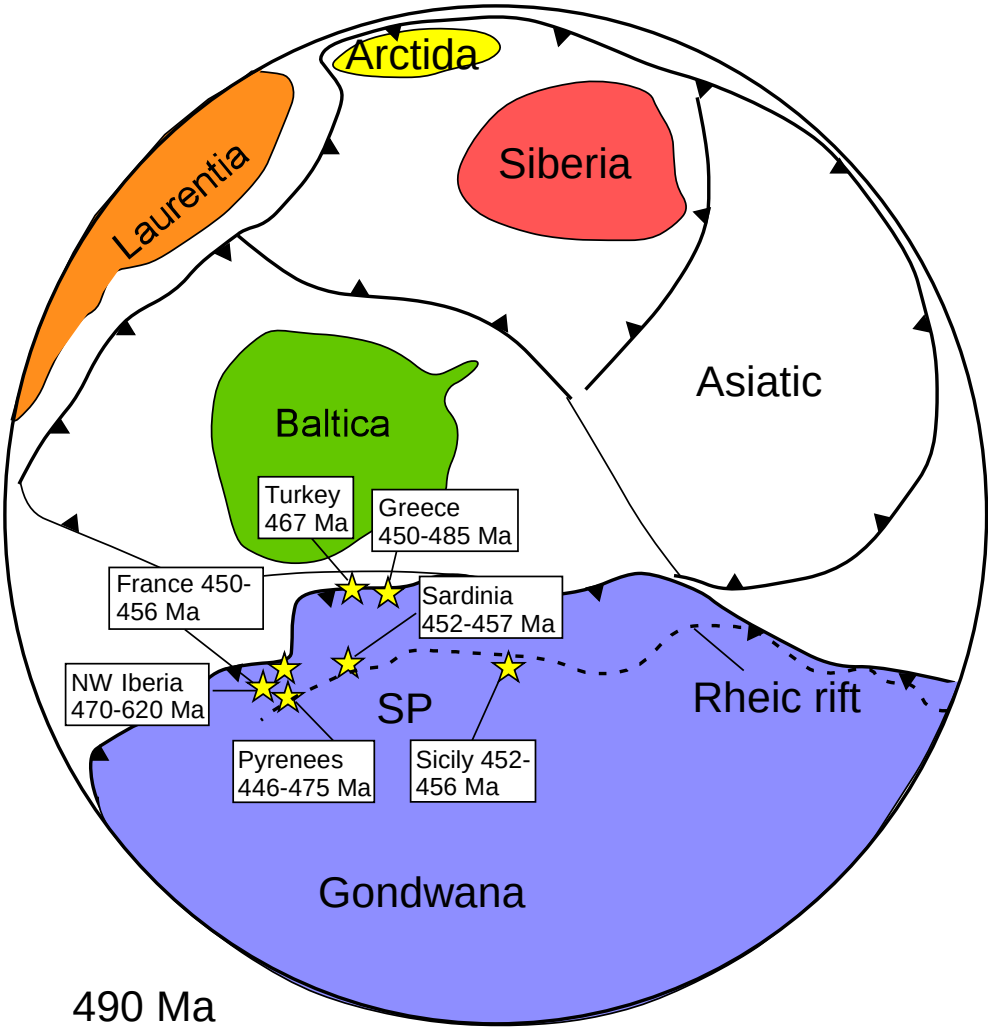

Figure 2.8: Paleogeographic reconstruction modified from von Raumer et al. (2003) at 490 Ma with recognized Ordovician volcanic rocks and metagranitoids.

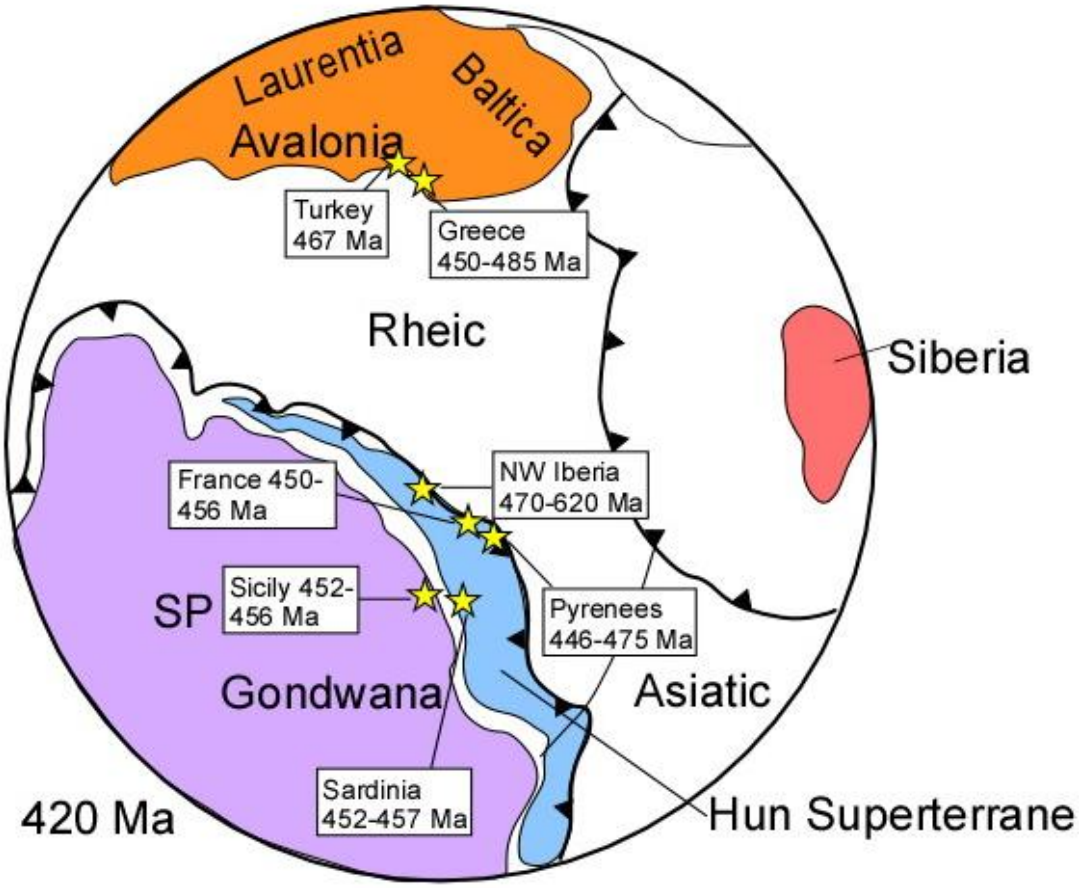

Figure 2.9: Location of pre-Variscan basement units with stars indicating Ordovician volcanic rocks and metagranitoids (modified from Stampfli, von Raumer, and Borel, 2002)

Works Cited

Cappelli, B., Carmignani, L., Castorina, F., Di Pisa, A., Oggiano, G. and Petrini, R., 1992, A Hercynian suture zone in Sardinia: geological and geochemical evidence: Geodinam. Acta., v. 5, p. 101-118.

Carmignani, L., and 15 others, 2001, Foglio 549, Carta Geologico di Muravera, Regione Autonoma della Sardegna, scale: 1:50,000: Carta Geologica D'Italia, Servizio Geologico D'Italia.

Carmignani, L., Barca, S., Cappelli, B., Di Pisa, A., Gattiglio, M., Oggiano, G., and Pertusati, P.C., 1992, A tentative model for the Hercynian Basement of Sardinia: "Contributions to the Geology of Italy". L. Carmignani and F.P. Sassi (eds), IGCP N^{o} 276, Newsletter, 5, v. 61-82.

Carmignani, L.,Carosi, R., Di Pisa, A., Gattliglio, M., Musumeci, G., Oggiano, G., and Pertusati, P.C., 1994, The hercynian chain in Sardinia (Italy): Geodinamica Acta (Paris), v. 7(1), p. 31-47.

Carmignani, L., Cocozza, T., Ghezzo, C., Pertusati, P.C., and Ricci, C.A., 1987, Structural Model of the Hercynian Basement of Sardinia. 1:500,000: Stabilimento L. Salomone, CNR, Progetto Finalizzanto Geodinamica, Roma.

Carmignani, L., Oggiano, G., Funnedda, A., Conti, P., Pasci, S., and Barca, S., 2008, Carta Geologica della Sardegna, scale: 1:250,000: Carta Geologica D'Italia, Servizio Geologico D'Italia.

Castiñeiras, P., Navidad, M., Liesa, M., Carreras, J., and Casas, J. M., 2008, U-Pb zircon ages (SHRIMP) for Cadomian and Early Ordovician magmatism in the Eastern Pyrenees: new insights into the pre-Variscan evolucation of the northern Gondwana margin: Tectonophysics, v. 461, p. 228-239.

Cocherie, A., Baudin, T., Autran, A., Guerrot, C., Fanning, M.C., and Laumonier, B., 2005, U-Pb zircon (ID-TIMS and SHRIMP) evidence for the early Ordovician intrusion of metagranites in the late Proterozoic Canaveilles Group of the Pyrenees and the Montagne Noire (France): new U-Pb zircon datings: Bull. Soc. Geol. Fr., v. 176, p. 269-282.

Conti, P. and Patta, E., 1998, Large-scale Hercynian west-directed tectonics in southeastern Sardinia (Italy): Geodinamica Acta (Paris), v. 11(5), p. 217-231.

Crowley, J.L., Schoene, B., and Bowring, S.A., 2007, U-Pb dating of zircon in the Bishop Tuff at the millennial scale: Geology, v. 35, p. 1123-1126.

Di Pisa, A., Gattaglio, M., and Oggiano, G., 1992, Pre-Hercynian basic magmatic activity in the Nappe Zone (Internal and External) of Sardinia: evidence of two within plate basaltic cycles: Contributions to the Geology of Italy, L. Carmignani and F.P. Sassi (eds) IGCP No 276, Newsletter 5, special issue, p. 107-116.

Garbarino, C., Maccioni, L., Padalino, G., Tocco, S., and Violo, M., 1981, Le mineralizzazzioni stratiformi di solfuri misti della Sardegna centrale quale prodotto di un vulcanismo di margine continentale di eta' ordoviciona: proposta di un modello geodinamico e genetico: Mem. Soc. Geol. It., v. 22, p. 145-150.

Gerstenberger, H. and Haase, G., 1997, A highly effective emitter substance for mass spectrometric Pb isotope ratio determinations: Chemical Geology, v. 136, p. 309-312.

Helbing, H. and Tiepolo, M., 2005, Age determination of Ordovician magmatism in NE Sardinia and its bearing on Variscan basement evolution: Journal of the Geological Society, v. 16(4), p. 689-700; DOI: 10.1144/0016-764904-103.

Krogh, T.E., 1973, A low contamination method for hydrothermal decomposition of zircon and extraction of U and Pb for isotopic age determination: Geochimica et Cosmochimica Acta, v. 37, p. 485-494.

Martínez Catalán, J.R., Fernández-Suárez, J., Meireles, C., González, C.E., Belousova, E., and Saeed, A., 2008, U-Pb detrital zircon ages in synorogenic dposits of the NW Iberian Massif (Variscan belt): interply of Devonian-Carboniferous sedimentation and thrust tectonics: Journal of the Geological Soiety, v. 165, p. 687-698.

Matte, P., 2001, The Variscan collage and orogeny (480-290 Ma) and the tectonic definition of the Armorica microplate: a review: Terra Nova, v. 13, p. 122-128.

Matte, P., 1991, Accretionary history and crustal evolution of the Variscan belt in Western Europe: Tectonophysics, v. 196 (3-4), p. 309-337.

Matte, P., 1986, Tectonics and plate tectonics model for the Variscan belt of Europe: Tectonophysics, v. 126, p. 329-374.

Mattinson, J.M., 2005, Zircon U-Pb chemical abrasion ("CA-TIMS") method: combined annealing and multi-step partial dissolution analysis for improved precision and accuracy of zircon ages: Chemical Geology, v. 220, p. 47-66.

Meinhold, G. and Frei, D., 2008, Detrital zircon ages from the islands of Inousses and Psaara, Aegean Sea, Greece: constraints on depositional age provenance: Geol. Mag., v. 145(6), p. 886-891.

Memmi, I., Barca, S., Carmignani, L., Cocozza, T., Elter, F.M., Franschelli, M., Gattiglio, M., Ghezzo, C., Minzoni, N., Naud, G., Pertusati, P.C., and Ricci, C.A., 1983, Further geochemical data on the pre-Hercynian igneous activity of Sardinia and on their geodynamic significance. IGCP n^{o}5, Newsletter, 5, p. 87-93.

Okay, A., Satir, M. and Shang, C.K., 2008, Ordovician metagranitoid from the Anatolide-Tauride Block, northwest Turkey: geodynamic implications: Terra Nova, v. 20(4), p. 280-288.

Pavamento, P. and Funnedda, A., 2009, pers. comm.

Prigmore, J., Butler, A. and Woodcock, N., 1997, Rifting during separation of Eastern Avalonia from Gondwana: Evidence from subsidence analysis: Geology, v. 25, n. 3, p. 203-206.

Roger, F., Respaut, J.P., Brunel, M., Matte, P., and Paquette, J.L., 2004, Premiére datation U-Pb des orthogneiss oeilles de la zone axiale de la Montagne Noire (Sud de Massif Central): nouveaux te'moins du magmatisme Ordovicien dans la chaîne varisque: C R Geosci, v. 336, p. 19-28.

Schmitz, M.D. and Schoene, B., 2007, Derivation of isotope ratios, errors and error correlations for U-Pb geochronology using ^{205}Pb-^{235}U-(^{233}U)-spiked isotope dilution thermal ionization mass spectrometric data: Geochemistry, Geophysics, Geosystems (G3) 8, Q08006, doi:10.1029/2006GC001492.

Stacey, J.S. and Kramers, J.D., 1975, Approximation of terrestrial lead isotope evolution by a two-stage model: Earth and Planetary Science Letters, v. 26, p. 207-221.

Stampfli, G. and Borel, G., 2002, A plate tectonic model for the Paleozoic and Mesozoic constrained by dynamic plate boundaries and restored synthetic oceanic isochrones: Earth and Planetary Science Letters, v. 196, p. 17-33.

Stampfli, G, von Raumer, J., and Borel, G., 2002, Paleozoic evolution of pre-Variscan terranes: From Gondwana to the Variscan collision: Geological Society of America Special Paper 364, p. 263-280.

Steiger, R.H. and Jager, E., 1977, Subcommission on geochronology: convention on the use of decay constants in geo- and cosmochronology: Earth and Planetary Science Letters, v. 36, p. 359-362.

Titorenkova, R., Macheva, L., Zidarov, N., von Quadt, A., and Petcheva, I., 2003, Metagranites from SW Bulgaria as a part of Neoproterozoic to early Paleozoic system in Europe: new insight from zircon typology, U-Pb isotopic data and Hf-tracing: Geophysical Research Abstracts, v. 5, n. 08963.

Trombetta, A., Cirrincione, R., Corfu, F., Mazzoleni, P. and Pezzino, A., 2004, Mid – Ordovician U–Pb ages of porphyroids in the Peloritan Mountains dating Ordovician magmatism in Sardinia (NE Sicily): paleogeographic implications for the evolution of the Alboran microplate: Journal of the Geological Society, London, v. 161, p. 1-13.

Vai, G.B., 1991, Paleozoic strike-slip rift pulses and paleogeographiy in the circum-

Mediterranean Tethyan realm: Paleogeography, Paleoclimatology, Paleoecology, v. 87, p. 223-252.

Vai, G.B., 1982, Fasi di “rifting” nuovi dati stratigrafici e consequenze paleografiche nel Paleozoico inferiore. In: Guida alla geologia del Paleozoico sardo: Guide Geologiche Regionali Soc. Geol. It., p. 193-195.

Vai, G.B. and Cocozza, T., 1986, Tentative schematic zonation of the Hercynian chain in Italy: Bull. Soc. Géol. Fr., v. 8(1), p. 95-114.

Valverde-Valquero, P. and Dunning, G.R., 2000, New U-Pb ages for Early Ordovician magmatism in Central Spain: Journal of the Geological Society, London, v. 157, p. 15-26.

von Raumer, J., Stampfli, G., and Bussy, F., 2003, Gondwana-derived-microcontinents-the constituents of the Variscan and Alpine collisional orogens: Tectonophysics, v. 365, p. 7-22.

STRUCTURAL AND KINEMATIC ANALYSIS OF VARISCAN DEFORMATION IN THE FLUMENDOSA AREA, SARDINIA, ITALY: EVIDENCE FOR AN OROGEN-PARALLEL TRANSITIONAL PHASE FROM CONTRACTION TO EXTENSION

Abstract

Collisional orogenic systems commonly express both contractional and extensional deformation; however, details of their kinematic interactions and the patterns of transitional strain as orogens switch from contraction to extension are not well constrained. The Variscan basement in Sardinia, Italy, contains a well preserved geologic record of Variscan orogenic contraction and extension. New mapping and structural analysis of the Flumendosa Area, located in the Variscan external nappe zone in southeastern Sardinia, suggest a complex deformational history with four stages, including an orogen-parallel phase that may represent one mode of transition from contraction to extension.

Within the detailed study area, the initial deformational phase (D1) is evidenced by a south-directed thrust fault related to the amalgamation of the composite Variscan nappe stack. The thrust contact is sharp, and visible in outcrops throughout the eastern half of the map area. The second phase of deformation (D2) is defined by the folding of the D1 thrust by the upright, gently SE-plunging Flumendosa antiform. Pi-analysis of bedding orientations from strata affected by the fold suggest a hinge line orientation of

142°, 13° indicating that D2 was a NE-SW directed contractional event. The third phase (D3) is expressed by top-to-the-east-southeast movement of the upper thrust sheet evidenced by penetrative deformation, shear, and a domino style series of N-S striking, high-angle faults within the lower sheet. This phase is interpreted to represent a transition from contraction to extension involving orogen-parallel transport. The fourth deformational event (D4) produced brittle fractures within the shale that cross-cut the penetrative deformation. Slickensides indicate a transport direction of 014°, 13°, consistent with extensional reactivation of the N-dipping D1 thrust surface during late stages of orogenic evolution.

Introduction

Collisional orogens generally involve early contractional deformation followed by syn- to post-collisional extension (Malavieille, Guihot, Costa, Lardeaux, and Gardien, 1990; Platt, 1993; LePichon, Henry, and Goffé, 1997; Milnes, Wennberg, Skår, and Koestler, 1997; Anderson, 1998; Leech, 2001). The geometric and kinematic interaction between these processes is a fundamental aspect governing the evolution of many collisional orogenic systems, including the Apennines (Carmignani and Kligfield, 1990; Scisciani, Tavarnelli, and Calamita, 2002), Betic Cordillera (Vissers, Platt, and van der Wal, 1995), Caledonides (Gee, Lobkowicz, and Singh, 1994; Northrup, 1996; Anderson, 1998), and Himalayas (Burchfiel et al., 1992). The structural features and patterns of 3-D movement that accommodate the transition between contraction and extension, however, are poorly understood for many orogens.

Several authors have documented contractional and extensional deformational features of Sardinian geology related to the Variscan Orogeny. Based on a synthesis of structural data, Helbing, Frisch, and Bons (2006) concluded that Sardinian basement rocks are related to the intra-Alpine terrane, and determined that the Variscan orogeny occurred in two general stages in the region: first, thrusting and second, normal faulting and exhumation. Similarly, the External Nappe zone was determined to have undergone contraction and later extension related to the Variscan orogeny (Carmignani et al., 1994). Conti, Carmignani, and Funedda (2001) further interpreted three phases of deformation: early contraction, followed by orogen parallel transport, then extension. Another significant structural feature is the Posada-Asinara Line, a potential Variscan suture zone related to the early phase of contraction that may extend across northern Sardinia (Conti et al., 2001).

Regional Setting

The Variscan belt of Western Europe was one of several collisional systems that were involved in the formation of Pangaea during the Paleozoic. As part of the 1,000 km broad and 8,000 km long system that extended from the Caucasus to the Appalachian and Ouachita Mountains, the Variscan Orogeny occurred in the Carboniferous during the later stages of Pangaea assemblage (Matte, 2001). Paleogeographic reconstructions place Sardinia at the suture zone between Laurentia-Baltica and Gondwana, suggesting that the mylonite zone known as the Posada-Asianara Line, may represent a part of a complex,

possibly anastomosing suture zone between these two supercontinents (Matte, 1986; Stampfli and Borel, 2002; Figure 3.1).

During the break-up of Pangaea, the Sardinia/Corsica block remained attached to the southern margin of Europe, however the position of reconstruction is still under debate. Rifting of the microplate containing Sardinia and Corsica did not occur until the late Miocene, pre- or syn-Alpine Orogeny (Gattacceca et al., 2007). The timing of rifting, along with the relative positioning of Sardinia to the west of the main zones of deformation for the Alpine Orogeny, are factors that allowed for the preservation of Variscan geology on Sardinia.

The Variscan exposures of Sardinia are divided into three major zones based on the degree of metamorphism and tectonic structure: the Axial/Internal Zone, the Nappe Zone and the Foreland Zone (Carmignani, Cocozza, Ghezzo, Pertusati, and Ricci, 1987; Figure 3.2). The Axial/Internal Zone is located in the northernmost section of the island, contains the Posada-Asinara Line, and comprises rocks metamorphosed to epidote/amphibolite facies. The Nappe Zone lies south of the Axial Zone and contains greenschist to non-metamorphosed units. The Arburesi thrust separates the Nappe and Foreland Zones, juxtaposing the autochthonous units of the Foreland Zone with the allochthonous units of the Nappe Zone.

The Nappe Zone of central Sardinia is composed of several nappes that were imbricated during the Variscan Orogeny (Carmignani et al., 1987). The Nappe Zone is further sub-divided into the northern Internal Nappes and the southern External Nappes. The External Nappe Zone consists of the Grighani Unit, the Rio Gruppa Unit, the Meano

Sardo Unit, the Gerrei Unit, and the Sarrabus Unit, from north to south (Carmignani et al., 1994). The first four nappes were structurally emplaced by south-directed thrust faults and the fifth, structurally highest nappe had a west-directed transport direction. The cause of change in transport directions is not known. The study area is located within the Gerrei unit, the third nappe sheet in the overall sequence of thrust emplacement (Figures 3.2 and 3.3).

Stratigraphy and Rock Unit Descriptions

Five rocks units comprise the Gerrei nappe; however, only four of these are found within the study area: the Cambrian San Vito Sandstone, Ordovician Volcanics, Gennemesa Formation, and the Silurian Shale (Figures 3.4 and 3.5). Devonian Limestone is present regionally in the Gerrei Unit, but not within the study area and will not be described (see Carmignani et al., 2001 for description).

Cambrian San Vito Sandstone

The San Vito Sandstone is composed of very fine to medium grained, tan to dark grey Cambrian sands. The age of this unit is based on fossil data regionally, including one locality near the study area (Carmignani et al., 2001). It is moderately to well sorted and cross-bedding is present locally. The unit has been metamorphosed under lower greenschist facies conditions. The San Vito can be distinguished in outcrop by its blocky appearance and darker color. Regionally seen in all of the thrust sheets, the San Vito Sandstone is the lowest stratigraphic unit. The depositional base of the unit is not visible.

Ordovician Volcanic Rocks

The Ordovician Volcanic unit is an undifferentiated package of shallow plutonic and volcanic rocks. The volcanic rocks contain variable amounts of quartz, potassium feldspar, and hornblende phenocrysts that range in size from 0.5-3 mm and occur within a dull light tan to light grey ash matrix. The plutonic rocks that compose the upper sections of the unit do not outcrop within the map area. The basal contact is sharp and unconformable with the Cambrian San Vito Sandstone. New U-Pb data constrain the age of the Ordovician volcanic unit (Chapter 2). U-Pb analyses of zircons from the lowermost part of the unit produced an age of 457.1 ± 0.14 Ma, indicating that deposition of this volcanic unit did not begin until the late Ordovician, which is later than previously thought. U-Pb analyses of zircons from a late porphyroid body that intrudes the upper sections of the volcanic unit yielded an age of 452.5 ± 0.1 Ma (Chapter 2), indicating magmatic activity ceased by this time.

The Gennemesa Formation

The Ordovician Gennamesa Formation is a light tan to grey arkosic sandstone. This unit is composed largely of reworked phenocrysts derived from the underlying volcanic rocks. Clear to milky quartz grains compose approximately 85% of the rock along with 1-3 mm, equant feldspars. Grain size varies throughout the unit from medium to very coarse sand. The unit is characterized by its cliff forming outcrops present through the center of the mapped area. The basal contact is not seen within the map area, but regionally is sharp and unconformable on the volcanics (Carmignani et al., 1994).

Silurian Shales

Stratigraphically highest in the study area are the Silurian Black Shales (Figure 3.3). The age of this unit is based upon the finding of graptolite fossils within the region (Carmignani et al., 2001). This unit is lustrous light to dark gray. The grain size is very fine and the rock displays well-developed penetrative foliation. The base of the unit is characterized by a less than 5m thick zone of darker gray color, blocky outcrops with a higher resistance to weathering. The basal contact is sharp with the Gennamesa Formation.

Structural Observations

A sharp thrust fault contact juxtaposes the Cambrian San Vito Sandstone and Ordovician Volcanic units against and structurally above the Silurian Shale (Figure 3.6). This contact separates the lower sheet (Arcu de su Bentu), which includes the shale and Gennemesa units, from the upper thrust sheet (Monte Lorna), which consists of the San Vito Sandstone and Ordovician Volcanic units. The fault ramps through the stratigraphy in the hanging wall block, cutting out the San Vito Formation to the south and placing the Ordovician Volcanic rocks directly in the hanging wall (Figures 3.4 and 3.5). This ramping geometry is consistent with overall south-directed transport during thrusting.

Bedding and tectonic foliation orientations display systematic variability within both the upper and lower sheets. The bedding orientations dip to the north in the northern portion of the area and to the south in the southern part, however, in the easternmost portion of the map area, bedding orientations dip to the east, consistent with the closure

of a fold (Figure 3.4). Pi analysis of bedding indicates a fold axis of 142°, 13° (Figure 3.7a). This regional scale feature is the Flumendosa antiform (Carmignani et al., 2001; Figure 3.5a).

Strong, complex penetrative deformation is present in the Silurian Shales, particularly within a few meters of the overlying fault contact. The bulk foliation and average stretching lineation taken within the unit are 314°, 22° to the NE and 276°, 01° respectively (Figures 3.7a and 3.7b). The bulk foliation was calculated from measurements on the north limb of the antiform where the kinematic observations were made (location A, Figure 3.4). Kinematic indicators observed on surfaces parallel to lineation and perpendicular to foliation include shear bands and S-C fabrics that are noted throughout the unit (Figure 3.8). Quartz veins have been stretched into boudins that are aligned with the S-C fabric (Figure 3.8). All of these kinematic observations are consistent with the top-to-the-east movement.

North-striking, high angle faulting is present throughout the lower sheet, juxtaposing the Gennemesa Formation against the Silurian shale in the western half of the map area and against different layers within the Gennemesa Formation in the eastern half of the map area. These faults are evident in map pattern from the alternating bands of the Silurian Shales and the Gennemesa Formation in the western half of the map area. Furthermore, cliff forming fault surfaces are recognizable within the Gennemesa Formation in the eastern half of the map area. Almost all of the faults are roughly N-S striking, high angle normal faults (Figure 3.4). Measurable fault surfaces give dips of 68° and 84° to the W-NW, however each of the faults dip roughly to the west while the

bedding planes dip north, east, or south in a regular pattern. The fault geometry and off-sets are consistent with domino-style block rotation with the top of the blocks rotating to the east (Figure 3.5b).

Brittle fractures that cross-cut the penetrative deformation are present, and particularly obvious in the shale. The average orientation of the fracture planes is 323°, 17° NNE (Figure 3.7c). Combined with the lineations found on the brittle fractures that indicate an average orientation of 016°, 30° and the stepping direction of the slickensides, these analyses and observations indicate a transport direction of top-to-the-NNE (Figure 3.7c).

The Gennemesa Formation also contains shear fractures with slickenlines that are in a different orientation than those in the Silurian Shales. The fracture surfaces are approximately vertical, with a strike of roughly 60°, and have subhorizontal slickenlines. Offsets of quartz veins along with the stepping direction of the slickenlines are consistent with a sinistral strike-slip movement. These localized features may be associated with the Alpine Orogeny as they are similar to recognized regional features associated with this later event.

Table 3.1. U-Th-Pb Isotopic Data for Samples SAR-07-01 and SAR-07-04.

							Radiogenic Isotope Ratios								Isotopic Ages					
Sample	Th/U	$^{206}Pb^*$ x10^{-13} mol	mol % $^{206}Pb^*$	Pb^*/Pb_c	Pb_c (pg)	$^{206}Pb/^{204}Pb$	$^{208}Pb/^{206}Pb$	$^{207}Pb/^{206}Pb$	% err	$^{207}Pb/^{235}U$	% err	$^{206}Pb/^{238}U$	% err	corr. coef.	$^{207}Pb/^{206}Pb$	±	$^{207}Pb/^{235}U$	±	$^{206}Pb/^{238}U$	±
(a)	(b)	(c)	(c)	(c)	(c)	(d)	(e)	(e)	(f)	(e)	(f)	(e)	(f)		(g)	(f)	(g)	(f)	(g)	(f)
SAR-07-01																				
z3	0.147	0.2885	93.84%	4	1.56	302	0.046	0.056308	1.678	0.573005	1.812	0.073805	0.296	0.516	464.5	37.2	459.96	6.70	459.04	1.31
z4	0.214	0.3687	97.01%	9	0.93	622	0.067	0.056334	0.814	0.571245	0.891	0.073544	0.102	0.775	465.6	18.0	458.82	3.29	457.47	0.45
z5	0.776	0.3896	95.02%	6	1.68	374	0.245	0.052250	1.378	0.346000	1.473	0.048027	0.145	0.681	296.4	31.4	301.71	3.84	302.40	0.43
z7	0.227	1.6181	99.36%	44	0.86	2903	0.071	0.056093	0.151	0.570125	0.187	0.073715	0.058	0.712	456.1	3.4	458.10	0.69	458.50	0.26
z9	0.725	0.8941	98.03%	16	1.47	946	0.229	0.052431	0.535	0.347054	0.582	0.048007	0.085	0.605	304.2	12.2	302.50	1.52	302.28	0.25
z10	0.301	0.4738	96.87%	9	1.26	594	0.095	0.052475	0.812	0.347564	0.877	0.048038	0.110	0.628	306.2	18.5	302.89	2.30	302.46	0.32
SAR-07-04																				
z2	0.519	3.4699	99.60%	76	1.14	4666	0.164	0.052081	0.113	0.327528	0.145	0.045611	0.054	0.720	288.96	2.57	287.68	0.36	287.52	0.15
z4	0.756	2.2333	99.50%	65	0.92	3742	0.239	0.052022	0.141	0.327207	0.172	0.045618	0.054	0.677	286.39	3.22	287.43	0.43	287.56	0.15
z6	0.687	3.9103	99.39%	52	1.99	3029	0.218	0.052053	0.163	0.326734	0.194	0.045525	0.055	0.652	287.73	3.73	287.07	0.48	286.99	0.15
z7	0.731	1.4693	99.54%	70	0.55	4085	0.231	0.051996	0.162	0.326948	0.189	0.045604	0.060	0.576	285.25	3.70	287.23	0.47	287.48	0.17
z8	0.671	1.8232	99.67%	96	0.50	5622	0.212	0.052025	0.166	0.326726	0.189	0.045548	0.066	0.500	286.51	3.79	287.06	0.47	287.13	0.19
z9	0.915	1.1302	95.95%	8	3.94	455	0.290	0.052163	0.576	0.327304	0.625	0.045508	0.073	0.702	292.57	13.16	287.51	1.57	286.88	0.21
z10	0.788	3.2918	99.69%	104	0.85	5944	0.249	0.052034	0.096	0.327305	0.132	0.045621	0.057	0.754	286.91	2.20	287.51	0.33	287.58	0.16
z11	0.324	3.9285	99.82%	157	0.60	10091	0.103	0.052167	0.067	0.332046	0.108	0.046164	0.056	0.853	292.72	1.54	291.13	0.27	290.93	0.16
z12	0.956	0.7100	99.29%	47	0.42	2605	0.303	0.052062	0.234	0.326886	0.277	0.045538	0.102	0.575	288.15	5.35	287.19	0.69	287.07	0.29
z13	0.662	1.1714	97.64%	13	2.33	787	0.209	0.051904	0.532	0.325995	0.581	0.045552	0.100	0.553	281.20	12.17	286.50	1.45	287.15	0.28
z14	0.307	1.2125	99.54%	62	0.46	4048	0.097	0.052119	0.139	0.332254	0.180	0.046235	0.078	0.678	290.62	3.18	291.29	0.46	291.37	0.22

(a) z1, z2 etc. are labels for fractions composed of single zircon grains or fragments; all fractions annealed and chemically abraded after Mattinson (2005).

(b) Model Th/U ratio calculated from radiogenic 208Pb/206Pb ratio and 207Pb/235U age.

(c) Pb* and Pbc represent radiogenic and common Pb, respectively; mol % $^{206}Pb^*$ with respect to radiogenic, blank and initial common Pb.

(d) Measured ratio corrected for spike and fractionation only. Mass fractionation correction of 0.22 ± 0.02 (1-sigma) %/amu (atomic mass unit) was applied to all single-collector Daly analyses, based on analysis of NBS-981 and NBS-982.

(e) Corrected for fractionation, spike, and common Pb; all common Pb was assumed to be procedural blank: 206Pb/204Pb = 18.60 ± 0.80%; 207Pb/204Pb = 15.69 ± 0.32%; 208Pb/204Pb = 38.51 ± 0.74% (all uncertainties 1-sigma).

(f) Errors are 2-sigma, propagated using the algorithms of Schmitz and Schoene (2007) and Crowley et al. (2007).

(g) Calculations are based on the decay constants of Jaffey et al. (1971). 206Pb/238U and 207Pb/206Pb ages corrected for initial disequilibrium in 230Th/238U using Th/U [magma] = 4.

Geochronology

Rhyolitic Dike (SAR-07-01)

A porphyritic rhyolite dike intruded the Silurian Shale unit at location A (Figure 4). The dike ranges from several centimeters to a half a meter thick and intruded just below the contact between the San Vito Sandstone and the Silurian Shales,with no outcrop showing the dike crosscutting the contact. The intrusion contains none of the penetrative deformation present in the surrounding shale; however, the brittle fractures that cross-cut the penetrative deformation discussed above also offset the dike, as seen in Figure 3.9. U-Pb ID-TIMS ages for six single zircon grains were analyzed from this dike (Table 3.1). The results cluster at two ages. The older population of Ordovician zircons (ca 457-459 Ma) may have been inherited (Figure 3.10a). The younger population yields a weighted mean $^{206}Pb/^{238}U$ date of 302.36 ± 0.36 Ma which is interpreted as the age of emplacement. This age provides a minimum age constraint for the event that produced the penetrative deformation within the shale and a maximum age for the N-dipping brittle fracture deformational event.

Sardic Batholith (SAR-07-04)

A late to post-Variscan granitoid of the Sardic Batholith outcrops approximately two kilometers north of San Vito at mile marker 1/85 on the highway from San Vito to Ballau. This location is a few kilometers to the southeast of the study area. The composition of this pluton is approximately 45% potassium feldspar, 25% plagioclase, 25% quartz and 5% biotite. This rock unit lacks any deformational fabric. Eleven single

grain zircons from this unit were analyzed by U-Pb ID-TIMS. All are effectively concordant grains cluster with three clusters of approximately 291, 287.5, and 287 Ma (Table 3.1). The four youngest zircons yielded a weighted mean $^{206}Pb/^{238}U$ date of 287.03 ± 0.89 Ma (Figure 3.10b), which is interpreted as the crystallization oage of the granite and may be interpreted as a minimum age for deformation related to the Variscan Orogeny.

Interpretations

D1: Contraction and Thrust Imbrication

Thrust juxtaposition of the Cambrian San Vito Sandstone and the Silurian Shales represents the initial phase of deformation within the map area (D1). Regional relationships from outside the mapped area suggest a top-to-the-south thrust direction and therefore this is assumed to be the thrusting direction for the mapped area as well. This transport direction is supported by the ramping direction in the hanging wall of the map area. This N-S oriented contractional event can be attributed to the amalgamation of the nappe stack during the main phase of the Variscan Orogeny. Previous geochronology to constrain this phase of deformation was calculated from in situ Ar/Ar analyses of a micaschist in NE Sardinia (Di Vincenzo, Carosi, and Palmeri, 2004). The analyses yielded an age of apporximately 340-315 Ma that is interpreted as the maximum thickening in the Internal Nappes, however this is the only known estimate for constraining the timing of this phase of deformation.

D2: N-S Contraction and E-W Upright Folding

The systematic change in orientations of the bedding foliation and D1 thrust reflects the regional scale antiformal feature known as the Flumendosa Antiform (Figure 3.5a). The exposure of the closure of the fold in the eastern edge of the study area (Figure 3.4), along with the gently east plunging hinge line, indicate a second N-S oriented contractional event (D2). The axial surface traces roughly E-W and the fold has an upright geometry. Field relationships could not discern whether D2 was a continued expression of the same progressive contractional event of D1. However, because the D1 thrust and both the upper and lower sheets are affected, the folding occurred after D1 thrusting of the upper thrust sheet. There is no previous geochronology for this phase of deformation.

D3: Orogen-parallel Transport

The third and previously undocumented phase of deformation is expressed by both the E-directed shearing in the Silurian Shale and the domino-style faulting and block rotation of the Gennemesa Formation in the lower sheet. These deformational features are consistent with a transition to orogen-parallel movement. Both suggest top-to-the-east reactivation of the D1 fault zone. The deformation appears to have been localized in the relatively weak shale of the lower sheet as there was no visible deformation related to this phase within the San Vito or volcanic units. The U-Pb age of the rhyolitic dike (SAR-07-01) provides a minimum age for this phase of deformation of 302.36 ± 0.18 Ma.

D4: N-S Extension

The fourth phase of deformation is a north-south oriented extensional event that postdates the three other phases related to the Variscan Orogeny (Figure 3.12). The slickensides on the fault surface are a new expression of the N-S extension that were previously interpreted as related to the thrusting event of D1 (Carmignani et al., 2001). N-S extensional reactivation of the thrust surface on the south dipping limb of the antiform would have had similar (top-to-the-S) movement as the original thrust, and be difficult to recognize. Therefore, our analysis was focused on the north dipping limb. The stepping of the slickenfibres is not consistent with south directed thrust transport on the northern dipping limb of the antiform (Figure 3.11), but rather with late, top-to-the-north movement. Reactivation of the D1 fault surface as a normal fault may have been facilitated by the rotation and steepening of the fault along the north limb of the D2 antiform. The U-Pb age of the Sardic Batholith of 287.03 ± 0.09 Ma provides a minimum age for D4 extension and the effective end of deformation related to the Variscan Orogeny.

Discussion

The deformational sequence interpreted for the Flumendosa area includes a transitional phase from contraction to extension through orogen-parallel movement. Orogen-parallel movement was referenced by Conti et al. (2001) as associated with the emplacement of the Sarrabus Unit. This was the fifth nappe sheet and records a change in transport direction from south directed emplacement to west directed emplacement.

Thus, the authors interpreted the orogen-parallel movement to be top-to-the-west movement related to contractional thrusting and nappe emplacement. However, this idea relies on the assumption that the Sarrabus Unit was thrust overtop of the Gerrei Unit and has since eroded away on the north side of the Flumendosa Antiform. In the present study area, orogen-parallel movement was interpreted as a D3 phase of deformation, and the kinematic indicators suggest top-to-the-east movement, rather than top-to-the-west as suggested by Conti et al. (2001). At least three possibilities exist: 1) multiple discrete phases of orogen-parallel movement, with changing transport directions; 2) a single phase of orogen-parallel deformation with heterogeneous strain expressed as local E or W-directed transport; or 3) strike-slip dominated strain with local zones of either transtension or transpression. Therefore, with the assumption that the orogen-parallel movement is still associated with the emplacement of the Sarrabus Unit, the nature of the contact needs to be reinterpreted. The juxtaposition of the Sarrabus Unit against the Gerrei Unit is thus interpreted to be a strike-slip fault, not a thrust fault.

Matte (1991) proposed a model for the compatibility of strike-slip and thrust faults in a convergent plate setting that can be used to interpret the significance of the strike-slip contact. Figure 3.13 is the cartoon sketch modified from Matte (1991) used for the Ibero-Armorican (a) and West Himalayan (b) vergences. Strike-slip faults are active along the sides of the leading edge as the converging plate (indentor) continues to migrate into the stationary plate. The fan-like nature of these boundaries allows for these strike-slip zones to occur. The Ibero-Armorican vergence is a result of the collision of the promontory of northern Gondwana with Laurentia or the Hun Superterrane during the

Variscan Orogen. The paleogeographic reconstructed position of Sardinia against mainland Europe places the island at the margin of the indenting promontory (Figure 3.13c). Therefore the emplacement of the Sarrabus Unit can be associated with later stages in the evolution of convergence of the Gondwanan promontory when strike-slip movement occurred along the margins of the indentor. This late stage emplacement created a high-angle, strike-slip zone with the contact between the Sarrabus Unit and the Gerrei Unit along the southern limb of the Flumendosa Antiform and top-to-the-west thrust direction of the Sarrabus Unit over the Foreland Zone. The strike-slip motion would have had dextral shear sense which coupled with top-to-the-east movement of the upper sheet relative to the lower sheet in the study area. This shear sense is supported by evidence for the D3 deformational event.

If valid, this reinterpretation also has significant implications for the timing of emplacement of the Sarrabus Unit. Previous work assumed that this unit was emplaced prior to the contractional event that folded the region into the Flumendosa Antiform and was subsequently eroded in the area north of the antiform (Carmignani et al., 1994; Conti et al., 2001). However, there is no field evidence to support the assumption that the Sarrabus Unit originally extended over the antiform to the north. Thus, the basis for interpreting the timing and nature of emplacement of the Sarrabus Unit is equivocal. An alternative is that the unit was emplaced by strike-slip movement after the formation of the Flumendosa Antiform.

Conclusions

The sequence of block diagrams seen in Figures 13a-13d represents the principle findings that there are four phases of deformation expressed within this region related to the Variscan Orogeny. The first two (D1, D2) were contractional events with north-south oriented shortening as evidenced by the thrust contact between the upper and lower sheets and the Flumendosa Antiform. The latter two deformational phases were extension in orthogonal directions, as D3 was orogen-parallel extension (at least locally), and D4 represents extension in a N-S orientation. It is the reinterpretation of the slickensides and the presence of the brittle fractures that cross-cut the penetrative deformation that require a late phase N-S extensional event. Early contractional events control the geometry and kinematics of the later phases of extension. The thrusting of the San Vito Sandstone over the less competent Silurian Shales localized the deformation within the shales and provided a zone of weakness for the top-to-the-east movement to reactivate the D1 fault surface. Similarly, the steepening of the fault surface as a result of the formation of the Flumendosa Antiform facilitated the reactivation of the D1 fault surface in a normal fault sense on each limb (D4).

The recognition of top-to-the-east orogen-parallel movement requires reevaluation of the nature and timing of emplacement of the Sarrabus Unit. This study proposes that the contact between the Gerrei and Sarrabus Units is a dextral strike-slip fault, not a thrust fault as previously interpreted. This shear sense is associated with the position of southeastern Sardinia at the margin of the promontory of northern Gondwana that acted as an indentor during late stages of orogenic evolution. The implications for

the timing of emplacement are also reinterpreted in this study as later than previously thought as the emplacement happened after the two stages of contraction, not as a later stage of the first contractional event.

Figures

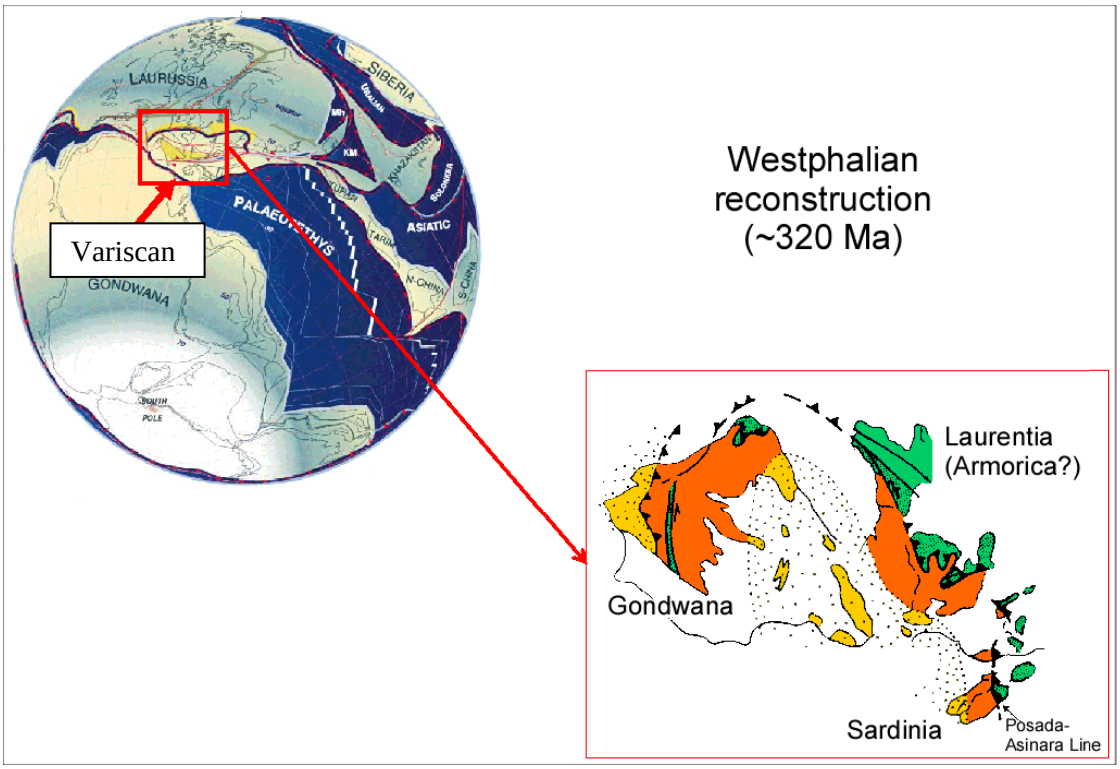

Figure 3.1: Paleogeographic reconstruction of Sardinia within the Variscan orogen based on Matte (1986) and Stampfli and Borel (2002).

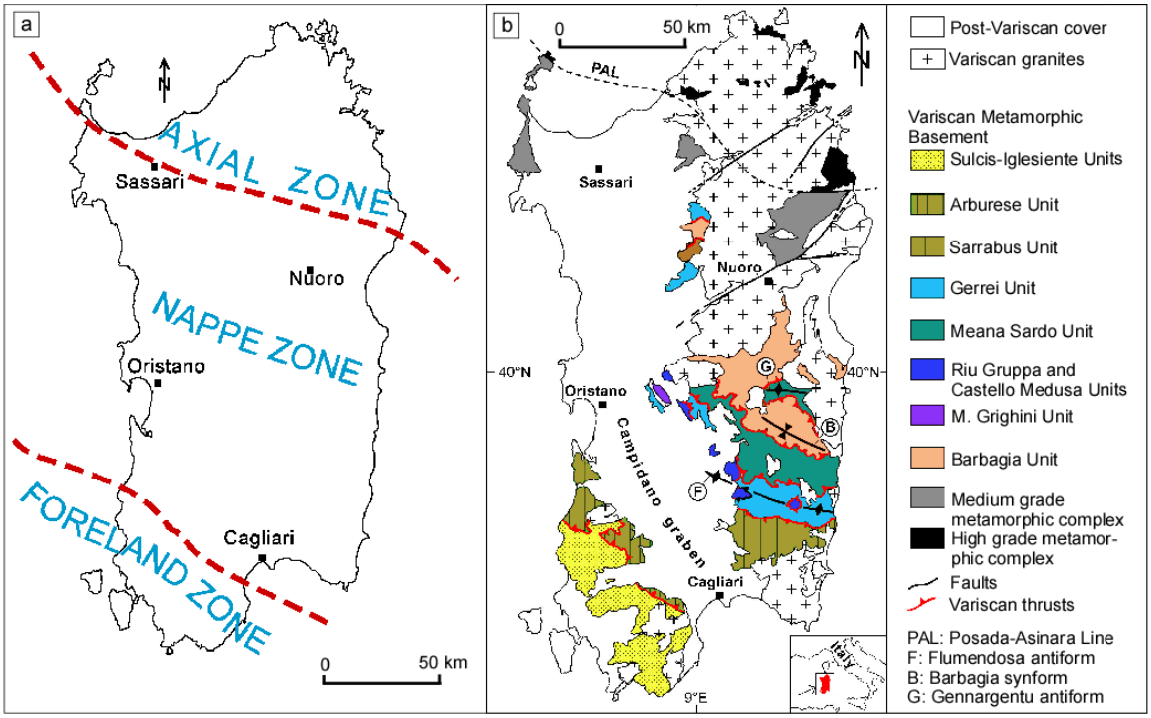

Figure 3.2: Tectono metamorphic zonation of Variscan metamporphism (a) and distribution of exposure (b) on Sardinia composed by Carmignani et al. (1987).

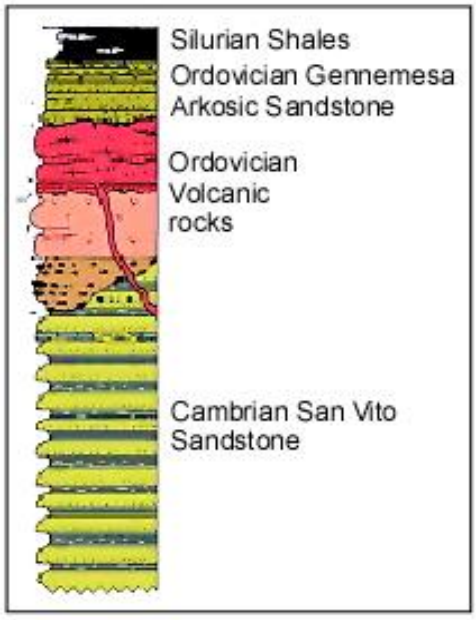

Figure 3.3: Simplified stratigraphic column illustrating the sequence of the rock units in the mapped area. Modified from Carmignani, et al. (1994).

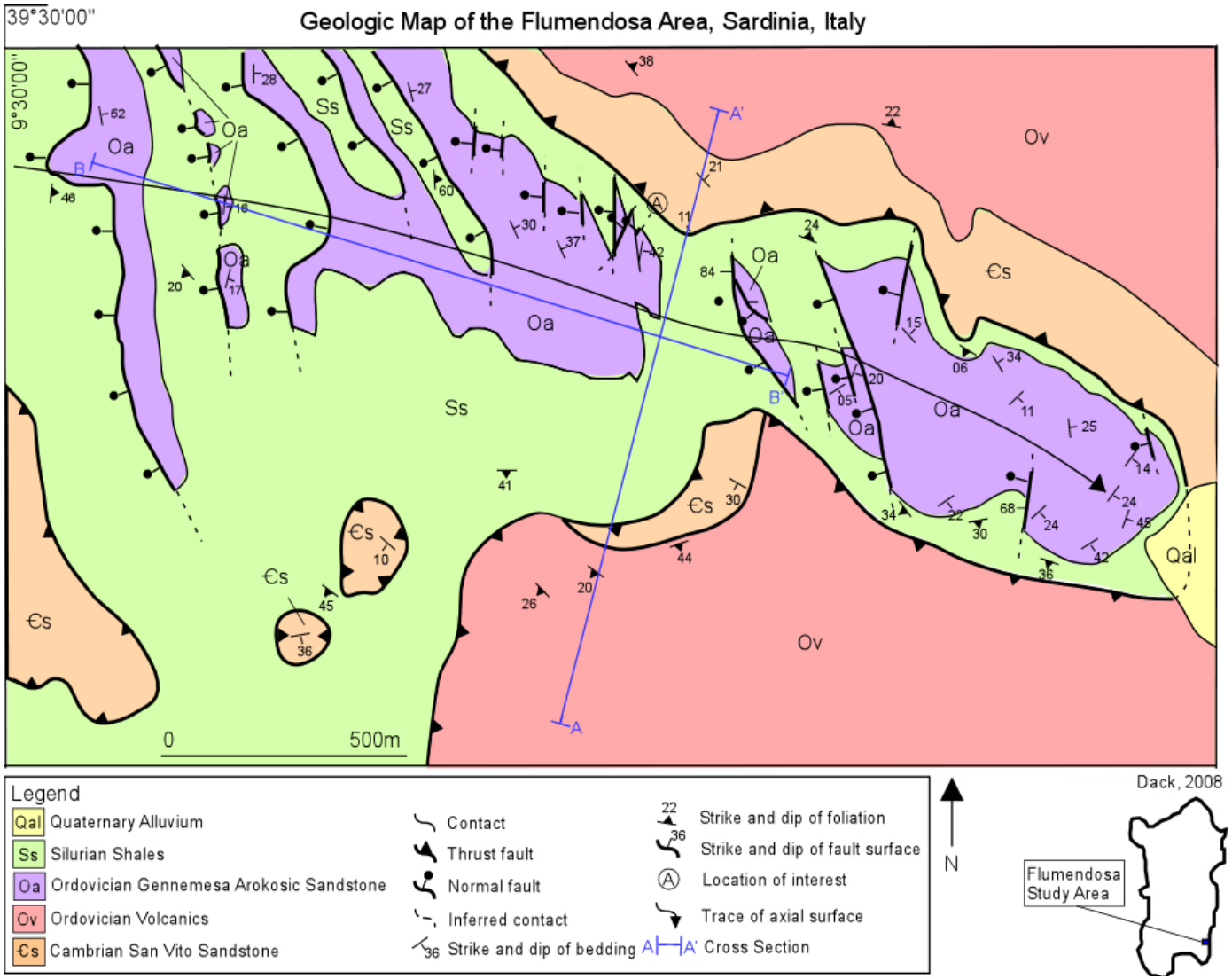

Figure 3.4: Simplified geologic map of the Flumendosa area of southeastern Sardinia. Cross sections are found in Figure 3.5.

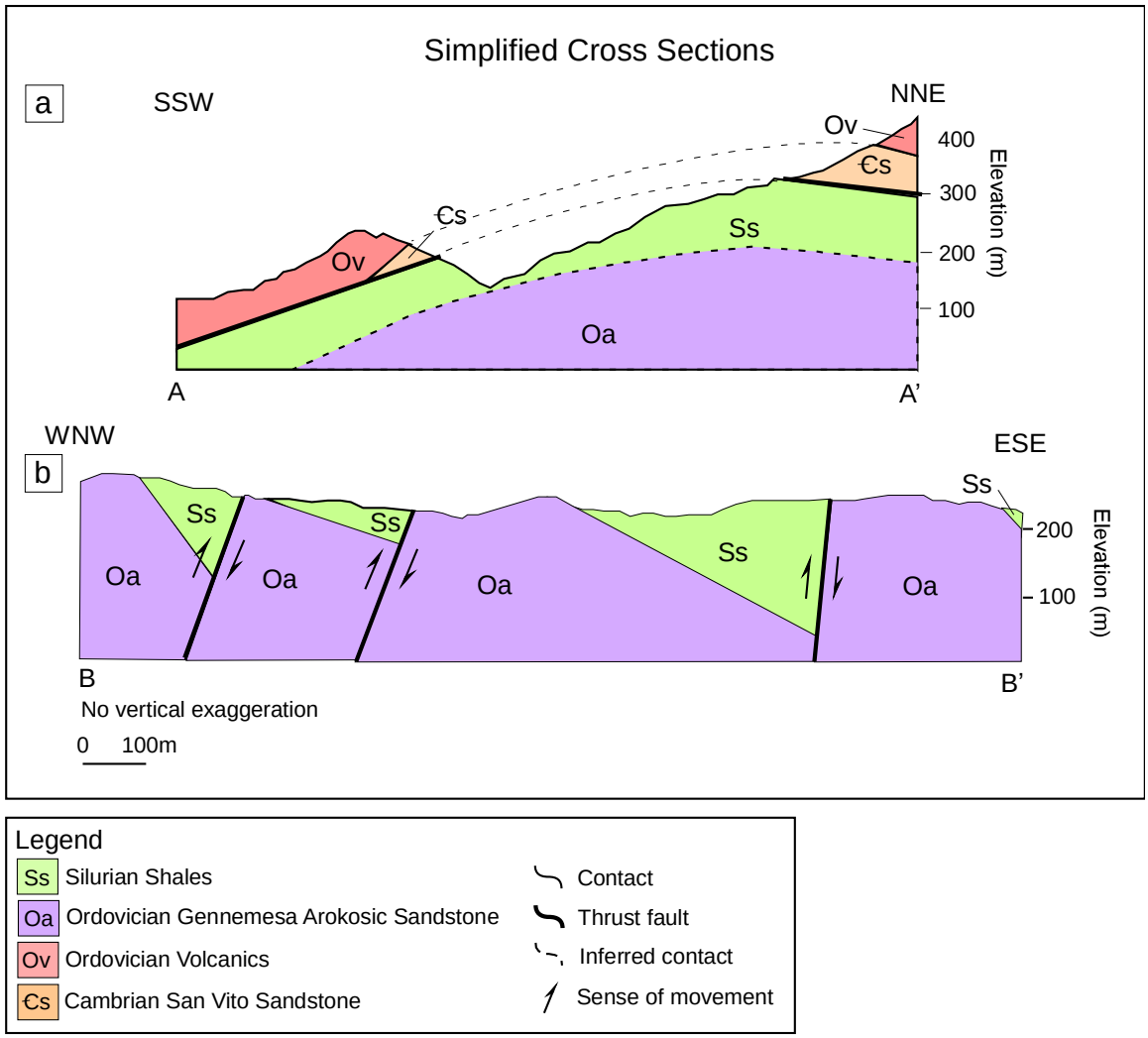

Figure 3.5: Simplified cross sections for transects A-A' (a) and B-B' (b) from Figure 3.4.

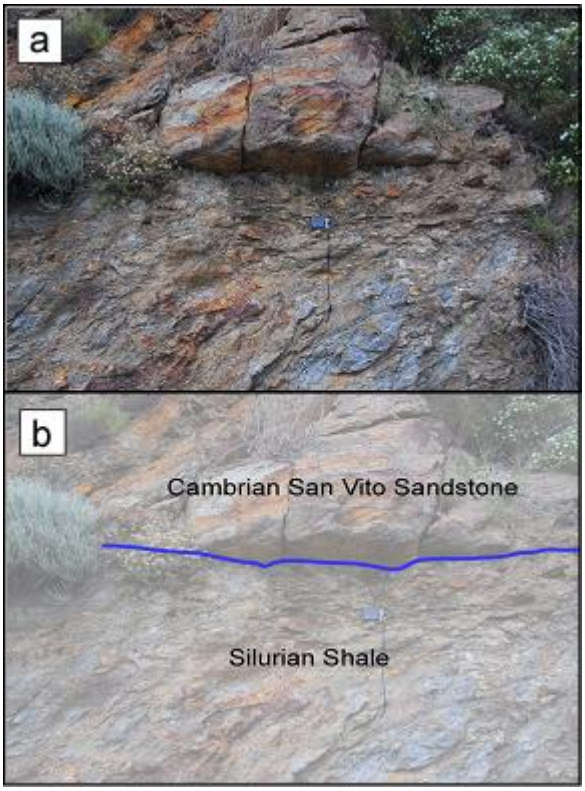

Figure 3.6: Field photograph (a) and interpretive sketch (b) show the thrust contact between the Cambrian San Vito Sandstone and the Silurian shale (view to the north, location A in Figure 3.4).

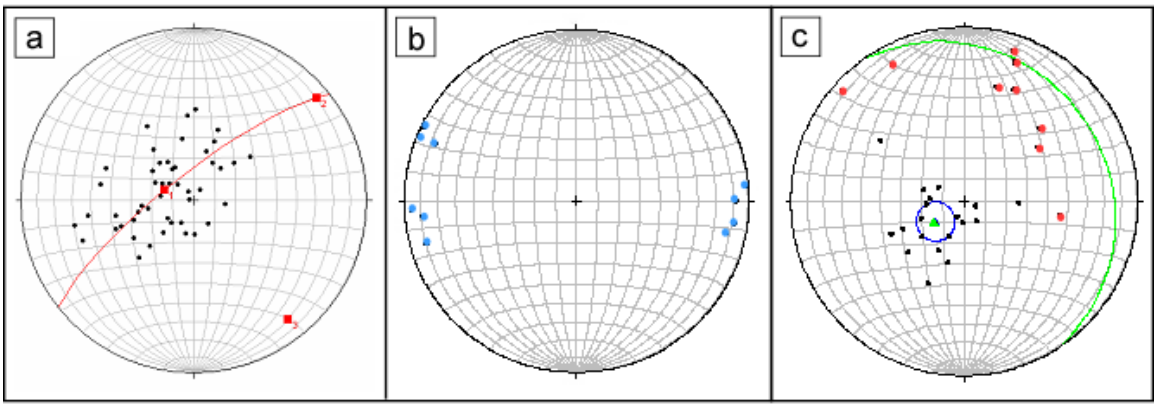

Figures 3.7: (a) Pi-analysis of the bedding orientations of both the lower and upper thrust sheets with measurements included from all four of the mapped units. The best-fit fold axis is 142°, 13°;(b) lineations within the shale unit that show the E-W trending shearing in response to the top-to-the-E movement of the upper sheet; (c) poles to fracture surfaces, vectoral mean yields an average orientation of 323°, 73° for the brittle fracture

measurements contained within the shale unit shown in the green great circle. The lineations on the fracture surfaces are shown in the red circles.

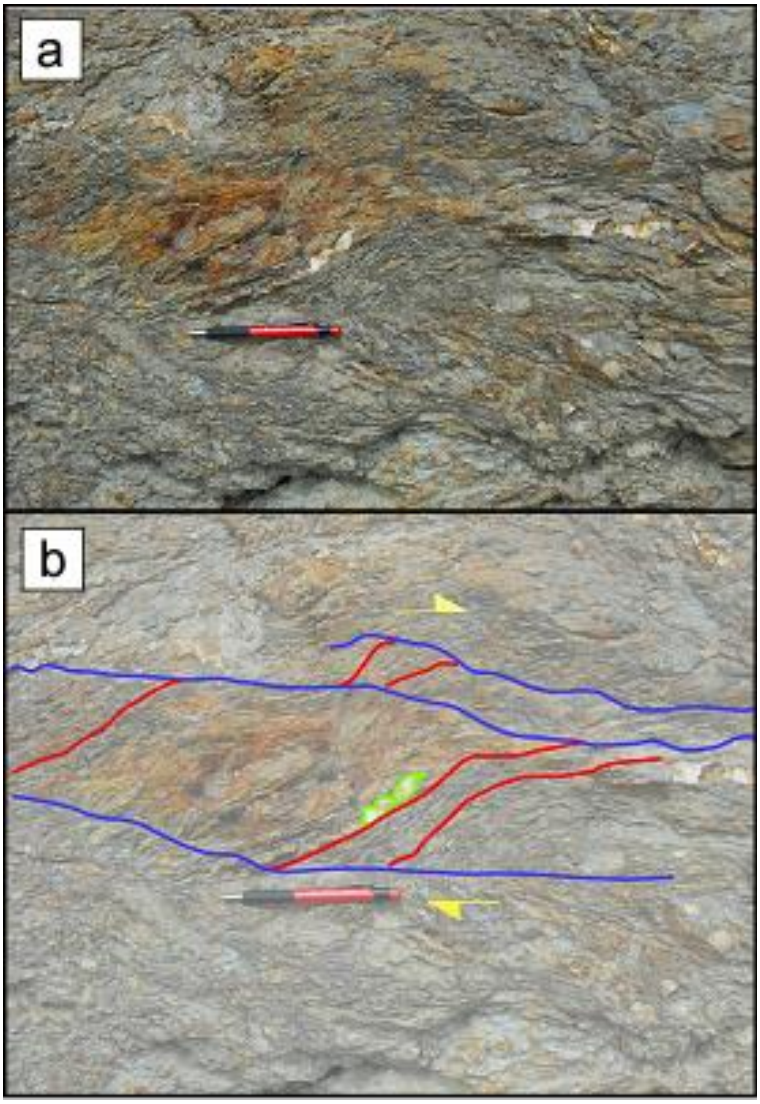

Figure 3.8: (a) field photo with the overlay of the observations in (b). The arrows indicate the sense of movement as dextral shear that is consistent with the S-C fabric and the stretching and wing patterns observed in the quartz veins. View looking north at outcrop surfaces oriented parallel to D3 stretching lineation and perpendicular to foliation.

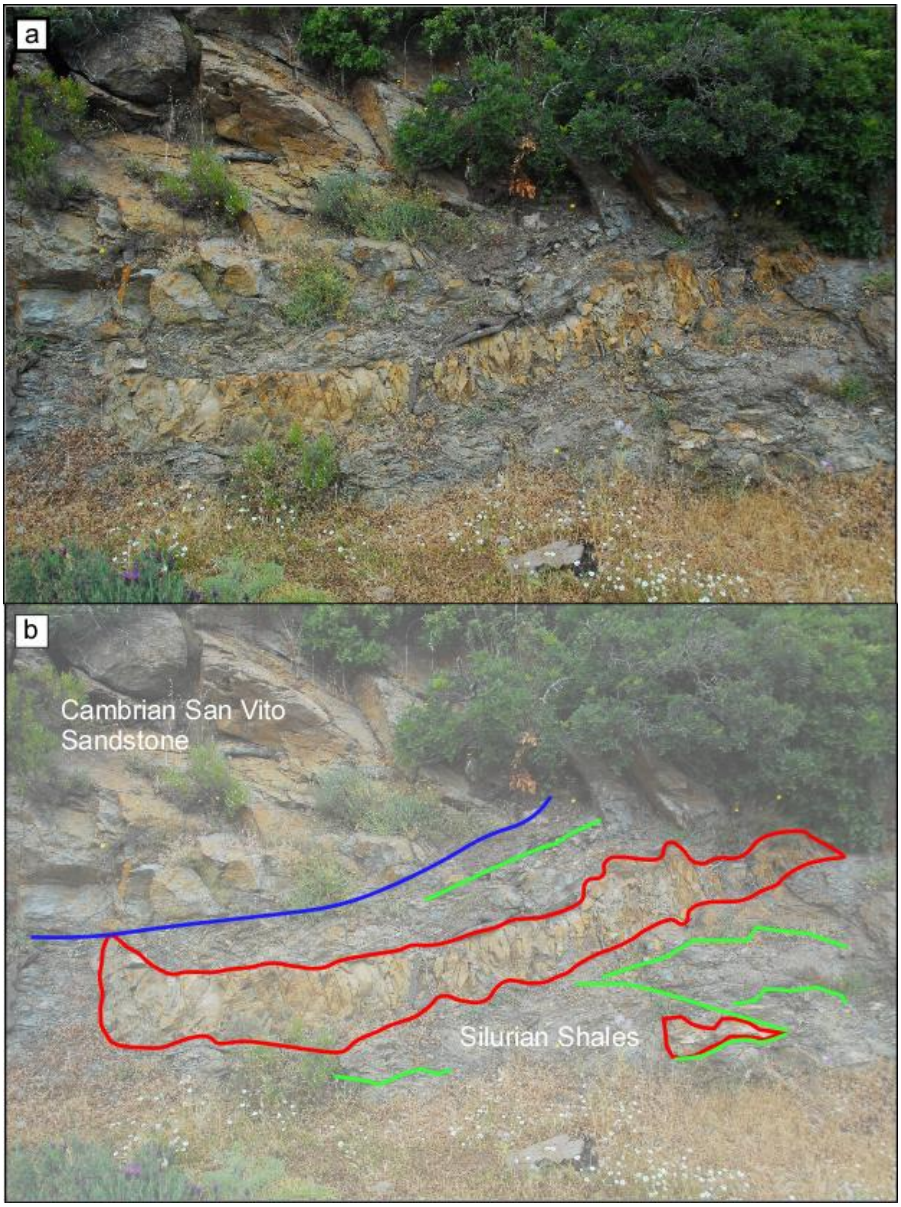

Figure 3.9: Visible in this field photo (a) and interpretation (b) is the dike (outlined in red) that contains none of the penetrative deformation that is included within the surrounding shale and is offset by the brittle fractures (green). The blue line represents the contact between the Cambrian sandstone and Silurian shales.

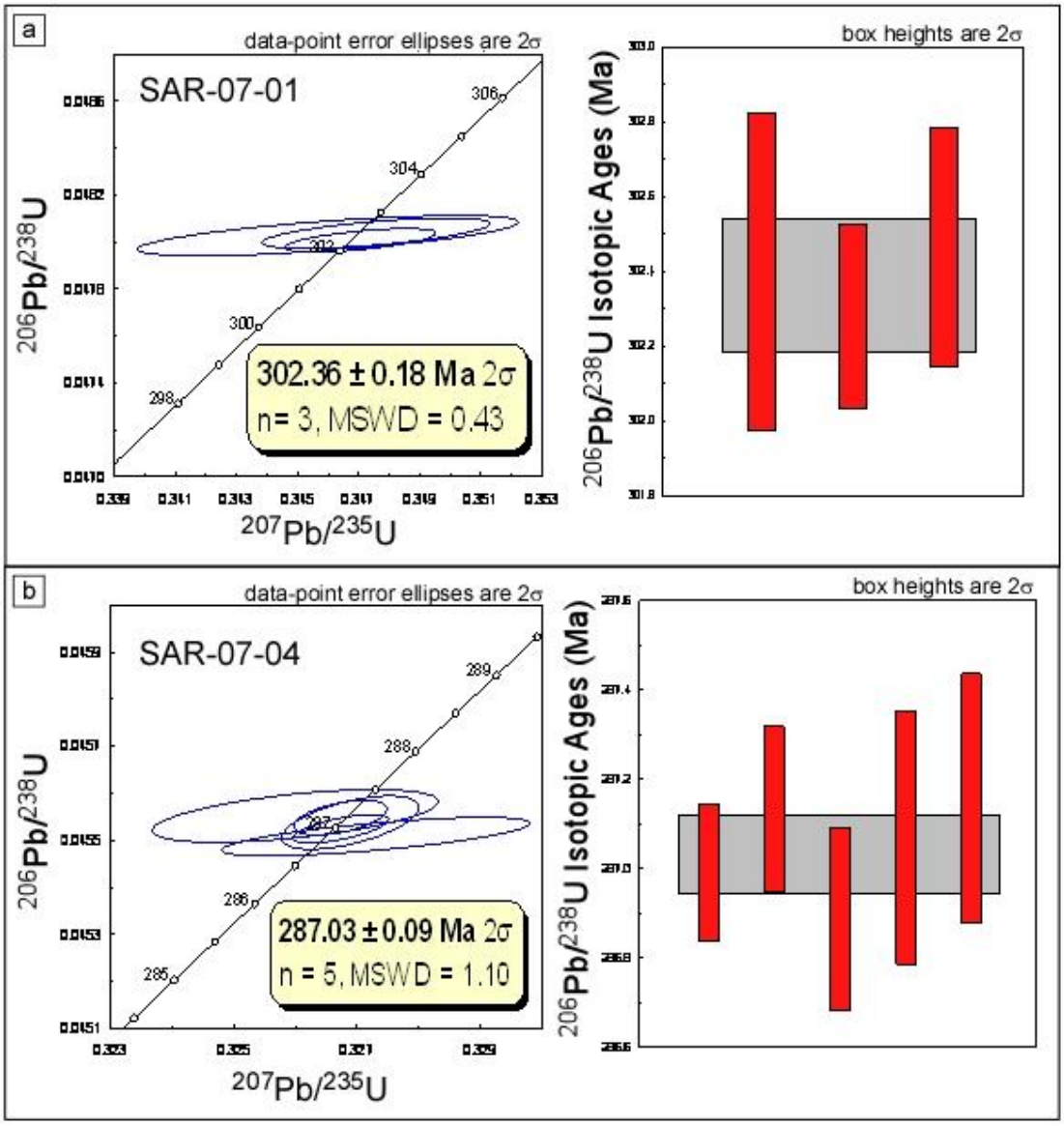

Figure 3.10: Concordia plots of U-Pb zircon analyses from the: (a) post-penetrative deformation intruded dike and (b) post-Variscan emplaced batholith.

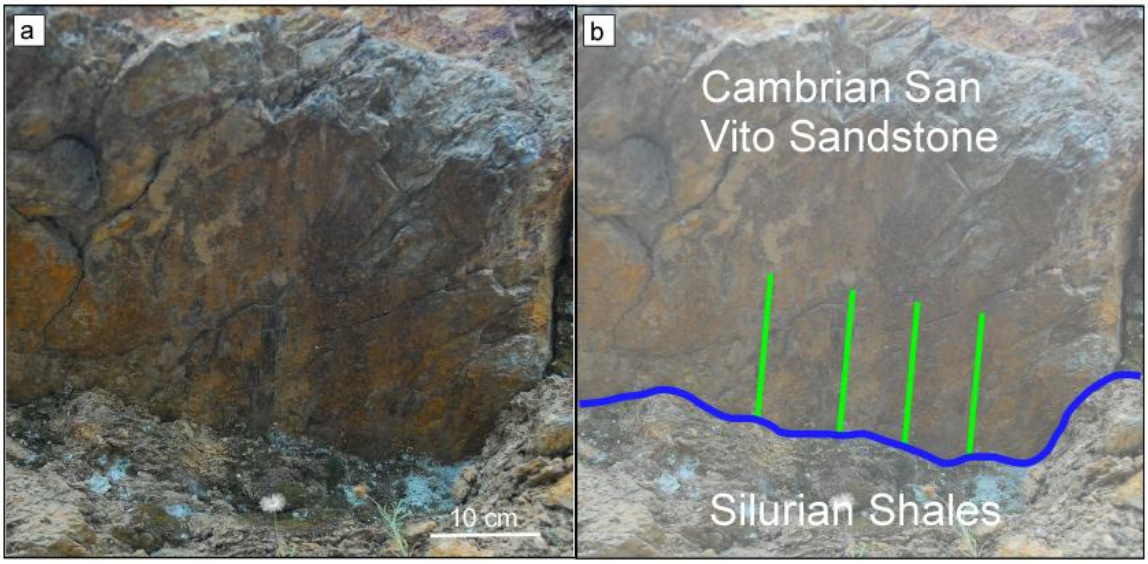

Figure 3.11: This picture was taken looking up at the contact surface from Figure 3.6a to focus on the slickenslides that are preserved on the surface.

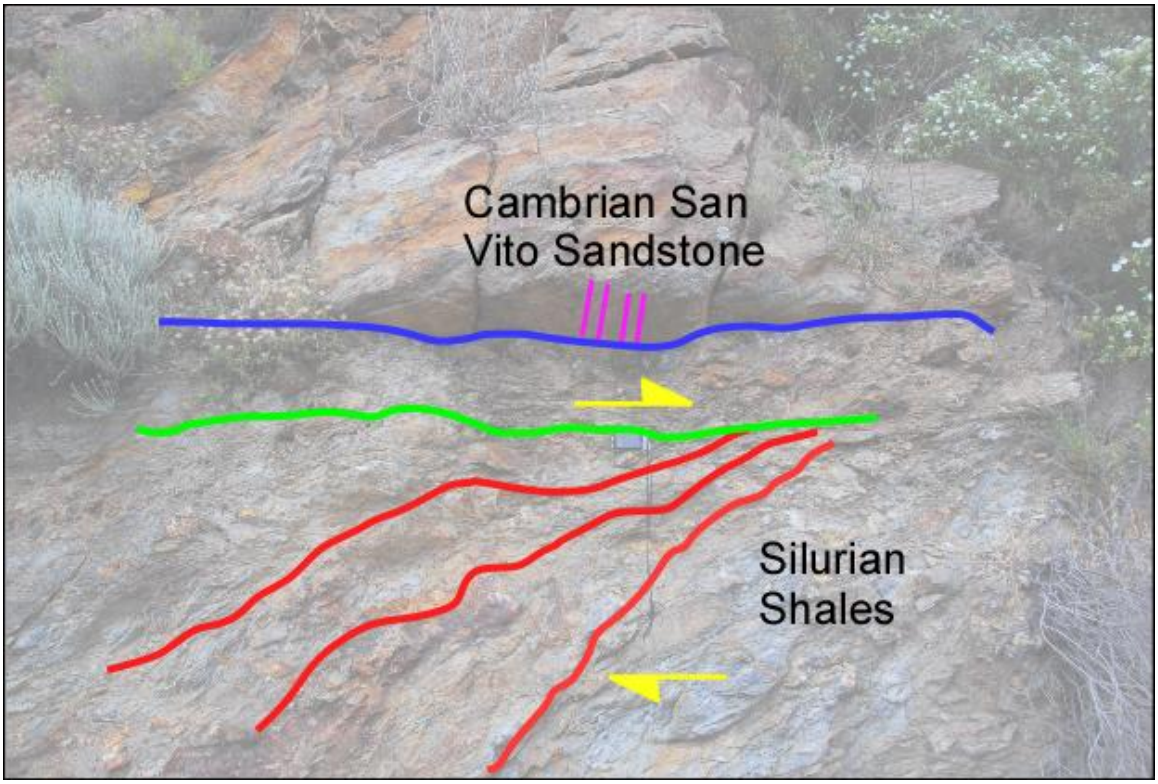

Figure 3.12: Field photograph looking north at location A in Figure 3.4. Traces illustrate features related to three of the four phases of deformation. D1 thrust contact (blue); D3 E-directed penetrative shearing (green, red, and yellow); and D4 top-to-the-NNE reactivation of fault surface based on slickenfibre kinematics (pink).

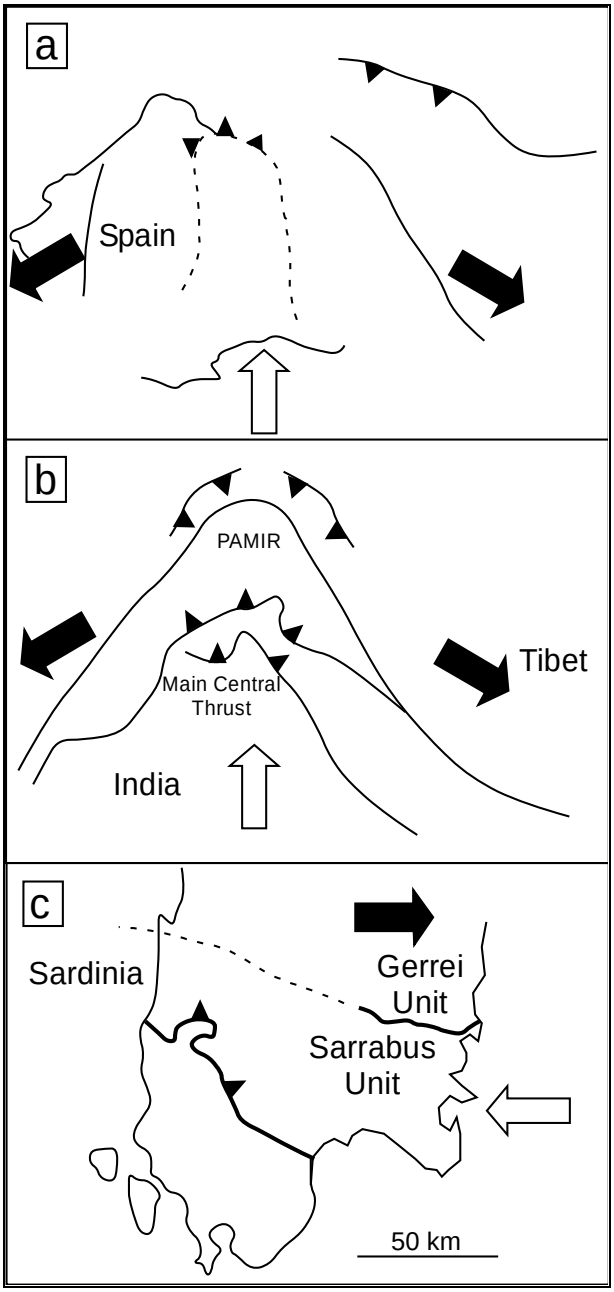

Figure 3.13: Sketch maps that illustrate relationship between thrusts and strike-slip faults in a fan-like converging system. The arrows indicate direction of movement. The examples above are from (a) the Ibero-Armorican, (b) the West Himalayan vergences (modified from Matte, 1991). A sketch of the proposed strike-slip contact between the Gerrei and Sarrabus Unit (c).

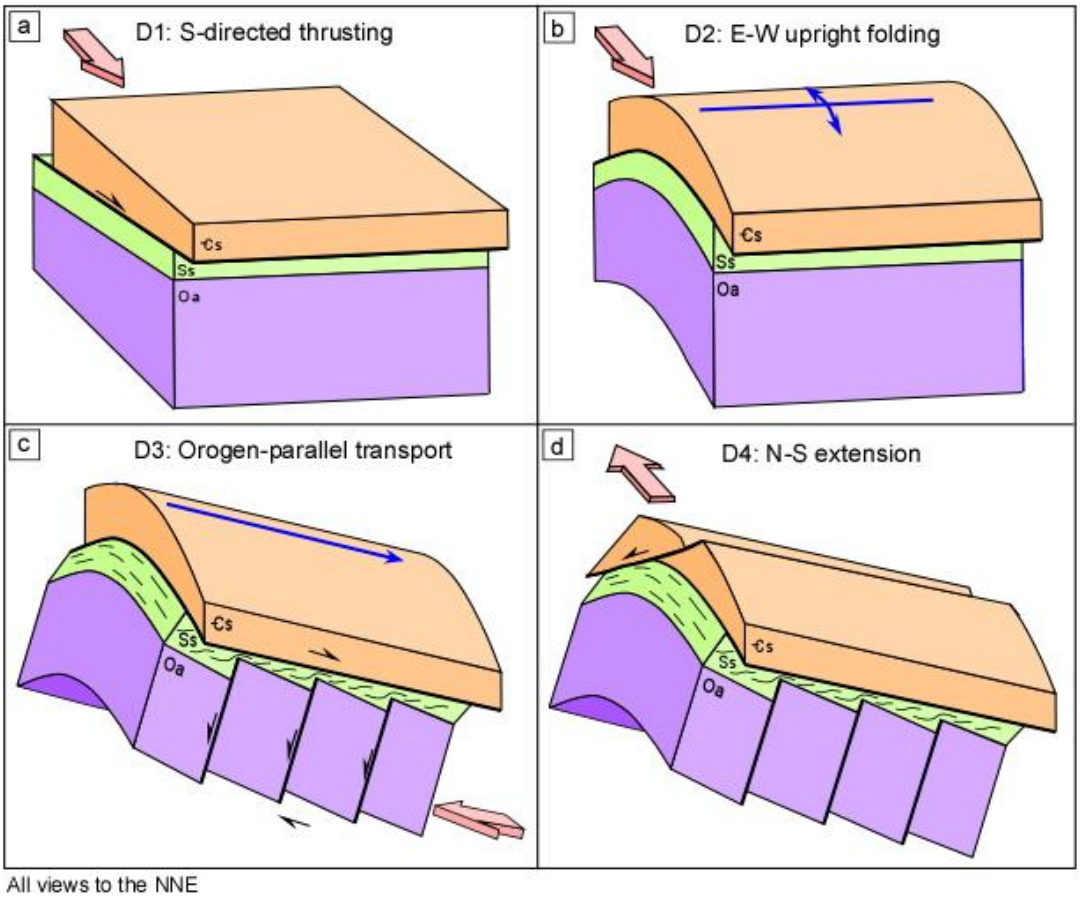

Figure 3.14: Block diagrams illustrating a conceptual sequence for the four phases of deformation that affected the Flumendosa region.

Works Cited

Anderson, T.B., 1998, Extensional tectonics in the Caledonides of southern Norway, an overview: Tectonophysics, v. 285, p. 333–351.

Burchfiel, B.C., Ziliang, C., Hodges, K.V., Yuping, L., Royden, L.H., Chanrong, D., and Jiene, X., 1992, The South Tibetan Detachment System, Himalayan Orogen: extension contemporaneous with and parallel to shortening in a collisional mountain belt: Spec. Pap. Geol. Soc. America, v. 269.

Carmignani, L. and 15 others, 2001, Foglio 549, Carta Geologico di Muravera, Regione Autonoma della Sardegna, scale: 1:50,000: Carta Geologica D'Italia, Servizio Geologico D'Italia.

Carmignani, L., Carosi, R., Di Pisa, A., Gattiglio, M., Musumeci, G., Oggiano, G. and Pertusati, P.C., 1994, The Hercynian chain in Sardinia (Italy): Geodinam. Acta., v. 7, p. 31-47.

Carmignani, L., Cocozza, T., Ghezzo, C., Pertusati, P.C., and Ricci, C.A., 1987, Structural Model of the Hercynian Basement of Sardinia. 1:500,000: Stabilimento L. Salomone, CNR, Progetto Finalizzanto Geodinamica, Roma.

Carmignani, L. and Kligfield, R., 1990, Crustal extension in the northern Appenines: the transition from compression to extension in the Alpi Apuane core complex: Tectonics, v. 9, p. 1275-1303.

Conti, P., Carmignani, L., and Funedda, A., 2001, Change of nappe transport direction during the Variscan collisional evolution of central-southern Sardinia (Italy): Tectonophysics, v. 332(1-2), p. 255-273.

Crowley, J.L., Schoene, B., and Bowring, S.A., 2007, U-Pb dating of zircon in the Bishop Tuff at the millennial scale: Geology, v. 35, p. 1123-1126.

Di Vincenzo, G., Carosi, R., and Palmeri, R., 2004, The relationship between tectono-metamorphic evolution and argon isotope records in white mica: constraints from in situ $^{40}Ar/^{39}Ar$ laser analysis of the Variscan basement of Sardinia: Journal of Petrology, v. 45, p. 1013-1043.

Gattacceca, J., Deino, A., Rizzo, R., Jones, D.S., Henry, B., Beaudoin, B., and Vadeboin, F., 2007, Miocene rotation of Sardinia: new paleomagnetic and geochronological constraints and geodynamic implications: Earth and Planetary Science Letters, v. 258, p. 359-377.

Gee, D.G., Lobkowicz, M., and Singh, S., 1994, Late Caledonian extension in the Scandinavian Caledonides-The Roragen Detachment revisited: Tectonophysics, v. 231, p. 139-155.

Helbing, H., Frisch, W., and Bons, P., 2006, South Variscan terrane accretion: Sardinian constraints on the intra-Alpine Variscides: Journal of Structural Geology, v. 28, p. 1277-1291.

Jaffey, A. Flynn, K., Glendenin, L, Bentley, W., and Essling, A., 1971, Precision measurement of half-lives and specific activities of ^{235}U and ^{238}U: Phys. Rev. C, v. 4, p. 1889–1906

Leech, M., 2001, Arrested orogenic development: eclogitization, delamination, and tectonic collapse: Earth and Planetary Science Letters, v. 185(1-2), p. 149-159.

LePichon, X., Henry, P., and Goffé, B., 1997, Uplift of Tibet: from eclogites to granulites-implications for the Andean Plateau and the Variscan belt: Tectonophysics, v. 273**,** p. 57–76.

Malavieille, J., Guihot, E, Costa, S., Lardeaux, J.M., and Gardien, V., 1990, Collapse of the thickened Variscan crust in the French Massif Central: Mont Pilat extensional shear zone and St. Etienne Late Carboniferous basin: Tectonophysics, v. 177, p. 139-149.

Matte, P., 2001, The Variscan collage and orogeny (480-290 Ma) and the tectonic definition of the Armorica microplate: a review: Terra Nova, v. 13, p. 122-128.

Matte, P., 1991, Accretionary history and crustal evolution of the Variscan belt in Western Europe: Tectonophysics, v. 196 (3-4), p. 309-337.

Matte, P., 1986, Tectonics and plate tectonics model for the Variscan belt of Europe: Tectonophysics, v. 126, p. 329-374.

Mattinson, J.M., 2005, Zircon U-Pb chemical abrasion ("CA-TIMS") method: combined annealing and multi-step partial dissolution analysis for improved precision and accuracy of zircon ages: Chemical Geology, v. 220, p. 47-66.

Milnes, A.G., Wennberg, O.P., Skår, Ø., and Koestler, A.G., 1997, Contraction, extension and timing in the south Norwegian caledonides: the Songefjord transect: J.-P. Burg, M. Ford (Eds.), Orogeny Through Time: Geological Society Special Publication No. 121, p. 123–148.

Northrup, C. J., 1996 Structural expressions and tectonic implications of general noncoaxial flow in the midcrust of a collisional orogen: the Northern Scandinavian Caledonides: Tectonics, v. 15, p. 490-505.

Platt, J.P., 1993, Exhumation of high-pressure rocks: a review of concepts and processes: Terra Nova, v. 5, p. 119–133.

Scisciani, V., Tavarnelli, E., and Calamita, F., 2002, The interaction of extensional and contractional deformations in orogenic belts: the example of the central Apennines, Italy: Journal of Structural Geology, v. 10, p. 1647-1658.

Schmitz, M.D. and Schoene, B., 2007, Derivation of isotope ratios, errors and error correlations for U-Pb geochronology using ^{205}Pb-^{235}U-(^{233}U)-spiked isotope dilution thermal ionization mass spectrometric data: Geochemistry, Geophysics, Geosystems (G3) 8, Q08006, doi:10.1029/2006GC001492.

Stampfli, G. and Borel, G., 2002, A plate tectonic model for the Paleozoic and Mesozoic constrained by dynamic plate boundaries and restored synthetic oceanic isochrones: Earth and Planetary Science Letters, v. 196, p. 17-33.

Vissers, R. L. M., Platt, M. J., and van der Wal, D., 1995, Late orogenic extenision of the Betic Cordillera and ASlboran Domain: a lithospheric view: Tectonics, v. 14, p. 786-803